Morphological Dynamics of Hybrid Dunes under Storm Conditions

A Field-Based Study on the Performance of Hybrid Flood Defenses

Msc Thesis - CIEM0500

R.G.C. Rosman

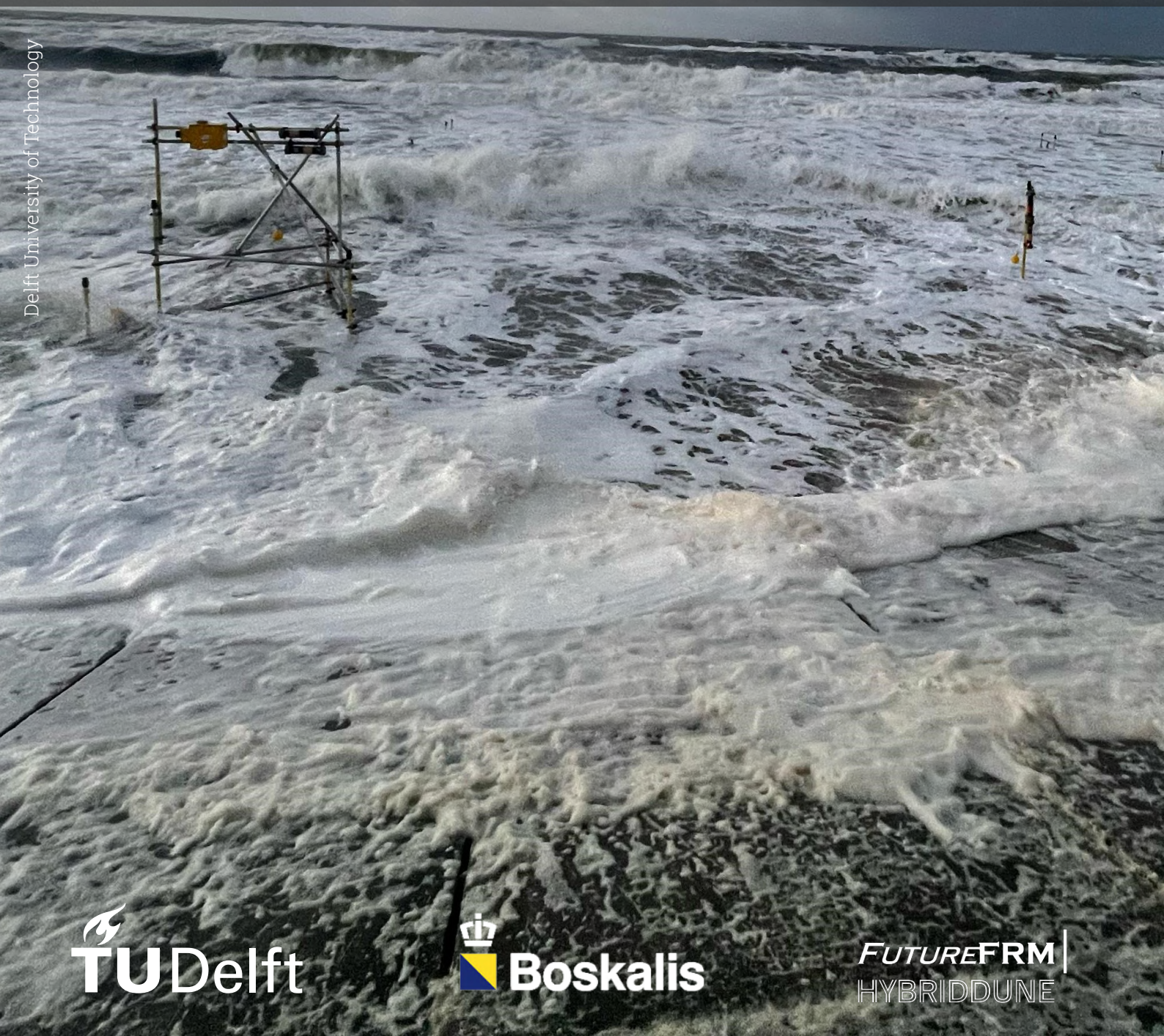

Delft University of Technology

TU Delft

Boskalis

FUTUREFRM | HYBRIDDUNE

Morphological Dynamics of Hybrid Dunes under Storm Conditions

A Field-Based Study on the Performance of Hybrid Flood Defenses

by

R.G.C. Rosman

Ruben Rosman 4905881

Supervisors:	Dr. ir. Sierd de Vries - TU Delft
	Dr. ir. Daan Poppema - TU Delft
	Dr. ir. Marrion Tissier - TU Delft
	Dr. ir. Mark Klein - Boskalis
Project Duration:	September 2024 - June 2025
Institutes:	Delft University of Technology,
	Royal Boskalis Westminster N.V.
Faculty:	Civil Engineering and Geosciences

TU Delft Boskalis FUTUREFRM | HYBRIDDUNE

Acknowledgements

This thesis marks the final step of my Master's in Hydraulic Engineering at Delft University of Technology, with a specialisation in Coastal Engineering. My passion for engineering started at a young age, building LEGO structures and creating water systems in the sand at the beach. During my Bachelor in Civil Engineering at TU Delft, this interest deepened, especially after following courses like Fluid Mechanics and Hydraulic Engineering, where I discovered how fascinating and complex water systems truly are. This fascination with water systems only grew stronger over the years, and with it came a deep appreciation for the world of dredging. The scale, impact, and technical challenges of working with sediment and shaping coastlines truly fascinate me.

Working on hybrid dunes at the Sand Engine has been an incredible experience. I especially enjoyed the fieldwork, whether it was building the dike sections together with contractors or going into the sea to deploy sensors in the middle of winter. It was cold, wet, and at times chaotic, but also deeply satisfying and unforgettable. Studying how these systems respond to storm conditions and presenting the results at the NCK Days were proud moments in this journey. I want to sincerely thank those who supported me throughout this project. Sierd de Vries, Daan Poppema, Marrion Tissier, and Mark Klein, thank you for your guidance, feedback, and enthusiasm along the way. Your support made this challenging project not only manageable but truly enjoyable.

I'm also very thankful to my family and friends. To my parents, for your endless support and belief in me. To my housemates and study friends, for making the long days more fun, keeping me motivated, and sharing the highs and lows of this adventure. Looking back, I feel proud of what I've learned, excited for what lies ahead, and grateful to everyone who helped make this experience so valuable.

R.G.C. Rosman
Rotterdam, June 2025

Disclaimer: Generative AI tools were used solely for practical support during the writing of this thesis. Their use was limited to grammar and spelling correction, as well as assistance with debugging Python code. AI was not used for sourcing information, generating interpretations or results, or making any methodological decisions. All academic content, analysis, and conclusions are entirely the work of the author.

Abstract

Hybrid dunes are a coastal flood defense structure that combines the sandy and wave-dissipating capacity of natural dunes with the robustness of hard structures. Their increasing application in coastal environments highlights the need for a better understanding of how these systems respond to storm forcing. This study investigates the morphodynamic behavior of hybrid dunes under storm conditions through a large-scale field experiment at the Sand Engine (NL), aiming to improve predictive insight into erosion mechanisms and structural performance. High-resolution LiDAR, pressure sensors, and acoustic instruments were deployed across four engineered dune configurations, ranging from a fully sandy dune to hybrid setups with embedded sea dike and seawall cores, to monitor morphological changes and hydrodynamic forcing during five consecutive storms.

The main research question is: *What are the dominant erosion mechanisms and structural influences of embedded hard elements in hybrid dunes during consecutive storm events?*

The findings show that hybrid dunes transition through three consistent erosion phases: (1) initial sand-dominated retreat characterized by notching, slumping, and offshore sediment transport, (2) reduced erosion once hard elements become partially exposed, and (3) structure-dominated stability after full exposure, during which landward retreat halts. Core geometry strongly influenced behavior: The Dike-in-dune (S1) supported smoother energy dissipation and profile adjustment, while the wall-in-dune (S4) halted retreat more abruptly but caused localized vertical beach erosion. In contrast, the Sandy dune (S2) continued to retreat by over 7 m, with cumulative erosion volumes exceeding 11 m^3/m.

Erosion volumes correlated significantly with 20 min time-averaged waterlevel, measured 80 m seaward of the dune foot. Field observation identified the total water level as the dominant driver of erosion. Once exposed, hard structures reduced wave run-up and changed energy distribution, influencing sediment mobility. Oblique wave conditions likely disrupted longshore sediment supply, especially toward unarmored sections, amplifying erosion near structural transitions. These interactions underscore the need to jointly assess cross- and longshore processes when evaluating hybrid dune behavior.

Key design factors include sand cover thickness, core geometry, and especially transition zone reinforcement. Structural flanking and undermining were critical failure mechanisms, as seen in the collapse of the Dike-in-Dune and Dike sections during the fourth storm. These results highlight the importance of integrated design strategies addressing not only structural shape, but also lateral sediment continuity and toe stability.

Hybrid dunes shift erosion from retreat-driven to structure-constrained behavior, offering localized resistance under storm conditions. However, their long-term performance depends on robust, system-scale design, balancing sand volume, structural exposure, and sediment pathways to deliver adaptable and resilient coastal protection.

Contents

Nomenclature

Abbreviations

Abbreviation	Definition
ADCP	Acoustic Doppler Current Profiler
ADV	Acoustic Doppler Velocimeter
GCP	Ground Control Points
IG	Infragravity Waves
LiDAR	Light Detection and Ranging
OBS	Optical Backscatter Sensor
RTK-GPS	Real-Time Kinematic Global Positioning System
TWL	Total Water Level
Ww	Wind Waves

List of symbols

Symbol	Definition	Units
D	Diameter	[m]
g	Acceleration due to gravity	[m/s^2]
H_0	Deep-water significant wave height	[m]
H_{m0}	Significant wave height	[m]
$H_{m0,IG}$	Infragravity wave height	[m]
L_0	Deep-water wavelength	[m]
$R_{2\%}$	2% exceedance wave runup height	[m]
R_{max}	Maximum runup elevation	[m]
S_{max}	Maximum scour point	[m]
S_t	Scour depth near seawall toe	[m]
T	Deep-water wave period	[s]
T_p	Peak wave period	[s]
$T_{-1,0}$	Mean absolute wave period	[s]
$T_{m-1,0}$	Spectral wave period	[s]
T_{m01}	Mean wave period	[s]
T_{m02}	Mean zero-crossing period	[s]
$z_{2\%}$	2% exceedance runup level	[m]
z_B	Dune base elevation	[m]

Symbol	Definition	Units
α	Slope angle	[rad]
β_f	Foreshore beach slope	[–]
η	Surface elevation relative to NAP	[m]
$\eta_{L,A,2\%}$	Lidar-derived 2% exceedance water level	[m]
γ	Overall reduction factor	[–]
γ_b	Berm reduction factor	[–]
γ_f	Roughness reduction factor	[–]
γ_β	Oblique wave attack reduction factor	[–]
ξ_{op}	Breaker parameter	[–]
$\xi_{s,-1}$	Surf similarity parameter	[–]
m_{-1}	Spectral moment of order -1	[m^2/s]
m_0	Zeroth-order spectral moment	[m^2]
s_{op}	Deep-water wave steepness	[–]
tan(α)	Slope angle	[–]

1 Introduction

Hybrid dunes are an innovative form of coastal flood defense that integrates engineered structures with natural sandy dunes. This design combines the wave-dissipating and adaptive properties of natural dunes with the robustness of hard infrastructure, enabling the system to withstand high-energy wave conditions and serve ecological and recreational purposes (Almarshed et al., 2020). In the Netherlands, hybrid dunes have been implemented at several coastal sites, most notably at Katwijk (Figure 1.1) and Noordwijk, with growing interest internationally. These systems can play an important role in present flood protection, especially in densely populated coastal zones, where roughly 40% of the global population resides within 100 km of a coastline (Small and Nicholls, 2003).

Despite their growing application, the understanding of the morphological response of hybrid dunes under extreme wave forcing remains incomplete. Storm-induced erosion presents a major risk to these systems, particularly when storm regimes exceed design conditions. Sallenger's storm impact scale categorizes dune erosion into four regimes: swash, collision, overwash, and inundation, based on the total water level and wave runup relative to the dune crest (Sallenger and Asbury, 2000). The collision regime is of particular concern for hybrid dunes, as repeated wave runup erodes the dune toe and triggers slumping on the upper slope (Van Wiechen et al., 2023). In addition, internal failure can be triggered by excess pore pressure resulting from repeated wave runup and rapid fluctuations of the phreatic surface within the dune body (Conti et al., 2024). Oblique wave conditions further amplify shoreline morphological variability by promoting beach cusp formation and swash zone instabilities, affecting cross-shore sediment transport patterns (Castelle et al., 2015). In hybrid configurations, the interaction between the soft sandy body and embedded hard structures complicates these processes. Experimental studies show that hard enhanced cores, such as revetments or dikes within the dune body, modify hydrodynamic conditions by enhancing wave reflection and concentrating energy at the structure's toe (Almarshed et al., 2020; Figlus et al., 2015). This leads to localized scour and increased overwash, which in turn redistribute sediment and reduce overall resilience (Boers et al., 2011). Laboratory experiments with 25 × 25 m wave basins confirm that hard structures amplify erosion near their interface with sand, altering natural morphodynamic behavior (Van Geer et al., 2009).

Designing sustainable hybrid dunes requires a deeper understanding of how these elements interact under storm conditions. The combined effects of altered wave runup, sediment transport, and internal pore pressure create a complex morphodynamic response. Currently, the long-term performance and failure mechanisms of hybrid dunes remain difficult to predict. This knowledge gap hinders the development of reliable, material-efficient, and climate-resilient flood protection strategies. This study addresses these challenges by investigating the morphodynamic behavior of hybrid dunes under storm conditions, with a focus on how hard structure configurations influence erosion patterns and stability. Through detailed analysis and large-scale field observations, this research aims to improve predictive capabilities and inform future coastal defense design.

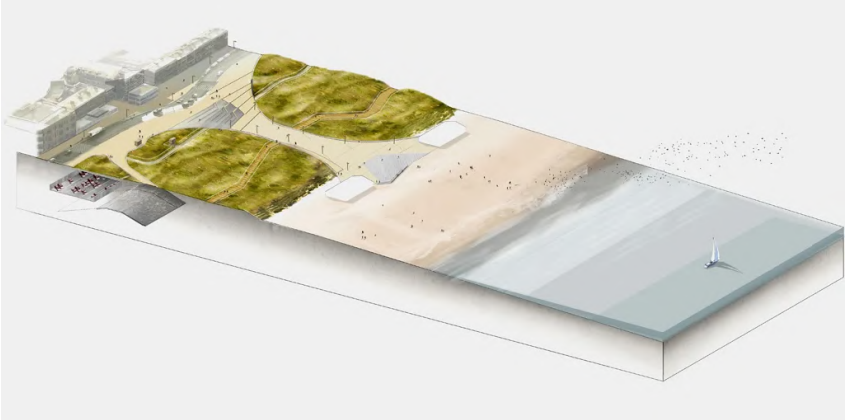

Figure 1.1: Schematic representation of the hybrid dune system at Katwijk. The figure illustrates the integration of a hard structural core (parking garage) embedded within a sandy dune. The dune is shaped with a natural profile, complete with vegetative cover, and functions as part of the coastal defense system. The beach lies in front of the dune, providing additional wave dissipation before reaching the sea-facing slope. Source: https://bouwenuitvoering.nl/weg_en_waterbouw/project-kustwerk-katwijk/

1.1. Research objective

This thesis forms part of the broader Hybrid-Dune Research Project, which aims to improve understanding of the interactions between sandy and hard structural components in coastal flood defenses. The overarching project includes a full-scale field experiment at the Sand Motor, commissioned under the NWO Perspectief program “Future Flood Risk Management Technologies,” and supported by Rijkswaterstaat. Its goal is to study dune erosion across four engineered cross-sectional configurations under storm conditions, enabling improved morphological predictions and more robust hybrid-dune designs (Poppema et al., 2025).

While the full Hybrid Dune project includes dune construction, measurement system deployment, and comprehensive analysis, this thesis focuses on a specific subcomponent: the morphological response of different hybrid-dune configurations to storm conditions. The objective of this study is to analyze erosion patterns, sediment transport, and structure-sediment interactions to identify the dominant processes influencing dune evolution. By using high-resolution datasets from extensive sensor arrays (including LiDAR, pressure sensors, ADVs, and RTK-GPS), this research aims to enhance understanding and provide actionable insights for coastal engineering.

The main research question of this thesis is:

> **What are the dominant erosion mechanisms and structural influences of embedded hard elements in hybrid dunes during consecutive storm events?**

To answer this, the following sub-questions guide the investigation:

- **1)** *How do different hard structures embedded within a hybrid dune affect cross-shore morphological evolution during storm events?*
- **2)** *What are the correlations between wave and current conditions and the observed morphological changes in hybrid dune configurations?*
- **3)** *What are the key design considerations that influence the resilience and erosion resistance of hybrid dunes under extreme hydrodynamic forcing?*

This study begins with a systematic analysis of morphological changes observed across four dune sections: a fully sandy dune, a dike-in-dune, a conventional dike with exposed revetment, and a wall-in-dune (sea container) setup. These configurations were deliberately chosen in the broader experiment to capture a wide range of hybrid typologies. Using integrated hydrodynamic and morphological data, the thesis quantifies differences in erosion behavior and evaluates how structural configurations influence sediment dynamics and dune stability. By isolating and comparing the performance of different designs under real storm conditions, this research provides insights that contribute to the optimization of hybrid dunes as sustainable and adaptable coastal defenses.

1.2. Report outline

This thesis is structured to distinguish between data collection and analysis, while presenting a coherent narrative that supports both scientific rigor and practical applicability. Following the introductory chapters (Chapters 1 and 2), the methodology chapter (Chapter 3) is presented in the format of a data paper. This chapter is designed to stand alone, offering a transparent and detailed account of the experimental setup, instrumentation, and data records from the full-scale hybrid dune experiment conducted at the Sand Engine. Its format facilitates reproducibility and allows independent use of the dataset by other researchers or practitioners.

The subsequent chapters (Chapters 4 to 7) focus on the interpretation and synthesis of the collected data. These chapters analyze the morphological and hydrodynamic response across the four hybrid dune configurations, identify key erosion mechanisms, and evaluate the role of structural design in shaping dune behavior under storm conditions. The discussion situates the findings within the broader literature and addresses the main research question and sub-questions. The thesis concludes with a summary of the key insights and a set of recommendations for future research and hybrid dune design improvements. An overview of the report structure is provided in Fig. 1.2. The hybrid layout, combining academic analysis with a technical data paper, ensures clarity for diverse audiences while preserving scientific depth and transparency.

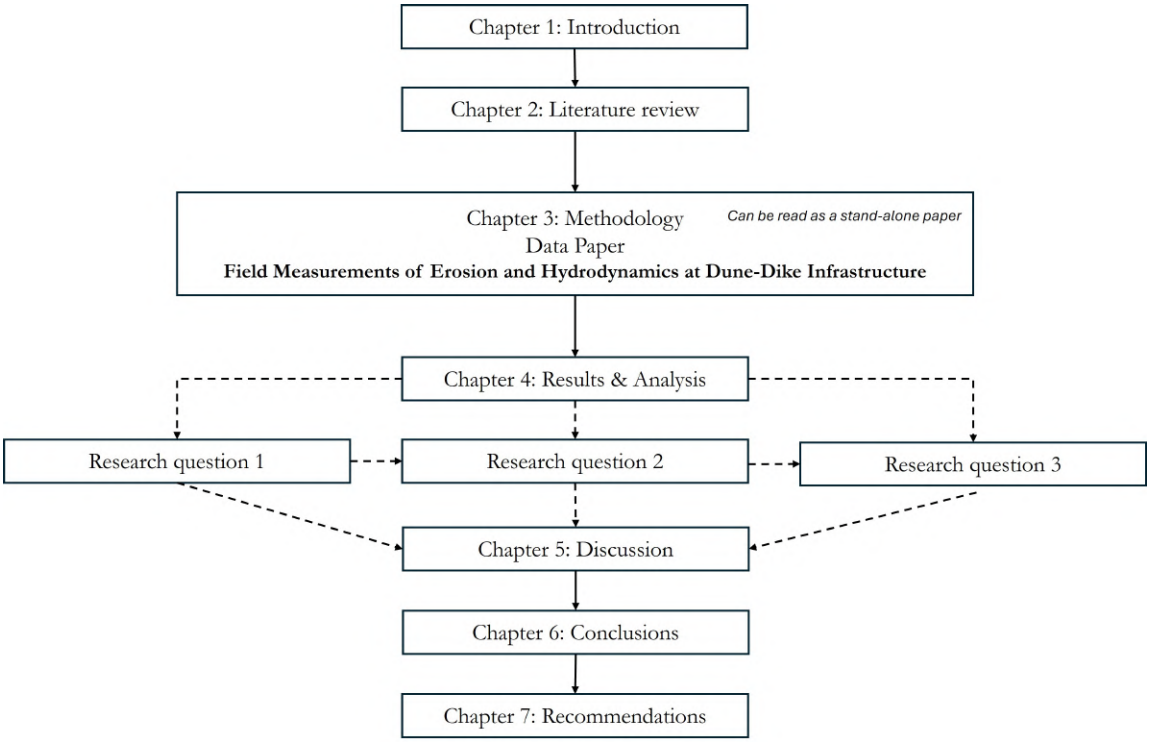

Figure 1.2: Overview of the thesis structure. Chapter 3 (Methodology) is presented in the format of a draft for a data paper and is designed to be read as a stand-alone publication.

2
Literature review

This chapter provides a comprehensive overview of the physical processes, structural behaviors, and design considerations relevant to hybrid dune systems. It establishes the scientific foundation for understanding how natural and engineered components interact under hydrodynamic forcing. The chapter is structured around three main system types: sandy dunes, hard structures, and hybrid dunes, each addressed in a dedicated section.

Section 2.1 focuses on natural sandy dunes, reviewing their morphodynamic and geotechnical responses to storm conditions. It covers storm impact regimes, wave runup dynamics, sediment transport processes, and soil mechanical properties. This section defines the baseline behavior of dunes without structural intervention, essential for evaluating hybrid performance.

Section 2.2 addresses hard structures, examining the primary failure mechanisms of sea dikes and revetments under wave attack. It outlines structural, geotechnical, and hydraulic failure modes, which become critical once a hybrid system's sand layer is lost.

Section 2.3 explores hybrid dune systems, presents current knowledge on their performance, configurations, and morphodynamic responses. It discusses the interaction between wave dynamics and buried structures, erosion patterns around exposed cores, and trade-offs in hybrid design. The section concludes with key insights into optimal material choices and design strategies.

2.1. Sandy dune

Sandy dunes play a central role in natural coastal protection, acting as dynamic buffers against storm surge and wave attack. This section reviews their morphodynamic and geotechnical response under wave forcing, highlighting the key physical processes, such as wave runup, sediment transport, and pore pressure effects, that govern erosion and failure. These mechanisms form the foundation for understanding how dunes respond with and without structural reinforcement.

2.1.1. Storm impacts and wave spectra

Understanding how sandy dunes respond to storm events begins with examining the nature of the hydrodynamic forcing that acts upon them. The primary agents of morphological change during storms are water levels and wave energy, both of which determine how and where waves interact with the dune system. This section introduces the key components of storm impact and describes the spectral characteristics of waves that govern dune behavior.

Storm impacts

Hydrodynamic forcing plays a critical role in shaping coastal morphology during storm events. In the North Sea, water levels are primarily influenced by semi-diurnal astronomical tides, dominated by the M2 (principal lunar) and S2 (principal solar) constituents, and further modulated by meteorological storm surges. This interaction produces two high and two low tides per day, with tidal ranges varying between one and four meters depending on local geography and weather conditions (Bosboom and Stive, 2023). In addition to these tidal and surge components, wave-induced processes such as wave setup and runup also contribute to the Total Water Level (TWL) at the shoreline. The TWL determines the vertical extent of wave interaction with coastal features such as dunes and hybrid defense systems. As TWL increases, the probability that waves reach and erode the dune toe or overtop the crest also increases, making TWL a primary determinant of storm impact severity (Sallenger and Asbury, 2000).

Based on this concept, Sallenger and Asbury (2000) developed a widely used classification framework that links TWL to four progressive storm impact regimes. Each regime represents a specific mode of wave-dune interaction and associated erosion response:

- **Swash regime (Impact Level 1)**: Wave runup remains confined to the foreshore and does not reach the dune toe. Erosion is limited to temporary redistribution of beachface sediments and is generally reversible through natural accretion.
- **Collision regime (Impact Level 2)**: runup exceeds the base of the foredune (dune toe), but not the crest. This leads to direct wave attack on the dune face, initiating scarping, slumping, and net sediment loss. This regime is especially relevant to hybrid dunes, where buried structural elements may become exposed prematurely.
- **Overwash regime (Impact Level 3)**: runup and surge levels exceed the dune crest, transporting sediment landward over the barrier and contributing to crest lowering, overwash fan deposition, and barrier rollover.
- **Inundation regime (Impact Level 4)**: The entire barrier is submerged for sustained periods due to extreme surge and wave setup. Wave energy reaches the back-barrier environments, causing large-scale sediment redistribution and morphological transformation.

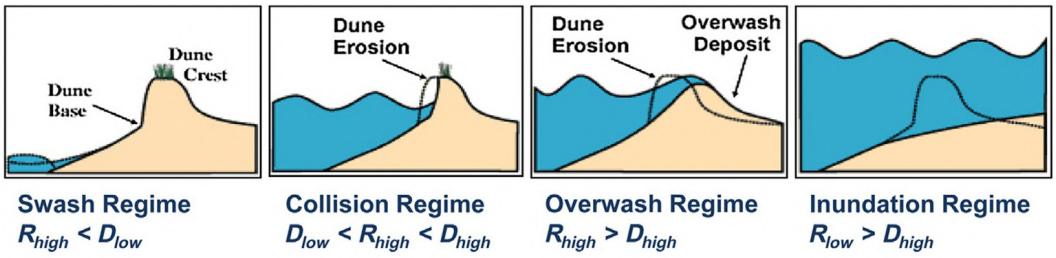

Figure 2.1: The Sallenger Impact Scale categorizes storm-induced coastal change into four regimes: (1) swash, (2) collision, (3) overwash, and (4) inundation. Thresholds are defined by the relative elevations of wave runup (R_{high}), total water level (R_{low}), dune toe (D_{low}), and dune crest (D_{high}). Adapted from the United States Geological Survey (USGS) Coastal and Marine Science Center. `http://coastal.er.usgs.gov/hurricanes/impact-scale/`

Understanding these impact regimes is fundamental for predicting the behavior of both natural and hybrid dunes under storm loading. In particular, the collision regime serves as the primary erosion mechanism observed in field-scale hybrid dune studies, where runup events erode the sandy cover and interact with embedded structures. Accurate classification of these regimes using TWL and runup metrics supports more effective design and management of resilient coastal defenses.

Wave Spectra and infragravity Wave Dynamics

Wave energy reaching the coast from wind and storm events offshore can be described using the wave spectrum, which illustrates how energy is distributed across different frequencies (and directions, in the case of a directional spectrum). This spectrum typically distinguishes between short-period wind waves and long-period infragravity (IG) waves.

Short waves dominate the offshore wave energy budget and are responsible for most of the wave breaking and turbulence in the surf zone (Bertin et al., 2018). As they shoal and break nearshore, their energy dissipates rapidly, particularly over the surf and swash zones. Their groupiness, natural fluctuations in wave envelope intensity, is critical in generating infragravity waves during the shoaling process (Bertin et al., 2018). Additionally, short waves are a primary driver of swash-scale sediment transport, especially along the lower beach face, and play a key role in shaping the beach profile under lower to moderate energy conditions (Ruessink et al., 2011).

Infragravity waves, generally defined within the frequency range of 0.004–0.05 Hz, are long-period waves that originate as bound components coupled to these short-wave groups. As the short-wave groups shoal and break, the associated bound long waves are released and propagate shoreward as free infragravity waves (Bertin et al., 2018). Because their energy is no longer constrained by the short-wave envelope, these waves persist and often grow in importance toward the inner surf and swash zones, particularly under energetic wave or storm conditions (Masselink and Puleo, 2006; De Bakker et al., 2014). The transformation and growth of infragravity waves from offshore to the swash zone is illustrated conceptually in Fig. 2.2, which highlights the inner surf zone as a key region for IG-driven modulation of runup and wave breaking. Unlike short waves, IG waves are capable of penetrating far into the swash zone, producing energetic, long-lasting runup motions. Their larger spatial and temporal

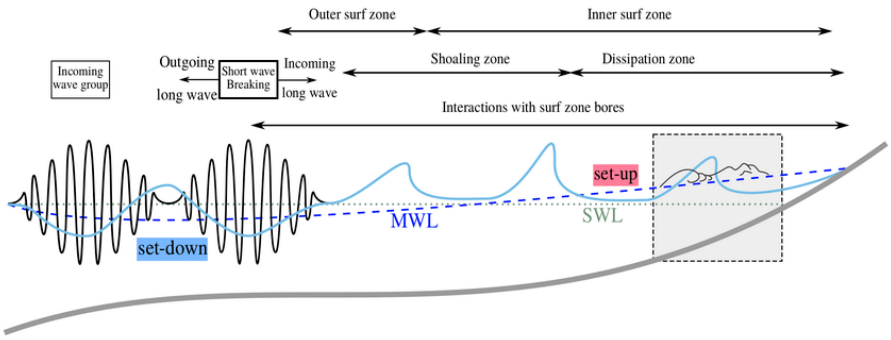

Figure 2.2: Conceptual model of infragravity wave transformation across the surf zone. The blue line represents the evolution of infragravity wave energy from the offshore to the swash zone. The inner surf zone (shaded area) marks the region where infragravity wave-induced water level fluctuations most strongly modulate incident wave breaking and swash processes. Adapted from Huntley and Kim (1984), Dongeren et al. (2007), and De Bakker et al. (2014).

scales enable them to modulate water levels at the dune toe effectively (Van Gent et al., 2008). Elevated runup driven by IG wave crests can allow short-wave remnants to reach higher elevations on the beach, increasing wetting and promoting dune slope instability through infiltration (Palmsten and Holman, 2011). Under high-energy conditions, infragravity waves often dominate nearshore hydrodynamics and contribute significantly to processes like dune erosion and barrier breaching (Bertin et al., 2018).

The role of infragravity waves in cross-shore sediment transport has been quantified by Ruessink et al. (1998), who showed that although their direct contribution is typically smaller than that of short waves or undertow, they play a crucial role in determining net sediment fluxes. This is because short-wave- and undertow-driven sediment transport often oppose each other and can partially cancel out, whereas the infragravity component provides a consistent directional influence, especially near the dune toe. The importance of IG waves in controlling dune erosion has been confirmed by both field and flume studies. Van Thiel de Vries et al. (2008) and Van Gent et al. (2008) showed that even under the same significant wave height, differences in wave period and spectral shape can result in substantially different erosion responses.

In summary, infragravity waves play a critical role in nearshore and swash zone dynamics due to their long periods and ability to propagate further shoreward than short waves. They significantly influence wave runup, water level variability at the dune toe, and cross-shore sediment transport. Their impact is especially pronounced during storm events, where they can dominate the physical processes driving dune erosion, underscoring their importance in coastal morphodynamics. These hydrodynamic drivers, particularly infragravity wave motions and elevated total water levels, set the stage for wave runup to reach and saturate the dune face. The next section explores the mechanics of wave runup and how it initiates sediment transport and infiltration processes that ultimately lead to dune instability and retreat.

2.1.2. Wave runup dynamics

As mentioned in the previous section, wave setup and runup are key components of the total water level (TWL). Wave setup refers to the quasi-steady increase in mean water level near the shoreline caused by the onshore transfer of momentum from breaking waves. This process results from gradients in radiation stress and leads to a rise in the water surface elevation (Gourlay, 2011). Setup initiates at the seaward edge of the surf zone, increases shoreward, and typically peaks in the inner surf zone, where wave breaking is most intense. Its magnitude depends on offshore wave height, wave period, and beach slope, with steeper profiles generally amplifying the effect.

Wave runup is the maximum vertical excursion of wave uprush above the still water level, encompassing both the mean setup and the superimposed swash oscillations. It directly governs whether waves reach the dune toe or crest, thus serving as a key indicator of storm impact regimes. runup increases with wave height, wave period, and beach steepness, and is typically greater on reflective profiles. Stockdon et al. (2006) proposed an empirical formula that incorporates both setup and swash components to estimate runup on sandy beaches (see Eq. 2.1).

However, the Stockdon formulation is based solely on deep-water wave parameters and does not account for structural elements or local wave transformations. As a result, it can misrepresent runup levels in engineered settings. In Section 2.1.2, two alternative models will be discussed that assess wave runup on hard structures, accounting for spectral evolution and wave-structure interactions.

Wave runup on steady sloped beaches

The formula estimates the 2% exceedance runup height, $R_{2\%}$, as a function of foreshore slope (β_f), deep-water significant wave height (H_0), and deep-water wavelength (L_0). It consists of two main terms: the first represents wave setup and incident-band swash, scaling with $\beta_f\sqrt{H_0L_0}$. The second captures both incident and infragravity swash, including a slope-independent component. Together, these terms describe the total vertical runup excursion due to mean and oscillatory wave processes during storm conditions. Fig. 2.3 illustrates the physical processes for the wave setup component of Eq. 2.1. As waves shoal and break on a steep, plane beach, mean water level initially decreases seaward of the breakpoint (set-down), then rises shoreward due to energy dissipation from breaking waves, this increase, or wave setup, directly corresponds to the first term of the Stockdon equation and contributes to total runup height.

While setup represents a mean water level shift, swash is the time-varying component. On dissipative beaches, swash is often dominated by infragravity waves, which enhance variability in runup and can drive more frequent or intense interactions with the dune toe (Masselink and Puleo, 2006; De Bakker et al., 2014). During high runup events, repeated swash exposure causes water to infiltrate horizontally into the unsaturated dune face via capillary action. This infiltration increases the pore water content and the weight of the dune's surface layer, leading to a rise in overburden stress. When the destabilizing forces from this added weight exceed the shear strength of the sediment, the wetted portion of the dune fails and slumps (Palmsten and Holman, 2011). This mechanism is a key process in storm-induced dune erosion, particularly relevant for hybrid dunes, where repeated slumping can prematurely expose underlying structural elements.

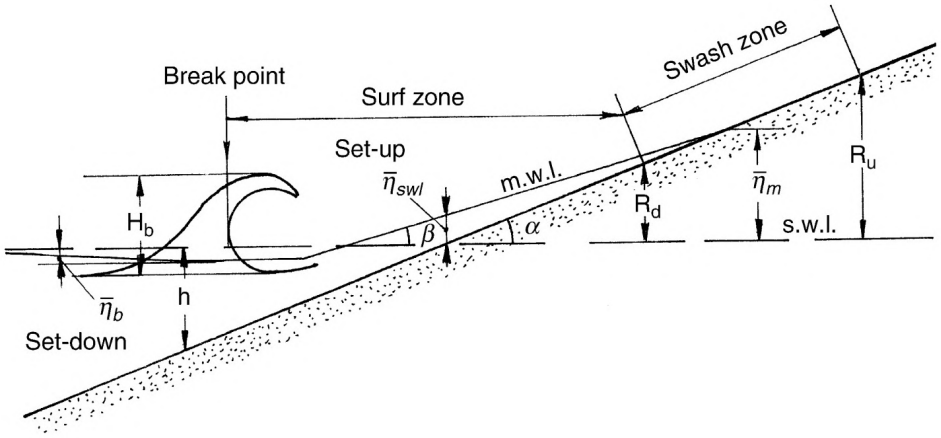

Figure 2.3: wave runup on beaches, with waves breaking on a steep, plane beach. Adapted from Gourlay (2011), originally published in the Encyclopedia of Modern Coral Reefs

$$R_{2\%} = 1.1\left[0.35\beta_f\sqrt{H_0L_0} + \frac{1}{2}\sqrt{H_0L_0\left(0.563\beta_f^2 + 0.004\right)}\right] \tag{2.1}$$

$$L_0 = \frac{gT^2}{2\pi} \tag{2.2}$$

Where:

- $R_{2\%}$: 2% exceedance wave runup height (m)
- β_f: Foreshore beach slope (dimensionless)
- H_0: Deep-water significant wave height (m)
- L_0: Deep-water wavelength (m)
- g: Acceleration due to gravity (≈ 9.81 m/s^2)
- T: Deep-water wave period, typically the peak period T_p (s)

Wave runup, comprising both setup and swash components, is a key control on storm-induced dune erosion. While setup elevates the mean water level, swash, especially infragravity-dominated on dissipative beaches, introduces high variability and dynamic forcing at the dune toe. The magnitude of runup depends on wave and beach characteristics, and its effects include infiltration-driven weakening of the dune face, often triggering slumping and scarp retreat. Accurate runup estimation is thus essential for understanding and predicting morphological response under storm conditions.

Wave runup on structures

While the empirical runup formula by Stockdon et al. (2006) is well-suited for gently sloping sandy beaches under deep-water wave conditions, it does not capture the complexity of wave-structure interactions at engineered structures such as dikes or hybrid dunes. In such cases, particularly when fronted by shallow foreshores or berms, shoaling, breaking, and energy dissipation significantly alter wave characteristics before reaching the structure. As a result, the Stockdon formula tends to misrepresent runup levels in these settings. To overcome these limitations, more physically grounded models have been developed. Notably, the formulations by Van der Meer (2017) and Van Gent (2001) incorporate local slope geometry, wave breaking dynamics, and spectral transformations. These approaches provide improved accuracy for structures with rough surfaces, berms, or complex foreshore profiles.

Van der Meer approach The runup formula (Eq.2.4) by Van der Meer (2017) is based on the breaker parameter ξ_{op}, which accounts for both the slope angle $\tan(\alpha)$ and deep-water wave steepness $s_{op} = \sqrt{H_s/L_0}$, where H_s is the significant wave height and L_0 the deep-water wavelength:

$$\xi_{op} = \frac{\tan(\alpha)}{\sqrt{H_s/L_0}} = \frac{\tan(\alpha)}{s_{op}} \tag{2.3}$$

The 2% exceedance runup level is then calculated as:

$$\frac{R_{u2\%}}{H_s} = 1.6 \cdot \gamma_b \cdot \gamma_f \cdot \gamma_\beta \cdot \xi_{op} \tag{2.4}$$

where:

- γ_b: berm reduction factor,
- γ_f: roughness reduction factor,
- γ_β: oblique wave attack reduction factor.

This formulation allows for deterministic or probabilistic applications and is suitable for composite and rough slopes, including configurations with berms and stepped geometries.

Van Gent approach The runup estimation (Eq. 2.6) used by Van Gent (2001) was developed to model dikes with shallow or barred foreshores, where local spectral transformation is significant. Unlike Van der Meer's approach, Van Gent uses the spectral wave period $T_{m-1,0}$, derived from the spectral moments m_{-1} and m_0, to better account for both short and long wave energy.
The surf similarity parameter is defined as:

$$\xi_{s,-1} = \frac{\tan(\alpha)}{\sqrt{2\pi H_s/gT_{m-1,0}^2}} \tag{2.5}$$

The corresponding 2% exceedance runup level $z_{2\%}$, normalized by the significant wave height and reduction factor γ, is given by a piecewise function:

$$\frac{z_{2\%}}{\gamma H_s} = \begin{cases} c_0 \cdot \xi_{s,-1}, & \text{if } \xi_{s,-1} \leq p \\ c_1 - \frac{c_2}{\xi_{s,-1}}, & \text{if } \xi_{s,-1} > p \end{cases} \tag{2.6}$$

This formulation reflects the nonlinear behavior of wave runup under spectral variability and allows better estimation in the presence of infragravity energy and double-peaked spectra. Together, the Van der Meer and Van Gent models represent accurate approaches for runup prediction on coastal structures. They incorporate both geometric complexity and wave spectral evolution, thereby significantly improving prediction accuracy over traditional empirical methods.

Comparison and application

The widely used empirical formula by Stockdon et al. (2006) is calibrated for open, sandy beaches with gently sloping, steady foreshores and assumes deep-water wave conditions. It relates runup to offshore wave steepness and beach slope, making it unsuitable for engineered or hybrid coastal structures where local bathymetry and wave transformations significantly influence runup. In contrast, both Van der Meer (2017) and Van Gent (2001) offer process-based formulations that explicitly account for wave-structure interactions and localized hydrodynamics, in contrast to the empirically derived Stockdon formula (Eq. 2.1).

- **Stockdon et al. (2006)**: Assumes unbroken, deep-water wave parameters. It lacks the capacity to represent the effects of wave breaking, roughness, or structural complexity. This results in systematic underestimation or overestimation of runup at structures fronted by shallow foreshores or berms.
- **Van der Meer (2017)**: Introduces the breaker parameter ξ_{op}, accounting for local slope and offshore wave steepness. It incorporates reduction factors for berms (γ_b), roughness (γ_f), and oblique wave attack (γ_β). This enables accurate estimation on composite or rough slopes, particularly in design conditions with complex geometry or multi-layer structures.
- **Van Gent (2001)**: Enhances predictive capability for structures fronted by shallow or barred foreshores. His method replaces the peak wave period T_p with the spectral wave period $T_{m-1,0}$, which better captures energy across long-period infragravity waves and multipeaked spectra. This approach significantly reduces uncertainty for non-Rayleigh spectral shapes and emphasizes the importance of spectral transformation effects.

Overall, while the Stockdon formula is effective for natural beach profiles under simplified conditions, the Van der Meer and Van Gent models provide more robust predictions in engineered or morphologically complex environments by accounting for nearshore wave transformation, structure-induced roughness, and spectral energy distribution.

2.1.3. Morphological and erosional responses

Sediment transport in the nearshore zone is a key driver of morphological change during storm events, particularly at the base of dunes and hybrid structures. Under high and low energy wave conditions, sediment is mobilized and redistributed through a combination of cross-shore and longshore transport processes. These transport mechanisms operate over different spatial and temporal scales and are influenced by wave direction, wave grouping, beach slope, and the presence of hard structures. In this section, the morphological response of the natural sandy dunes is discussed.

Hydrodynamic and sediment transport processes in the swash zone are very complex, characterized by rapidly varying flows in both time and space, nonlinear wave transformations, wave–wave interactions, and multiphase flows that may involve infiltration and exfiltration. These dynamics make the study and prediction of swash zone behavior particularly challenging. (Larson et al., 2004b) Cross-shore sediment transport dominates in the swash and surf zone during storm conditions and is primarily driven by the asymmetry between uprush and backwash flows. On steep and dissipative beach profiles, uprush may deposit sediment temporarily at the dune toe, but stronger backwash and infragravity-driven undertow tend to remove more sediment seaward, resulting in net erosion (Masselink and Puleo, 2006; Ruessink et al., 1998).

Field experiments by Larson et al. (2004b) and Masselink and Puleo (2006) demonstrated that the swash zone, often referred to as the foreshore, is shaped by these hydrodynamic forces. They showed that altering the initial beach slope initiated a natural readjustment of the beach profile toward an equilibrium state, regardless of its starting geometry. This indicates that, independent of the initial conditions, a specific set of hydrodynamic forcings consistently drives the beach toward a characteristic equilibrium profile, particularly when local gradients deviate from equilibrium conditions (Masselink and Puleo, 2006).

High-energy wave conditions

During sustained storm activity, intense wave action frequently erodes the dune toe, leading to the formation of notches that destabilize the slope and can trigger slumping and scarp retreat (Conti et al., 2024). The eroded sediment can temporarily act as a protective buffer at the dune face, but is typically transported offshore shortly afterward (Van Thiel de Vries et al., 2007).

Wave energy is a critical factor controlling sediment transport dynamics. Under high-energy wave conditions, breaking waves generate strong turbulence. This formation of steep, unstable wave fronts in the inner surf zone has been found to correlate with increased sediment resuspension and enhanced offshore-directed transport rates, particularly at the base of the dune (Ruessink et al., 1998; Van Thiel de Vries et al., 2008). Field observations confirm that during storm events, sediment transport is dominated by the suspended load, rather than bedload, with fluxes primarily driven by short-wave energy and undertow currents (Ruessink et al., 1998). Illustrated in Fig. 2.5, Van Wiechen et al. (2024a) identified three key mechanisms that simultaneously contribute to sediment suspension during storm conditions.

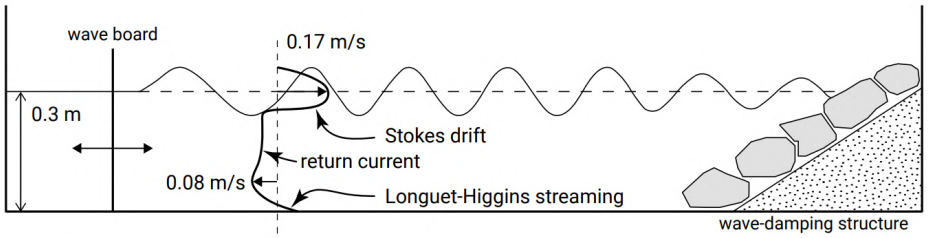

Figure 2.4: Simplified illustration of undertow, a return current that develops below the wave trough level to compensate for the onshore mass flux in the surf zone. The velocities shown are averaged over a wave cycle in a wave flume. Even under non-breaking wave conditions, a weak return flow is present. Adapted from Bosboom and Stive (2023).

Breaking waves in the nearshore zone generate complex circulation patterns, with undertow playing a central role in cross-shore transport. Undertow is the seaward-directed near-bed return flow that balances the shoreward mass transport caused by breaking waves, maintaining mass conservation within the surf zone (Stive and Wind, 1986; Reniers et al., 2004). It arises from the imbalance between the onshore wave momentum flux and the offshore-directed pressure gradient associated with wave setup. This process of return current (undertow) is illustrated in Fig. 2.4. The strength of the undertow depends on wave height and breaking intensity, with stronger flows typically observed under high-energy conditions (Stive and Wind, 1986). Field studies show that undertow velocities peak near the seabed beneath breaking waves, whereas under non-breaking wave conditions, return flows are more evenly distributed throughout the water column (Reniers et al., 2004). This variability is influenced by factors such as turbulence levels, bed roughness, and wind forcing, all of which modulate sediment suspension and transport during energetic events.

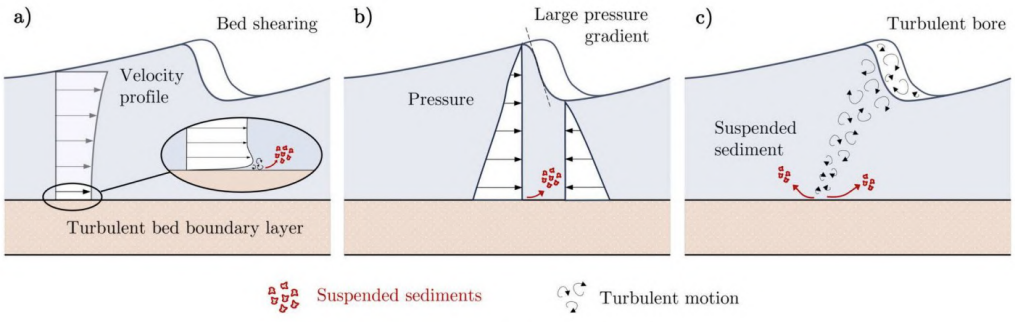

Figure 2.5: Sediment suspension drivers identified by Van Wiechen et al. (2024a): (a) bed shear stress induced by near-bed velocities, (b) horizontal pressure gradients beneath steep wave fronts, and (c) bore-induced turbulence reaching the bed.

Low-energy wave conditions

As waves propagate shoreward, they undergo shoaling and refraction, gradually aligning more perpendicular to the coastline as they interact with the seabed. During this transformation, nonlinear effects cause the wave shape to deform, increasing both asymmetry and skewness. Wave asymmetry refers to the steepening of the wave's front face relative to its back, while skewness describes the deviation from a sinusoidal profile, characterized by sharper crests and flatter troughs (Elgar and Guza, 1985).

These morphological changes can affect sediment transport, especially under low-energy wave conditions, where wave breaking is limited. Skewed waves enhance net onshore-directed transport (stokes-drift), whereas asymmetric waves, such as a saw-tooth shaped profiles, tend to promote a net offshore transport (Ruessink et al., 2009). In the nearshore zone, elevated wave asymmetry and skewness have been shown, through both numerical modeling and field measurements, to influence bed load dynamics. Strong wave asymmetry facilitates enhanced bed load transport, while skewed wave profiles are associated with ripple formation and variations in cross-shore sediment flux (Ruessink et al., 2011). These processes collectively contribute to the sediment re-distribution and dune morphology under under low-energy wave regimes.

In summary, wave-induced cross-shore sediment transport plays a critical role in shaping dune morphology, with distinct responses under high- and low-energy conditions. During storm events, high-energy waves generate intense turbulence and undertow, leading to re-suspension and offshore sediment transport and erosion at the dune toe. In contrast, low-energy conditions promote net onshore transport through wave skewness and Stokes drift, contributing to sediment accumulation and morphological adjustment. The interplay of wave shape, energy, and nearshore hydrodynamics governs the dynamic behavior of sandy dunes under varying wave climates. These processes are therefore a central focus of measurement in the field campaign of the Hybrid-Dune project.

Transport due to avalanching of the dune face

Avalanching refers to the episodic slumping of the dune face and crest following excessive steepening due to toe erosion. This gravity-driven process substantially contributes to cross-shore sediment transport, particularly during the later stages of storm-induced erosion (Van Thiel de Vries et al., 2008).

Fig. 2.6 illustrates the slumping mechanism based on laboratory observations. In panel (1) initially, drag-induced sediment removal below the maximum runup elevation (R_{max}) steepens the face beyond its angle of repose. As incoming swash further saturates the dune material, slope failure occurs when the weight of wet and dry sand layers exceeds the resisting shear strength, panel (2). The slumped material accumulates temporarily at the base, attenuating subsequent wave impact and temporarily reducing further erosion, panel (3). And finally in panel (4) the cycle repeats. (Van Thiel de Vries et al., 2007; Van Wiechen et al., 2023).

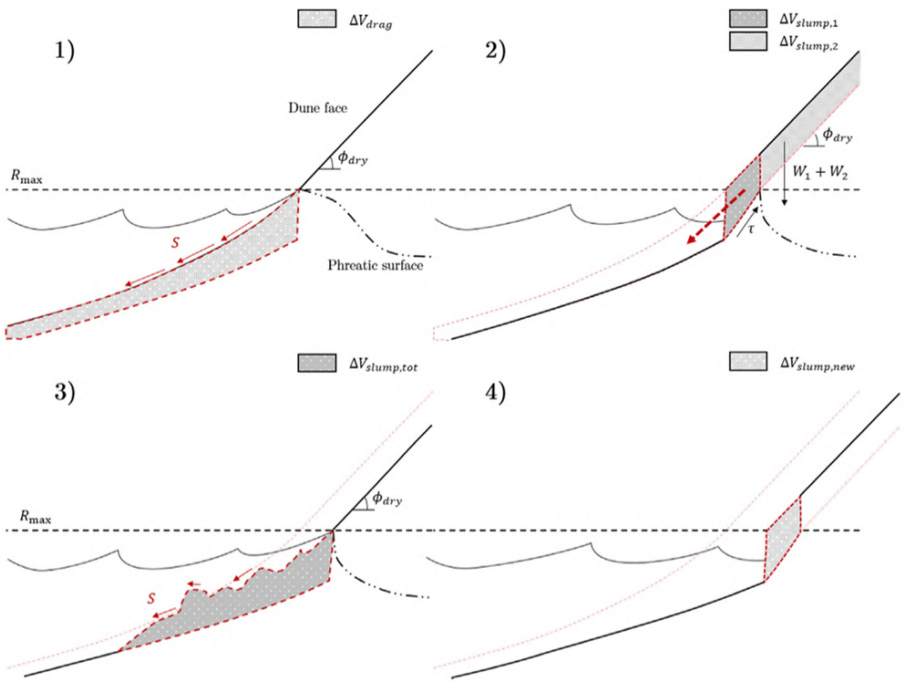

Figure 2.6: Illustration of the slumping mechanism based on laboratory observations. (1) Initial sediment removal due to drag below the maximum runup elevation (R_{max}) steepens the slope beyond the angle of repose. (2) Continued swash saturation reduces shear strength, triggering slope failure as the weight of wet and dry sand layers exceeds resisting forces. (3) The slumped material accumulates at the dune toe, temporarily absorbing wave energy and reducing further erosion. (4) The cycle then repeats with successive wave impacts. Adapted from Van Wiechen et al. (2023).

Over time, wave action redistributes the slumped material offshore, re-exposing the dune face and triggering the next cycle of erosion and collapse. Van Wiechen et al. (2024b) conducted field measurements and found that erosion rates increase with two rising water level indicators: (1) the 15-minute averaged water level measured approximately 16.5 meters seaward of the dune ($r = 0.77$, $p = 2.61 \times 10^{-4}$), and (2) the total water level, measured 5–6 meters in front of the dune face, that was exceeded 2% of the time ($r = 0.89$, $p = 2.00 \times 10^{-6}$). The strongest correlation was observed between the erosion rate and the square of the elevation difference between the dune base and the total water level exceeded 2% of the time ($r = 0.91$, $p = 4.05 \times 10^{-7}$). Their data further indicated that each slumping event was preceded by the near-complete removal of previously slumped sediment, highlighting the cyclic and self-sustaining nature of this process.

2.1.4. Soil mechanical response

Dune stability during storm events is governed not only by external hydrodynamic forcing but also by internal soil mechanical properties. Key factors include shear strength, pore pressure, and capillary forces, all of which are influenced by soil moisture content. These factors determine the dune's resistance to deformation and failure under wave-induced loading.

Shear strength and soil suction

Shear strength plays a central role in dune stability and is strongly influenced by matric suction in unsaturated sandy soils. Matric suction, generated by capillary forces, increases apparent cohesion by drawing water toward soil particles, thereby enhancing shear resistance. Conti et al. (2024) observed that dunes with high matric suction, typically under drier conditions, exhibit greater resistance to erosion and slumping. However, as moisture content increases toward saturation, matric suction decreases sharply. This leads to a corresponding reduction in shear strength, making the dune more susceptible to failure, particularly during prolonged storm exposure or tidal inundation.

Pore pressure

Pore pressure rises when water infiltrates the dune body, especially during high tide or storm surge. This increase in pore pressure reduces the effective stress within the soil matrix, which can trigger slope failure. Turner (1993) found that rapid fluctuations in pore pressure during dynamic hydraulic loading, such as wave attack or tidal cycles, significantly increase the likelihood of collapse. Supporting this, Erikson et al. (2007) noted that a rapidly rising water table contributes to instability by limiting the drainage potential of the dune, causing elevated internal water pressures to persist. While infiltration from individual wave runup events contributes to wetting, Conti et al. (2024) emphasized that such infiltration is not the primary driver of failure. Instead, their work points to rapid oscillations in the phreatic surface as the key mechanism behind excess pore pressure generation. These fluctuations disturb the sediment matrix and promote conditions for large-scale slumping or face collapse.

Capillarity and grain size

Capillary action in the unsaturated zone above the water table plays an important stabilizing role. The capillary fringe, the zone where water is held above the phreatic surface, provides cohesion by retaining moisture between sand grains, especially in finer-grained sediments (Turner, 1993). This additional suction strengthens the upper layers of the dune and delays failure. The height of the capillary fringe is inversely related to grain size. Finer sediments have smaller pore spaces, which produce a higher capillary rise. Coarser sands result in a lower capillary rise and thus a thinner fringe. Turner's findings indicate that while the capillary fringe can significantly enhance dune stability, excessive wetting eventually overwhelms these stabilizing effects. Once saturation is reached, capillary cohesion is lost, and the risk of mass failure increases (Turner, 1993).

Fig. 2.7 illustrates the beachface response under different wave conditions. When the beachface is flatter than its equilibrium gradient (Fig. 2.7a), sediment is transported up slope by swash processes until equilibrium is restored. Conversely, when the beachface is too steep (Fig. 2.7b), backwash processes dominate, leading to net offshore sediment transport and erosion of the upper beachface. Fig. 2.7c and Fig. 2.7d, show a more realistic response to changing wave conditions. These sediment dynamics interact with internal soil processes, further influencing the stability of the dune system during storm events (Masselink and Puleo, 2006).

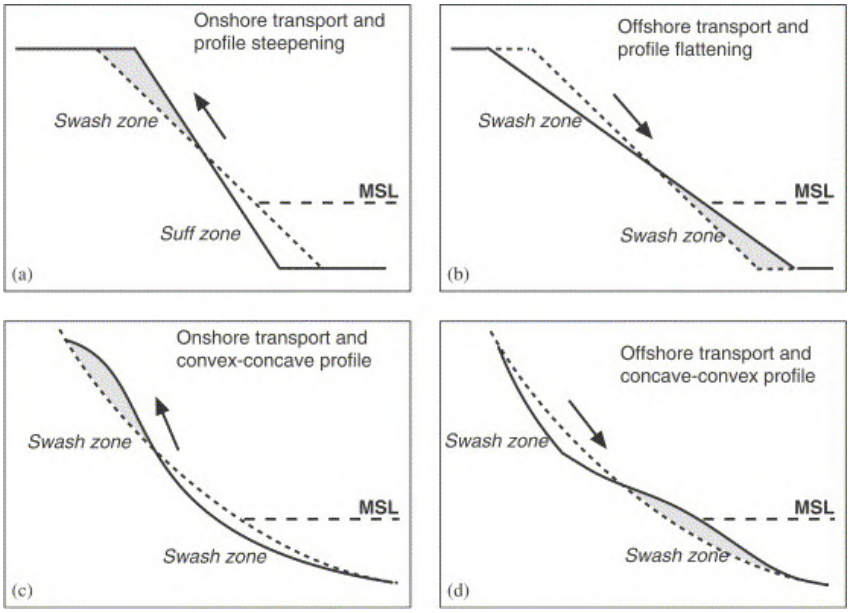

Figure 2.7: Comparison of beachface morphological responses. Panels (a) and (b) show idealized situations where maximum erosion and accretion occur in the upper swash zone, an area typically associated with low wave energy, making such patterns less realistic. In contrast, panels (c) and (d) illustrate more realistic morphological outcomes, with maximum bed level changes occurring in the mid-to-lower swash zone. These are characterized by the development of a convex profile during accretion (c) and a concave profile during erosion (d). (Masselink and Puleo, 2006).

2.1.5. Sandy dune Overview

The response of sandy dunes to storm events is controlled by a complex interplay between wave-induced hydrodynamic forcing and internal geotechnical properties. Cross-shore sediment transport, driven by wave asymmetry, undertow, and infragravity wave motions, plays a central role in shaping dune morphology. Under high-energy wave conditions, sediment is transported offshore and erosion at the dune toe intensifies. In contrast, low-energy conditions tend to promote onshore sediment deposition. Gravity-driven processes, such as slumping, further contribute to dune retreat, often occurring in repetitive, cyclic patterns.

Internally, dune stability is governed by soil mechanical factors, including shear strength, pore pressure, and capillary cohesion. These are highly sensitive to variations in soil moisture and hydrodynamic loading. During storm events, rising water levels, infiltration, and rapid fluctuations in the phreatic surface can significantly reduce the dune's resistance to failure, thereby accelerating erosion and collapse. Dune failure typically results from the interaction between external erosion at the toe and internal geotechnical weakening of the dune face. These processes often unfold sequentially and are interconnected through feedback loops. Based on insights from flume experiments, field observations, and recent conceptual models, five primary failure modes have been identified:

- **Toe erosion and notching:** Wave runup repeatedly impacts the dune base, removing sediment and forming a notch. This undercutting steepens the slope and destabilizes the overhanging sand mass. Notch depth is strongly linked to scarp retreat (Erikson et al., 2007; Van Wiechen et al., 2023).
- **Slumping and mass failure:** As the upper slope exceeds the angle of repose, gravitational collapse occurs. This can take the form of shear-type sliding or beam-type toppling, depending on moisture content and tensile strength. The failed block temporarily shields the dune toe before being reworked by waves (Erikson et al., 2007).
- **Infiltration-induced instability:** Repeated wave runup raises the phreatic surface, generating excess pore pressure and reducing effective stress in the sediment matrix. This internal weakening triggers slope failure, especially in partially saturated sand near field capacity (Conti et al., 2024; Palmsten and Holman, 2011).
- **Crest erosion and overtopping:** Under extreme water levels, wave runup may exceed the crest, causing erosion from the top down and accelerating landward retreat. If sustained, this can transition into breaching (Van Gent et al., 2008; Castelle et al., 2015).

- **Progressive instability from repeated slumping:** Individual slumping events rarely remove all unsupported sand. As waves continue to attack the face, new slumps occur before the profile can stabilize. This cyclical process leads to stepwise landward migration of the dune scarp and is especially evident in prolonged storm sequences (Van Wiechen et al., 2023).

These mechanisms are highly interdependent. Infiltration-driven weakening accelerates slumping, while mass failure exposes previously protected dune faces to renewed wave attack. The combined influence of these internal and external processes governs the rate of dune retreat and the total volume of sediment eroded during storm events. This integrated response forms a critical baseline for evaluating the performance of natural, hybrid, and engineered dune systems. In summary, the interaction between hydrodynamic forcing and geotechnical instability defines the dynamic behavior of coastal dunes. A comprehensive understanding of these processes is essential for predicting dune evolution and assessing coastal vulnerability in the face of rising sea levels and intensifying storm climates.

2.2. Hard structures

This section reviews the damage and failure mechanisms of hard coastal structures. Understanding these mechanisms is essential because, once the sand layer above a hybrid structure is fully eroded, the underlying hard element becomes directly exposed to incoming wave forces. These exposed structures are then vulnerable to damage and failure under hydrodynamic loading. In this section, the main damage processes and failure mechanisms affecting hard structures are discussed. Their influence on surrounding morphology, particularly in hybrid dune systems, will be addressed in Section 2.3.

2.2.1. Dike failures in hard coastal structures

Despite their robustness, hard structures such as sea dikes and seawalls are susceptible to failure under extreme hydrodynamic conditions. Failure mechanisms are typically classified into structural, geotechnical, and hydraulic categories, and often occur in combination during high-energy storm events.

A widely accepted framework for dike failure modes is summarized by the Technical Advisory Committee for Flood Defenses (TAW), as shown in Fig. 2.8. The primary failure mechanisms include wave overtopping and erosion, toe scour and undercutting, internal erosion and seepage, and slope instability or micro-instability.

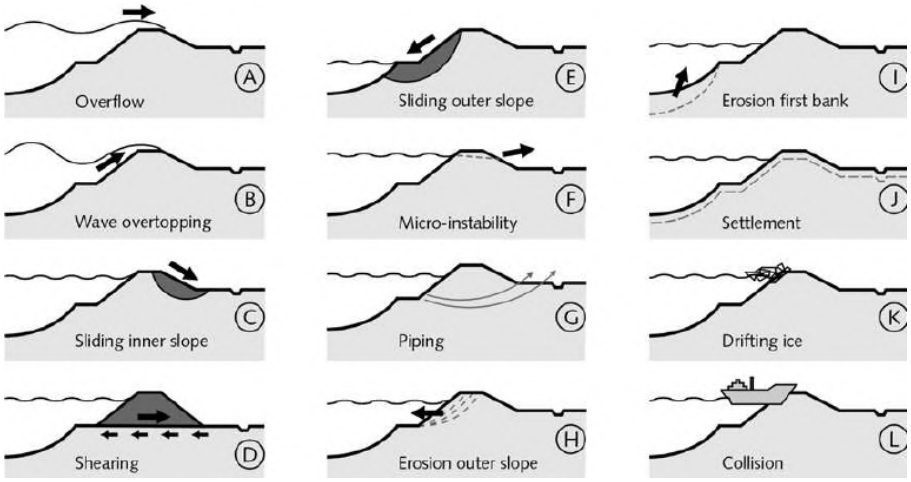

Figure 2.8: Overview of primary dike failure mechanisms, as classified by the Technical Advisory Committee for Flood Defence (TAW, 1998). The schematic highlights structural, geotechnical, and hydraulic failure modes, including overtopping, internal erosion, and slope instability.

Wave overtopping and surface erosion

Wave overtopping occurs when incident waves exceed the crest elevation of the dike, allowing water to flow over its landward slope. Repeated overtopping can lead to surface erosion, especially if protective layers (e.g., grass or asphalt) are absent or damaged. The erosive impact is magnified by wave period and storm duration(Mai et al., 2006). Thao and Tuan (2019) observed that crown walls can exacerbate overtopping-induced scour by increasing runup and backwash energy.

Toe scour and undermining

As detailed in previous section, toe scour poses a critical threat to dike stability. When sediment is removed from the base of the slope, the foundation becomes unsupported, increasing the likelihood of sliding or rotational failure. Toe scour can also contribute to indirect failure mechanisms: erosion of the foreshore increases water depth in front of the dike, allowing larger nearshore waves to develop under certain design conditions, which in turn raises the hydraulic loading on the structure (Mai et al., 2006). Experimental studies, such as Saponieri et al. (2018), have also shown that toe scour is most severe under irregular wave conditions and can evolve rapidly during the early stages of a storm.

Internal erosion and seepage

Internal erosion, or piping, occurs when water infiltrates the dike body, mobilizing fine particles and creating voids. This weakens the internal structure, potentially resulting in collapse. Seepage through the dike core can also increase pore pressure, lowering effective stress and promoting failure from within. These processes are difficult to observe directly, making early detection and monitoring essential (Schiereck and Verhagen, 2012).

Micro-instability and slope failures

Micro-instability refers to surface instabilities on the seaward or landward slope of a dike. These are often triggered by local saturation, rapid drawdown, or wave impact, and can evolve into larger slope failures under sustained loading. Such failures are especially critical for grass-covered dikes, where the loss of vegetative cover reduces shear resistance and increases vulnerability to runoff-induced erosion. While initially small, these failures can evolve under sustained loading. (Steendam et al., 2014).

Compound and progressive failure

In real-world conditions, dike failures are rarely caused by a single mechanism. For example, toe scour may trigger slope instability, which in turn may expose inner layers to wave overtopping and internal erosion. These progressive interactions highlight the importance of integrated failure analysis in the design and assessment of hard coastal structures.

2.2.2. Hard structures overview

Hard coastal structures, while robust, are vulnerable to a range of failure mechanisms under extreme wave conditions. Key processes include wave overtopping, toe scour, internal erosion, and slope instability, often acting in combination and evolving progressively during storm events. Understanding these interrelated mechanisms is critical for designing resilient structures and for assessing the performance of hybrid systems when the protective sand cover is lost.

2.3. Hybrid dunes

Hybrid coastal defense systems combine engineered core structures (e.g., rock, clay, concrete, or geotextile) with a sand cover that mimics the morphology of natural dunes. This integrated approach aims to combine the erosion resistance and structural reliability of hard infrastructure with the dynamic, wave-dissipating, and ecological benefits of sandy systems. While hybrid dunes do not fully replicate the long-term behavior of natural dunes, they represent a promising compromise between robust protection and environmental compatibility (Almarshed et al., 2020; Nordstrom, 2019; Figlus et al., 2015).

The section begins with an overview of earlier hybrid flood defence research, followed by a discussion of morphological responses around traditional sea dikes and vertical seawalls. It concludes with a summary of key design considerations and a concise closing overview.

The addition of a sacrificial sand layer atop the hard core provides several benefits. It dissipates wave energy before it reaches the core, delays core exposure, reduces direct wave-structure interaction, and can enhance aesthetics and habitat potential. This layered approach contributes to coastal resilience by attenuating erosion, limiting damage to inland infrastructure, and enabling adaptation to sea-level rise and increasing storm intensity (Almarshed et al., 2020). Field installations and laboratory studies have demonstrated that hybrid dunes can reduce total sediment loss compared to purely sandy systems, especially under moderate storm conditions. Case studies in the Netherlands and along the U.S. Atlantic coast illustrate their potential to improve flood protection and reduce damage during storm events. However, performance varies significantly depending on core type, sand cover thickness, and hydrodynamic conditions.

Despite growing interest, major knowledge gaps remain in understanding how hybrid dunes evolve over time. In particular, the interaction between wave dynamics and the sand–structure interface, the role of internal drainage and pore pressure, and the performance of various core materials under extreme loading require further investigation. Current research emphasizes the need for improved physical and numerical modeling to capture the complex morphodynamic response of hybrid dunes and to support the development of robust design criteria for site-specific applications (Almarshed et al., 2020; Figlus et al., 2015; Maximiliano-Córdova et al., 2023).

2.3.1. Hybrid dune configurations

This section reviews hybrid dune configurations evaluated in both laboratory and field studies. These designs aim to replicate the external morphology of natural dunes while incorporating structural reinforcement at the core. Core materials commonly used include armor stone, concrete (e.g., T-walls), clay, and geotextiles. Comparative studies have assessed the performance of these configurations in terms of erosion resistance, profile evolution, and failure mechanisms under storm conditions (Figlus et al., 2015; Maximiliano-Córdova et al., 2023; Nordstrom, 2019).

Armor stone embankment

Figlus et al. (2015) conducted large-scale flume experiments to assess the performance of different hybrid dunes. Their results showed that the sand cover eroded rapidly within the first 10 minutes of wave action, exposing the underlying armor layer. However, once exposed, the armor stone core significantly reduced further retreat of the dune scarp and limited overall sediment loss. Although the profile evolution resembled that of natural dunes, the presence of the armor stone provided enhanced stability, making this configuration an effective option for settings where rapid initial erosion is anticipated.

T-wall

Figlus et al. (2015) tested a T-wall embedded within a sand-covered dune, revealing a distinct erosion pattern. Wave attack concentrated at the interface between the sand and the vertical wall, accelerating sand loss in that zone. Once the sand cover was removed, the T-wall effectively halted landward dune retreat. However, significant scouring at the base of the wall raised concerns about foundation stability under prolonged wave exposure.

Clay levee

Flume tests with a clay-core hybrid dune showed rapid erosion of the overlying sand, with the clay becoming exposed after only 5 minutes (Figlus et al., 2015). Due to the smooth surface of the clay core, waves ran up with minimal energy dissipation, increasing retreat at the crest. While the clay core provided structural stability, it did not reduce wave runup or energy as effectively as coarser, rougher materials.

Geotextile tube core

Geotextile tubes (geotubes) are frequently used as artificial dune cores due to their cost-effectiveness and ease of installation. These synthetic fabric tubes are typically filled with sand or slurry and covered by a sacrificial sand layer. Harris and Ellis (2020) analyzed five geotube installations and found that while they offered initial erosion resistance and economic benefits, they also led to steeper dune slopes and narrower beaches. Beach volume decreased by an average of 23.4% landward of the core, and long-term performance required frequent reburial to maintain protection and aesthetics. Maximiliano-Córdova et al. (2023) further found that dunes with geotextile cores lost more sediment under storm conditions than those without cores. Additionally, they altered wave reflection patterns, limiting recovery and disrupting early dune formation. Despite these trade-offs, geotubes remain attractive for temporary or constrained settings, especially where visual intrusion must be minimized.

Rocky core with vegetation

Recent experiments by Maximiliano-Córdova et al. (2023) compared vegetated and non-vegetated dunes with either rocky or geotextile cores. Their results showed that vegetated dunes with rocky cores performed best across all storm intensities. The porous structure of the rock allowed better root anchoring and water retention, enhancing vegetation effectiveness. Morphodynamically, rocky cores preserved a more natural sediment exchange between the beach and dune, supporting recovery and resilience. Rocky-core dunes showed minimal alteration in erosion regime and reduced the likelihood of large-scale collapse, particularly during intense storm phases. As such, they are increasingly viewed as sustainable components of nature-based hybrid solutions, especially when paired with strategic planting.

2.3.2. Morphological response around hard structures

When the sacrificial sand layer of a hybrid flood defence is fully eroded, the underlying structure is most likely to behave like a conventional hard sea defence. Therefore, this subsection reviews the morphological response around two traditional coastal structures. It begins with previous studies on sloped sea dikes, followed by an overview of research on vertical seawalls.

Sloped sea dike

Thao and Tuan (2019) conducted wave flume experiments to investigate the role of crown walls, slope roughness, and overtopping on toe scour. Their findings show that low dikes with crown walls experienced greater scour depths compared to high dikes without crown walls, primarily due to enhanced wave reflection and increased overtopping volumes.

Scour depth was found to scale with the Iribarren number and inversely with relative water depth. Increased slope roughness mitigated scour, demonstrating the importance of surface texture in energy dissipation. Further insights were obtained from the WALOWA experiments in the Deltares Delta Flume (Saponieri et al., 2018), which studied scour development at the toe of a 1:2 sloped dike under various wave conditions, including bi-chromatic and irregular waves. The highest erosion rates occurred early in the test duration, particularly under irregular wave forcing. Scour stabilized after approximately 11 hours. Results from these tests showed a maximum laboratory scour depth of 0.3 m, equivalent to 1.3 m at full scale. The affected area extended 9 meters in front of the structure, with a mean scour depth of 0.2 m and a total eroded volume of 8 m^3.

Vertical sea wall

Laboratory experiments by Herbich et al. (1980) showed that ultimate scour depth scales with wave height, while its location is linearly related to wave length. Field studies by Kraus and McDougal (1996) found that longshore transport and return of overtopping water often dominate scour development, rather than the influence of cross-shore wave action. These results underline the need to consider both cross-shore and longshore processes in scour prediction.

Vertical seawalls reflect wave energy, intensifying sediment transport and scouring near their base. In 34 medium-scale lab tests, Sutherland et al. (2006) found that local water depth and the Iribarren number significantly influence scour depth near the seawall toe (S_t) and the maximum scour point (S_{max}). Interestingly, changing the wall slope from vertical to 1:2 had little effect, suggesting that hydrodynamics and sediment availability are more critical factors. Ruggiero and McDougal (2001) used analytical modeling to study vertical seawalls' influence on longshore transport. They found that wave reflection shifts the breaking point seaward, narrowing the surf zone and altering current intensity. Depending on seawall geometry and wave angle, longshore currents may either increase or decrease. Additionally, interactions between incident and reflected waves can generate resonance effects, leading to spatially uneven

erosion or accretion alongshore. These findings highlight the importance of accounting for longshore dynamics in hard structure design to avoid unintended morphological impacts.

2.3.3. Design considerations and trade-offs

Hybrid dunes must be designed with site-specific wave climates, sediment availability, and space constraints in mind. As noted by Nordstrom (2019) and Almarshed et al. (2020), hard cores are best placed close to infrastructure to maximize available space for natural dune morphodynamics on the seaward side. Additionally, periodic sand nourishment and reburial are essential maintenance practices for most hybrid systems, particularly those using geotextile or clay cores.

While no hybrid solution fully replicates the adaptive capacity of natural dunes, combining hard cores with ecological design elements, such as vegetation and aeolian transport pathways, can enhance performance and sustainability. Trade-offs remain between protection efficiency, maintenance needs, ecological impact, and aesthetic considerations, which must be balanced in the selection of core materials and structural layouts.

2.3.4. Hybrid dune overview

Hybrid dunes combine engineered cores (e.g., rock, concrete, clay, or geotextiles) with a sacrificial sand cover to merge the structural robustness of hard coastal defenses with the dynamic, wave-dissipating behavior of natural dunes. While the sand layer typically erodes early during storm events, the core beneath serves to limit further retreat and provides essential structural stability. Among the different configurations, vegetated rocky cores and armor stone embankments perform most effectively, preserving dune shape and supporting ecological recovery after storms. T-walls and clay cores can resist landward erosion but often accelerate local scouring or enhance wave runup. Geotextile cores are a low-cost and flexible solution, but they tend to steepen beach profiles and narrow the active zone, requiring more frequent reburial and maintenance. Once the protective sand cover is lost, hybrid dunes begin to behave like hard structures, with increased wave reflection, localized scour, and altered sediment transport. This transition underscores the need for hybrid dune designs to consider both the covered and exposed states, accounting not only for physical stability but also for maintenance, visual impact, and ecological performance.

Understanding this complex behavior is central to the Hybrid-Dune Project, which investigates how hybrid dunes respond to wave forcing in both laboratory and field settings. By measuring hydrodynamics, sediment transport, and structural exposure over time, the project provides needed insight into the processes that govern hybrid dune evolution and failure. These measurements aim to inform improved modelling and design guidance. In summary, hybrid dunes combine the soft, adaptive characteristics of sand with the durability of hard structural cores. This dual nature offers improved storm resilience while also creating space for nature, recreation, and landscape integration. However, their morphological behavior, particularly the dynamics of erosion, recovery, and sediment redistribution, remains insufficiently understood. Bridging this knowledge gap is essential for the successful implementation and long-term performance of hybrid dune systems.

3

Methodology: Data paper

Field Measurements of Erosion and Hydrodynamics at Dune-Dike Infrastructure

D.W. Poppema, S. De Vries, R.G.C. Rosman, J.W. Mol, S. Pluis, A. Antonini

June 2025

Note to the reader:
The experimental setup and collected dataset described in this chapter have been structured as a self-contained data paper. This format ensures reproducibility, transparency, and accessibility of the research. A standalone version of the data paper is currently being prepared for separate publication.

Contribution of authors:
This draft of the data paper was written by R.G.C. Rosman under the supervision of D.W. Poppema, S. De Vries, and A. Antonini. R.G.C. Rosman was responsible for the full structure and content of the manuscript, based on the template provided by the journal Nature `https://www.nature.com/sdata/submission-guidelines`. D.W. Poppema contributed to final editing and provided feedback on the abstract, introduction, instrumentation, and overall clarity of the manuscript.

3.1. Abstract

To study the interactions between sandy dunes and hard coastal structures, a 100-metre-long test dune was constructed just above the high-water line at the Sand Motor near Kijkduin, the Netherlands. Four different cross sections were constructed to compare the hydrodynamics and erosion under storm conditions: a sandy dune, a dike-in-dune, a seawall-in-dune, and a dike. This dataset contains the observed hydro- and morphodynamics between December 18, 2024, and January 8, 2025, when substantial dune erosion occurred from five subsequent storms. The morphodynamic data contains continuous measurements of the dune face during storms by a multi-line lidar scanner at each of the four cross sections, as well as bathymetric and topographic surveys and optical backscatter sensor data in the surfzone. The hydrodynamic data include pressure sensor and velocimeter data at four cross-shore transects, offshore wave conditions, and pressures observed at the hard constructions (wall, revetments) for wave impact and soil pore pressure analysis. This dataset can be used to A) study cross-shore and alongshore hydromorphodynamic processes that occur at the beach-dune interface during storms and B) to improve or validate the implementation of hard elements in dune erosion models.

3.2. Background & summary

Hybrid dunes, also known as hybrid flood defenses, integrate hard engineering elements with natural sandy dunes. This enables them to combine the erosion resistance of traditional hard defenses with the ecological and recreational functions and natural growth capabilities of natural dunes (Almarshed et al., 2020). The concept of hybrid dunes has gained significant attention in coastal protection strategies, with successful implementations in, for instance, the Netherlands (e.g. the dike-in-dune protection at Katwijk), Australia (the partially buried seawall in Gold Coast, Queensland), and the USA (the buried seawall at Dam Neck, Virginia). However, despite their growing adoption, the fundamental understanding of their morphological response to extreme hydrodynamic forcing remains incomplete.

Especially, the interaction between their soft and hard components is not yet fully understood. Incorporating hard structures within dunes significantly alters the hydrodynamics and sediment dynamics, by changing wave reflection and runup, sediment availability, and soil permeability. Wave reflection against hard structures can induce localized toe scour (**?**Dette et al., 2002) and affect foreshore development. Previous wave basin experiments (Boers et al., 2011; Van Geer et al., 2009) showed that revetments embedded within dunes can locally intensify erosion at the transition from hard elements to neighbouring sandy dune.

Due to the complex interplay between sandy and hard elements, it remains a challenge to accurately assess the flood safety of existing hybrid dunes or effectively design new hybrid dune projects. The Hybrid Dune experiment aims to address these knowledge gaps by simultaneously measuring dune morphology, hydrodynamic forcing, and sediment transport processes at a hybrid dune test setup in the field. This experiment involved the construction of a 100-metres-long test dune just above the high-water line at the Sand Motor. The dune contained four distinct cross-sections, each representing different (hybrid) dune typologies commonly found in engineered and natural coastal systems. Methodologically, this can be regarded as a follow-up to the RealDune-REFLEX experiment (Van Wiechen et al., 2024b), both with prototype-scale sand dunes tested in-situ at the beach, but now including various hard dike elements in four different cross sections:

- Section 1: A dike-in-dune section, containing a buried hard revetment within the dune
- Section 2: A fully sandy dune, as a control case
- Section 3: A dike, with an exposed revetment slope
- Section 4: A wall-in-dune, with an unerodable vertical structure embedded within the dune

This dataset presents the beach-dune evolution and hydrodynamics during storms at the setup, as observed during the winter of 2024-2025. The concurrent high-resolution observations of hydrodynamics, sediment transport, morphological evolution of the dune and foreshore, and wave load on the structures enable researchers to analyze key coastal morphodynamic processes and assess the stability of (hybrid) dunes in response to varying hydrodynamic forcing conditions.

3.3. Methods

This section provides a detailed overview of the data collection procedures employed during the field experiment. It outlines the site characteristics, dune configurations, instrumentation layout, and measurement protocols. The experimental setup is documented to ensure transparency, reproducibility, and clarity for future users of the dataset.

3.3.1. Design setup and dune sections

The experiment took place at the Sand Motor near Kijkduin, the Netherlands. An artificial hybrid dune, approximately 100 meters in length, was constructed just above the high-water line to study the response of hybrid dune configurations to storms. Four distinct cross sections, each 24 to 30 m wide, were compared in the test dune (Figure 3.1, 3.2, and 3.3) 1) A hybrid dike-in-dune section, with a concrete revetment slope buried under the sand; 2) a classical sand dune section as baseline; 3) a dike, with an exposed revetment slope; and 4) a wall-in-dune, with a vertical sea wall made from shipping containers placed within the dune. The (initial) outline of the test setup was alongshore uniform, except that the dike section (S3) was placed 3.7 m landwards, aligning the revetment of S1 and S3. The revetments are made from concrete 2×2 m tiles, placed directly on the sand. The toe of the dune, i.e., the (initial) intersection of the dune slope with the beach, was at 2 m NAP. At the toe of the hard elements (concrete tiles resp. containers), scour protection was added in the form of wooden sheet piling covered with geotextile, to prevent toe erosion.

The sediment composition of the Sand motor was analysed in the laboratory facilities of Utrecht University. Sieving results classified the sediment as slightly gravelly sand, with a gravel content of 0.2% and a sand content of 99.8% and a grain size distribution of $D_{10} = 236.0$ μm, $D_{25} = 287.3$ μm, $D_{50} = 362.3$ μm, $D_{75} = 443.0$ μm, and $D_{90} = 557.6$ μm (Van Wiechen et al., 2024b).

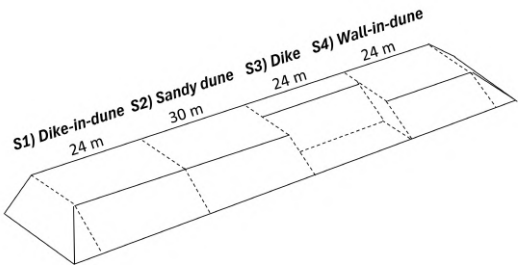

Figure 3.1: Schematic overview of the Hybrid Dune setup

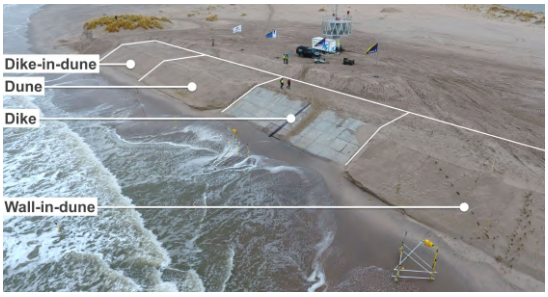

Figure 3.2: The test setup overlaid on an aerial photograph

The measurement setup was designed to capture both hydrodynamic conditions and morphological changes in the dune and foreshore. A combination of in-situ sensors, remote sensing equipment, and periodic surveys was employed across the study area.

Each cross-section was instrumented with:

- Acoustic Doppler Velocimeters (ADV) with connected Optical Backscatter Sensors (OBS) to measure water velocity and suspended sediment concentrations.
- Pressure sensors to monitor water level fluctuations due to waves and tides.
- LiDAR scanners to track dune profile changes and assess local wave conditions.
- GoPro cameras to visually capture dune evolution and wave impacts over time.

Additional instruments were deployed in hybrid and hard dune cross-sections:

- Pressure sensor arrays at the sand-hard structure interface to measure pore pressure variations and wave impact forces.
- Echo sounders to monitor scour development at the base of the hard structures.

Two Acoustic Doppler Current Profilers (ADCPs) were installed offshore to measure incoming wave characteristics. Additionally, RTK-GPS and LiDAR drone surveys were conducted periodically to track dune erosion and foreshore evolution. More details of the instruments and settings can be found in section 3.3.3.

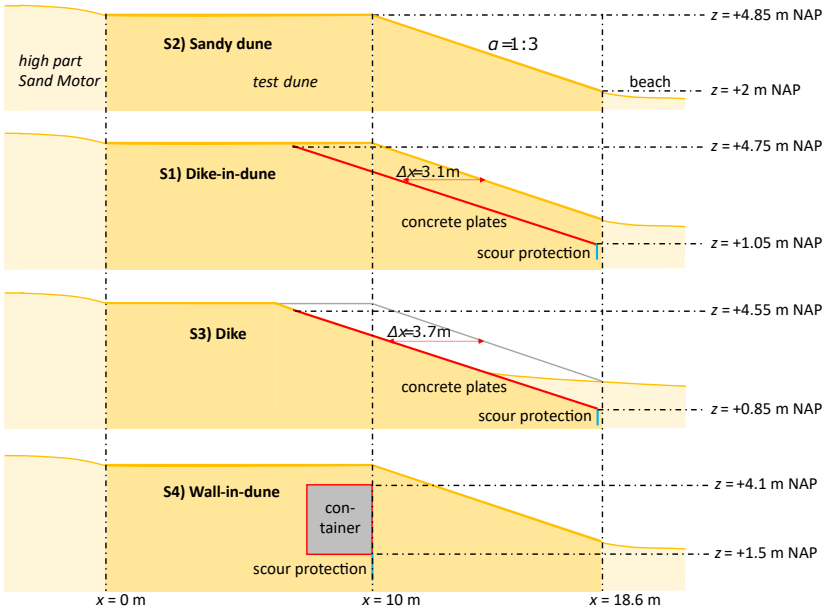

Figure 3.3: Overview of the four tested hybrid dune cross-sections

3.3.2. Deployments and storm events

Figure 3.4 provides an overview of the instruments used during the experiment. A combination of permanent and event-based sensor deployments was employed. LiDAR scanners and GoPro cameras were activated only during storm events, while most other sensors operated semi-continuously. The instrumentation setup varied slightly between storm events.

In total, five storm events were recorded during the field campaign: two occurred between *19–22 December 2024*, and three between *1–7 January 2025*. Figure 3.5 provides an overview of the experiment timeline, from construction through to completion, with the storm periods indicated. A more detailed summary of instrument deployments and corresponding nearshore wave conditions, measured by pressure sensor S3.P3, is shown in Figure 3.7. This figure includes time series of water level, significant wave height (H_{m0}), wind-wave and infragravity components of significant wave height ($H_{m0,ww}$ and $H_{m0,Ig}$ respectively), and peak wave period (T_p), displayed above the deployment intervals of each instrument. Wave data were collected using pressure sensors (RBR and OSSI), and velocity measurements were obtained from ADVs and ADCPs during the extended offshore monitoring periods: *17–23 December* and *31 December–13 January*. LiDAR scanners were deployed during each storm event, as indicated in the lower panel of Figure 3.7.

A summary of the five recorded storm events is provided below, and an overview can be seen in Table 3.1. All wave parameters referenced were derived from nearshore conditions measured by S3.P3, the most seaward pressure sensor in the S3:Dike array. This instrument was installed 0.4 m above the bed, at a bed elevation (z_b) of −1.2 m NAP and a sensor elevation (z_i) of −0.70 m NAP. The processing of the raw pressure signal into wave parameters, including water depth (h), significant wave height (H_{m0}), and peak wave period (T_p), is described in Section 3.5.1. All storm events were classified within the collision regime (Regime 2).

- **Storm 1** (*2024-12-19 00:00 – 2024-12-20 00:00*): The first storm of the experiment featured two high tides (numbered 1.a and 1.b) at 1.85 m and 2.05 m NAP, with moderate to high nearshore wave conditions. The significant wave heights at the peaks of the high tides were approximately 1.42 m and 2.12 m, respectively, with peak wave periods of 6.0 s and 7.5 s.
- **Storm 2** (*2024-12-22 02:00 – 2024-12-23 02:00*): Occurring just two days after Storm 1, this event included two high tides at 1.99 m and 1.75 m NAP. The corresponding nearshore significant wave heights were approximately 1.94 m and 1.92 m, with peak periods of 7.5 s and 8.6 s.
- **Storm 3** (*2025-01-01 11:00 – 2025-01-02 12:00*): Following eight days of relatively calm conditions, Storm 3 lasted two tidal cycles, with peak water levels at 1.86 m and 1.69 m NAP. The significant wave heights were 1.96 m and 1.71 m, with associated peak periods of 8.6 s and 7.5 s.

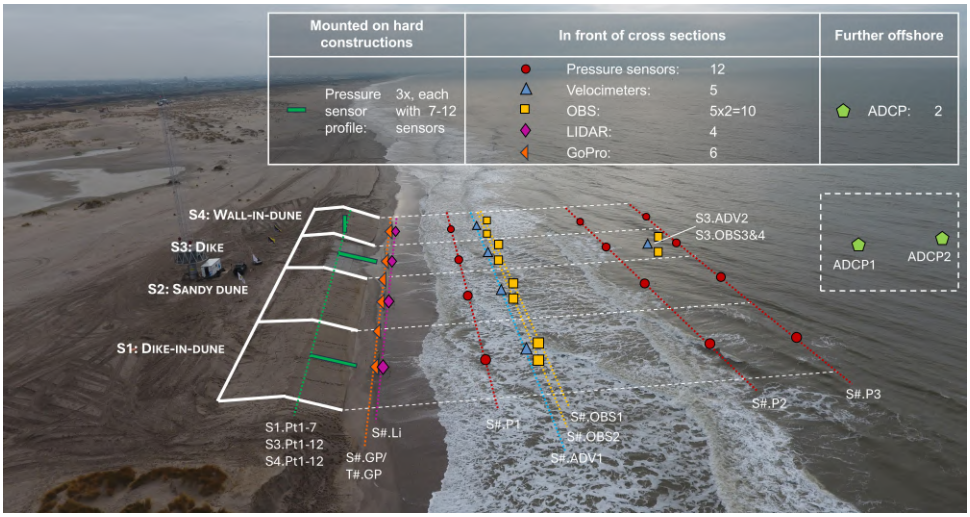

Figure 3.4: Overview of deployed instruments, indicated on an aerial photo of the setup. NB: The ADCP locations are in reality approximately 2.7 and 1.2 km offshore.

- **Storm 4** (*2025-01-03 12:00 – 2025-01-03 23:59*): This short, unexpected storm occurred shortly after Storm 3. A single high-water of 1.99 m NAP was observed, with a peak significant wave height of 2.24 m and a peak period of 10.0 s.
- **Storm 5** (*2025-01-06 12:00 – 2025-01-07 14:00*): The final storm of the campaign included two high-waters at 1.90 m and 1.75 m NAP. The corresponding significant wave heights were 1.89 m and 1.78 m, with peak periods of 7.5 s and 8.6 s, respectively.

Table 3.1: Measured wave characteristics from the S3.P3 RBR pressure sensor. Hydrodynamic conditions are reported per high tide, indicated with postscripts '.a' and '.b' for storms that lasted multiple tidal cycles.

Storm	1.a	1.b	2.a	2.b	3.a	3.b	4	5.a	5.b
η [m + NAP]	1.85	2.05	1.99	1.75	1.86	1.69	1.99	1.90	1.75
H_{m0} [m]	1.42	2.12	1.94	1.92	1.96	1.71	2.24	1.89	1.78
T_p [s]	6.0	7.5	7.5	8.6	8.6	7.5	10.0	7.5	8.6

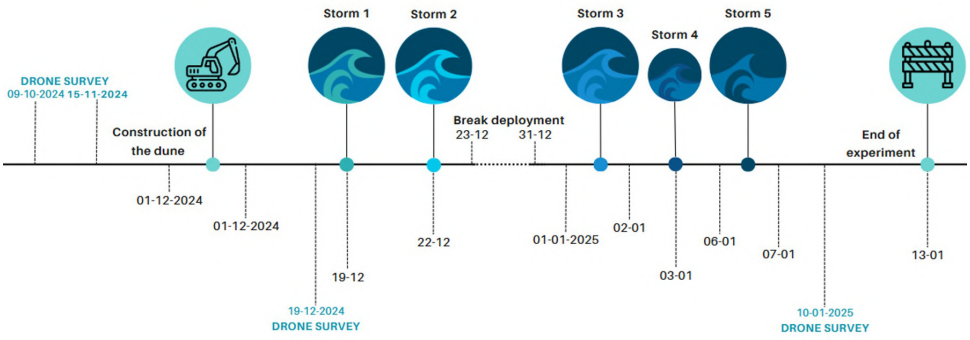

Figure 3.5: Timeline of the experiment, with the dune construction, storms, and instrument deployment

All four LiDAR scanners and all six GoPro cameras were deployed during the first three storms. They were not operational during the fourth storm. For the fifth storm, they were reinstalled only at the dune section (S2) and wall-in-dune section (S4), as the dike and dike-in-dune sections (S1 and S3) had failed already. All pressure sensors (12), ADVs (5), and OBS sensors (10) were deployed during the first and second storms to provide a comprehensive view of cross-shore and alongshore hydrodynamics. These sensors were temporarily removed during the calm period between Storms 2 and 3 to allow for data retrieval and battery replacement. A subset of the instruments was re-deployed for the final three storms (for details, see Figure 3.7). The high-frequency (10–1000 Hz) pressure sensor arrays installed on the hard structures recorded data throughout the first three storms. During the fourth and fifth storms, these arrays were primarily active at the wall-in-dune section (S4), as other hard sections had sustained too much structural damage to maintain sensor operation.

In addition to the fixed sensors, two ADCPs were installed offshore to continuously monitor incoming wave conditions at depths of −13m NAP and −11m NAP, located 2.7 km and 1.2 km offshore, respectively. LiDAR drone surveys were conducted at the start and end of the campaign to capture the initial and final morphology of the beach-dune area. RTK-GPS was used for regular topographic surveys, inclusing beach profiles and surveys of the dune toe. Echo sounders were installed in front of hard structures to monitor real-time scour development during storm events. Fig. 3.7 summarizes the instrument deployment schedule, indicating the operational periods of each sensor type in relation to the storm events. Fig. 3.6 shows the offshore wave conditions during Storms 1 and 2, as recorded at the Hollandse Kust West Zuid (HKWZ) wind farm, approximately 18 km offshore. The waves predominantly came from directions between southwest and northwest. No wave data were available for Storm 3. As the waves approach the coast, they undergo shoaling and refraction, which typically reorient them to a more shore-normal direction relative to the coastline.

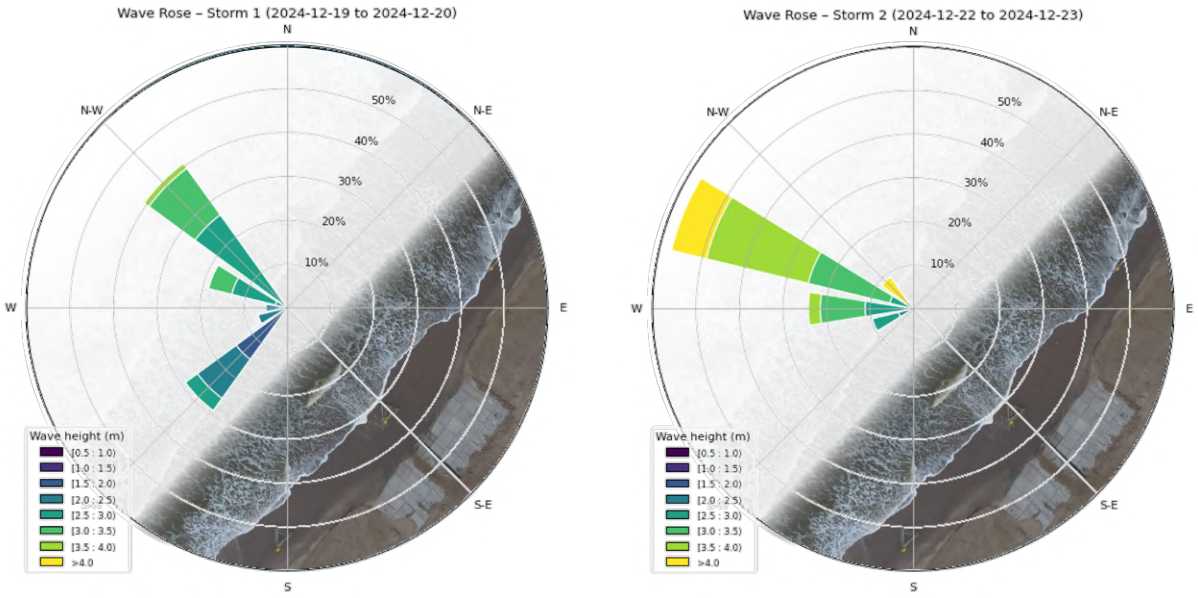

Storm 1 Storm 2

Figure 3.6: Windrose plots of Storm 1 (left) and Storm 2 (right). Each plot shows wind direction and magnitude distribution during the respective storm.

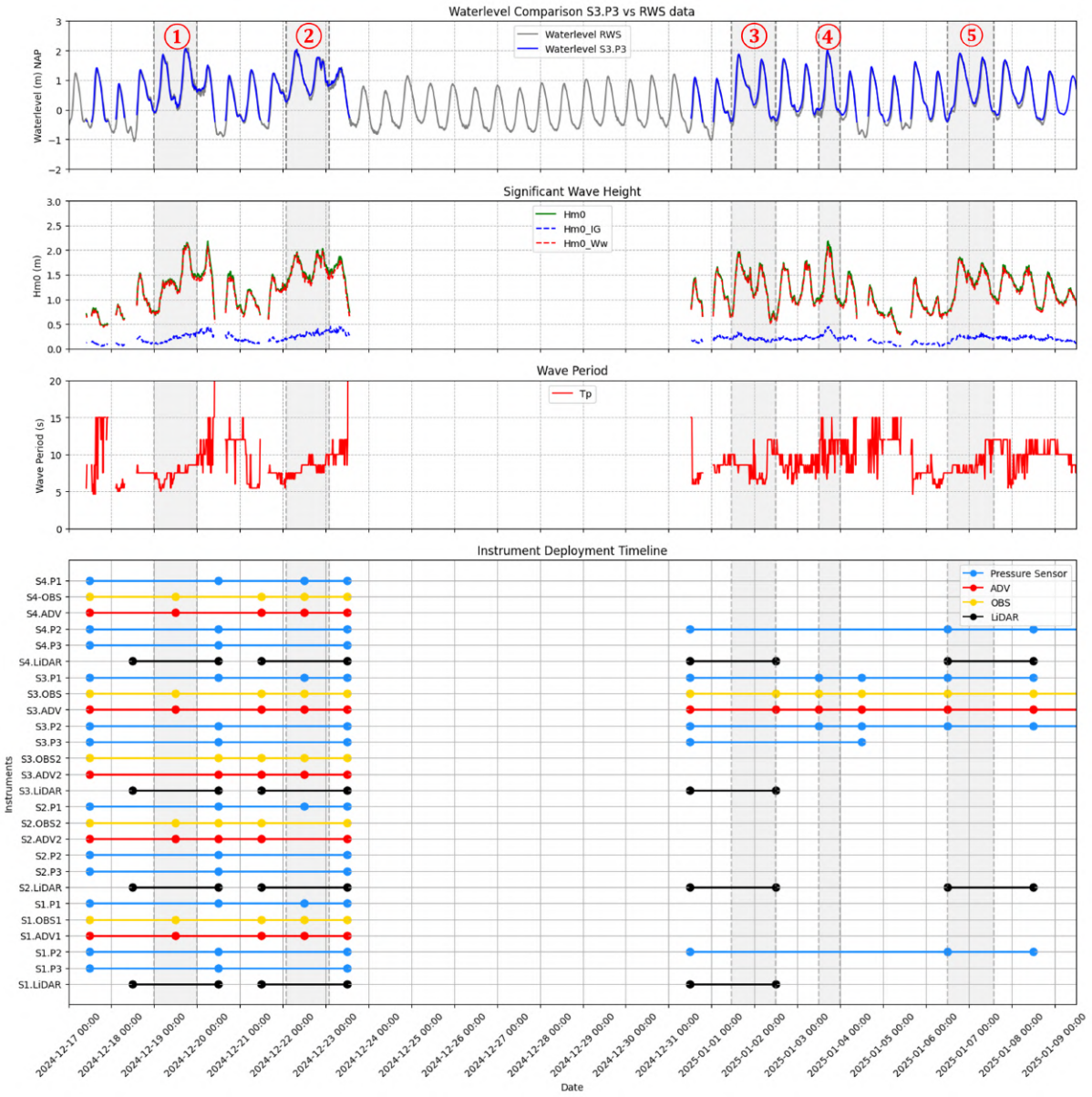

Figure 3.7: Overview of storm conditions and instrument deployment during the hybrid dune field campaign. **Top panel:** Water levels (in m +NAP), with data from the RWS gauge at Scheveningen (gray line) and the pressure sensor 80 m in front of the dune (S3.P3-RBR06) (blue line). **Second panel:** Significant wave heights measured at S3.P3-RBR06, including the full spectrum (H_{m0}), wind-wave component ($H_{m0,Ww}$), and infragravity component ($H_{m0,IG}$). **Third panel:** Peak wave period (T_p) at S3.P3-RBR06. **Bottom panel:** Instrument deployment timeline, showing frame positions (left axis) and deployment periods (colored lines) over time (x-axis). Dots indicate adjustment or maintenance actions on the instruments. LiDAR drone survey periods are not shown, as most flights occurred outside the depicted timeframe (Fig. 3.5).

3.3.3. Instrumentation

This section provides a detailed overview of the instrumentation deployed during the Hybrid Dune field campaign. A diverse set of sensors was used to monitor hydrodynamic forcing and morphological change across (hybrid) dune profiles. The deployed instruments include pressure sensors (from RBR and OSSI), acoustic Doppler velocimeters (ADVs), optical backscatter sensors (OBS), acoustic Doppler current profilers (ADCPs), and LiDAR scanners. Each instrument was strategically placed to capture cross-shore and alongshore variability in wave conditions, sediment transport, and topographic change. The following subsections describe the sensor types, deployment configurations, measurement settings, and operational periods for each system.

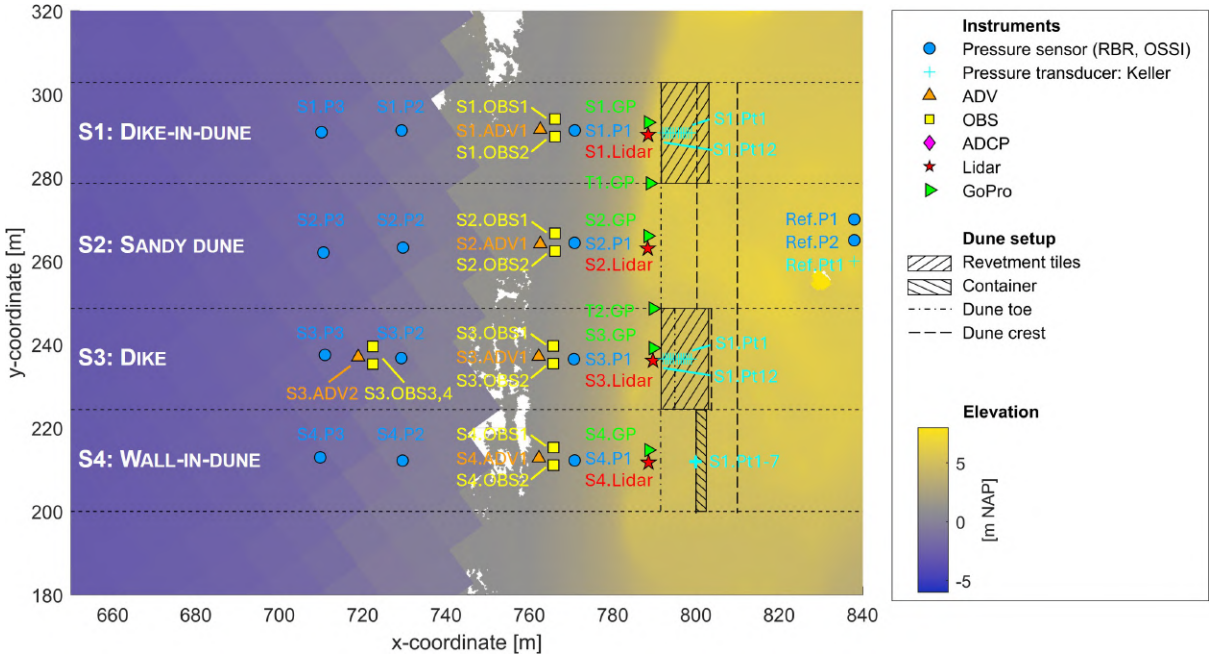

Figure 3.8: Plan view of the hybrid test dune and instrumentation.

Intertidal pressure sensors

Pressure sensors were used to record wave field characteristics and water levels, enabling the derivation of key hydrodynamic parameters such as significant wave height, wave period, and storm surge elevation. Three types of pressure sensors were used: OSSI Wave Gauges with a frequency of 20 Hz, and RBRsolo8 and RBRsolo16 pressure loggers with frequencies of 8 and 16 Hz. Sensors were mounted on poles, spread throughout the intertidal area to capture spatial variations in water depth. They were installed approximately 40 cm above the bed level and were checked and adjusted during field visits to maintain proper elevation. Exact sensor deployment per pole varied between the first and second deployment (Table 3.2). As a reference, one sensor of each type measuring atmospheric pressure was installed on the dry beach landward of the setup (above 6 m NAP).

Table 3.2: Pressure sensors deployed during the first deployment (first two storms) and second (mostly storm 3-5)

Instrument type	First deployment	Second deployment
OSSI	8, at S1.P1-S4.P1; S2.P2-S4.P2; ref.P1	0
RBRsolo8	4, at S2.P3; S4.P2; S1.P2; ref.P2	4, at S1.P2; S3.P2; S4.P2; ref.P2
RBRsolo16	2, at S1.P3; S3.P3	2, at S3.P1; S3.P3

Calibration of all sensors was conducted before and after deployment by submerging the sensors in known water depths to correct for any factory offset. This procedure provided a reliable time-stamped reference in the dataset to verify pressure accuracy and ensure consistency across instruments.

Pressure sensors on hard constructions

In the hybrid and hard dune sections, high-frequency Keller pressure transducers were installed at the sand–structure interface to monitor dynamic pressure variations during wave impact. These sensors are essential for evaluating wave loading on the structures and identifying potential failure mechanisms, such as slumping, local scour, or pore pressure buildup. The sensors, type 36XW, had a range of 0.8-2 bar absolute pressure, so approximately 0-10 m water depth. Their factory accuracy is 0.15% of their full range (i.e. ± 1.8 cm water depth). They were connected via cables to a central data logger housed in a mobile lab positioned on elevated ground behind the experimental site. De analog 4-20 mA signal was digitized using two 16-channel USB DAQs from MCC (type USB-1608G). This setup allowed for real-time monitoring and data acquisition during storm events. The sensors operated at sampling frequencies of 1000 Hz during storms, and 10 Hz in between storms.

To ensure accurate measurements, each sensor was housed in a protective casing designed to prevent sediment burial and mechanical damage. For the dike-in-dune (S1) and dike (S3) sections, the sensor housings were mounted flush with the concrete surface in the middle of each cross section. At the wall-in-dune section (S4), the sensor casing was vertically mounted between two adjacent sea containers, aligned with the centerline of the section. One reference sensor was installed landward of the setup to measure atmospheric pressure. Photographic documentation of the sensor mounting and setup is shown in Figure 3.9.

Figure 3.9: (a) and (b) Installation of Keller pressure sensors at Section S1, mounted flush between the concrete panels of the dike-in-dune. (c) and (d) Placement of Keller pressure sensors at Section S4, positioned vertically between two sea containers in the wall-in-dune setup.

Acoustic Doppler Velocimeter (ADV)

The Acoustic Doppler Velocimeter (ADV) measures three-dimensional water velocity using the Doppler shift principle. It emits short bursts of acoustic pulses that scatter off suspended particles in the water. By analyzing the frequency shift of the returning signal, the instrument calculates instantaneous velocity components in the x, y, and z directions. This makes the ADV especially suited for studying turbulence, sediment transport, and wave-induced currents in the swash and surf zones.

In this study, ADVs (Nortek Vector Acoustic Doppler Velocimeters) were deployed within the swash zone to capture near-bed velocity fluctuations under storm and non-storm conditions. Every dune section contained an ADV 20 m in front of the dune toe for alongshore comparison of the waves attacking the dune (S#.ADV1 in Figure 3.8). A fifth ADV was installed 60 m in front of the dike to measure cross-shore wave evolution (S3.ADV2). Each ADV was mounted on a stable seabed frame, with the measurement volume positioned approximately 20 cm above the bed. To ensure data quality, the frame elevations were periodically verified and adjusted, and any instrument tilt or displacement was documented. Each ADV was connected to two Optical Backscatter Sensors (OBSs), positioned at different elevations on the same frame. These paired measurements allowed for the simultaneous recording of velocity and turbidity, enabling the estimation of sediment transport rates. The ADVs operated with a sampling frequency of 8 Hz, configured in burst mode. Each burst lasted 3,590 seconds (approximately one hour), capturing 28,720 samples per burst. The burst interval was set to 3600 seconds, resulting in near-continuous coverage.

Optical Backscatter Sensor (OBS)

The Optical Backscatter Sensor (OBS) measures turbidity by detecting the amount of light scattered by suspended sediment particles in the water column. The sensor emits infrared light and quantifies the intensity of the backscattered signal, which correlates with sediment concentration. This information is essential for understanding sediment suspension, resuspension, and transport processes relevant to dune erosion. OBS sensors (8Hz) were co-located with the ADV units and mounted on the same seabed frames. Each ADV frame included two OBS's: one positioned at 15 cm and the other at 25 cm above the bed. This dual-sensor setup enabled the capture of vertical gradients in sediment concentration. Two different types of OBS sensor were used: Cambell OBS3+ for the eight sensors in front of the

dune toe (S1.OBS1-S4.OBS2 in Figure 3.8), and Seapoint STM for the two more offshore (S3.OBS3 and S3.OBS4). Calibration of the OBS sensors was performed after the deployment using sediment samples from the field site to develop site-specific turbidity-to-concentration relationships. This ensured accurate conversion of voltage signals to sediment concentrations during post-processing.

Acoustic Doppler Current Profiler (ADCP)

The Acoustic Doppler Current Profilers (ADCP) captured offshore hydrodynamic conditions over the water depth at 2.7 and 1.2 km offshore, to monitor wave transformation as waves approached the dune system. ADCPs operate by emitting acoustic pulses into the water column, which reflect off suspended particles. By analyzing the frequency shift (Doppler effect) of the returning echoes, the ADCP provides vertical profiles of current velocities across multiple depth layers. Both ADCPs were Teledyne Workhorse 1200 kHz upward-looking models. They recorded in a 2-hour measurement cycle, consisting of a 1-hour burst of 7200 samples at 2 Hz. Further deployment details can be found in Table 3.3. Due to sediment burial, only a subset of the data was deemed valid for analysis, especially in case of ADCP2.

Table 3.3: ADCP locations and main settings

	ADCP 1	**ADCP 1**
Deployment depth [m NAP]	-13	-11
Offshore distance [km]	2.7	1.2
Operating period	17-12-2024 14:00 to 22-12-2024 13:59; 03-01-2025 16:00 to 21-01-2025 09:59	17-12-2024 14:00 to 20-12-2024 05:59
Vertical resolution	30 vertical depth cells with a resolution of 0.70 m, starting 1.46 m above the transducer.	50 vertical depth cells with a resolution of 0.35 m, starting 0.78 m above the transducer.

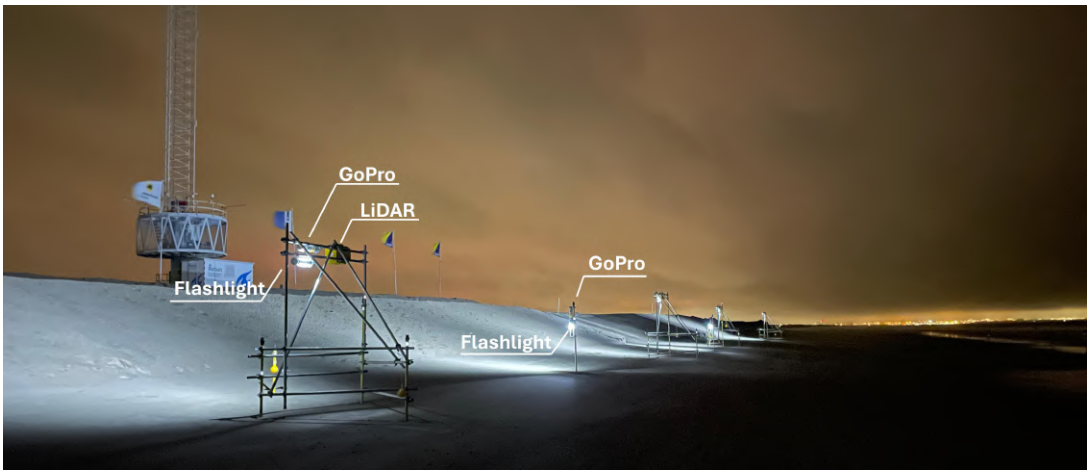

Figure 3.10: Overview of a GoPro and flashlight mounted on a LiDAR frame and in front of the hybrid dune transitions (S1-S2) and (S2-S3).

LiDAR Scanner

LiDAR (Light Detection and Ranging) technology was employed to create high-resolution digital elevation models of the study area. The system works by emitting laser pulses from the scanner and measuring the time it takes for the pulses to reflect off the surface and return. By dividing this time delay by the speed of light, the distance is calculated, generating a detailed 3D point cloud of the terrain.

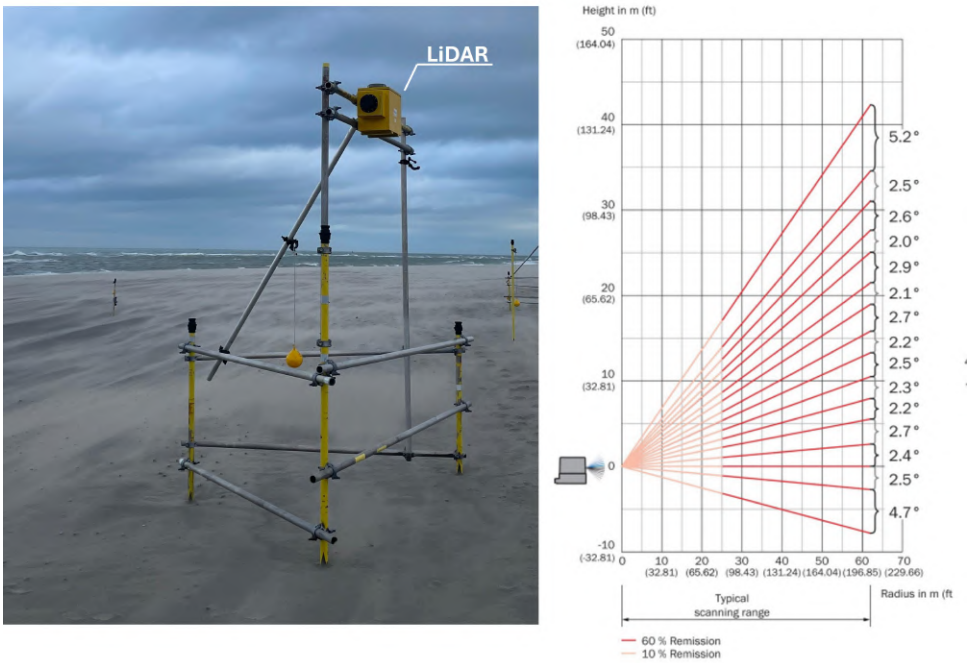

Figure 3.11: LiDAR frame setup and scanning geometry of the SICK Multiscan 165, showing its working range and angular scanning pattern. Figure adapted from SICK product documentation.

SICK Multiscan 165 LiDAR devices were positioned in front of each cross-section at a 90-degree angle to scan segments perpendicular to the dune face. They were only operational during storms. The scanners were mounted on fixed frames to ensure stability and minimize movement errors, placed at around 4.5 m NAP elevation and roughly 2.5 m above the bed level, depending on the beach state. They operated at a frequency of 4 Hz, continuously monitoring dune changes during deployment. At low tide, the LiDAR captured the exposed bed profile, while at high tide, it also recorded wave characteristics. By selectively sampling the LiDAR data, the bed level during high water, incoming bore height, and the upper part of the swash oscillation can be determined. The LiDAR sends out laser signals in 16 transects at various (horizontal) angles (Figure 3.11), vertically covering 360° around the scanner puck with 0.5° angular resolution. The scanned area becomes wider with increasing distance from the scanner, meaning the exact distance between lines depends on the horizontal distance from the scanner, making it vary over time with changing bed and water levels.

GoPro Cameras

GoPro cameras were installed to provide visual documentation of dune erosion processes and wave dynamics. The cameras (model GoPro Hero10) captured two images per second, which were compiled into timelapse videos at 30 frames per second. They were all oriented toward the dune for a clear view of wave runup and sediment dynamics, allowing for the visual identification of scarp retreat, sediment slumping, and wave impacts. The cameras were mounted a few metres in front of the (initial) dune toe: four at fixed positions on each LiDAR frame and two at the transition between S1–S2 (Dike-in-dune – Sandy dune) resp. S2–S3 (Sandy dune – Dike), see Figure 3.8. They were positioned approximately 2.5 m above the bed level on the LiDAR frames, and around 2.0 m above the bed level in front of the dune transitions. Each unit was equipped with a light sensor-triggered flashlight to ensure nighttime visibility (Figure 3.10).

LiDAR Drone

A LiDAR-equipped drone was periodically deployed to perform high-resolution topographic surveys of the study area (DJI Matrice 300RTK drone with Yelloscan Mapper+). The drone captured large-scale elevation changes, enabling precise monitoring of dune erosion. The drone surveys were conducted under calm weather conditions to minimize disturbances from wind and precipitation. Flight paths were pre-programmed to ensure consistent coverage of the dune system. The drone's LiDAR sensor operated at a high scan frequency, producing dense point cloud data with centimeter-scale accuracy. Post-processing included filtering out non-ground returns such as vegetation and wave reflections to generate accurate digital terrain models.

The drone-based LiDAR surveys were performed on the following dates:

- 15 November 2024
- 19 December 2024
- 10 January 2025

Real-Time Kinematic GPS (RTK-GPS)
Real-Time Kinematic GPS was used for high-precision topographic mapping. With centimeter-level accuracy, RTK-GPS was employed to track sensor locations and measure beach profiles, dune toe elevation and dune morphology over time. Data collection was conducted during low tide to maximize beach coverage.

3.4. Data records

All the data can be downloaded with the following link **link to repository**. The repository contains the following datasets:

- Lidar data, converted to netCDF file (with local coordinate system as well as RD)
- Pressure signal: Raw data and filtered & processed
- Adv signal: Raw data and filtered & processed
- OBS: Raw data with calibration files
- Echo sounder: Raw data and filtered & processed
- ADCP: Data processed by RWS

3.5. Data processing

This section outlines the data processing procedures applied to the LiDAR and pressure sensor datasets. The section begins with the processing of the pressure sensor data, detailing the filtering steps followed by the reconstruction of surface elevation and wave parameters. Next, the LiDAR data processing is described, including the transformation of measurement points to the Dutch RD coordinate system and filtering to remove unintended reflections. Other sensors referenced in this data paper, such as ADVs, ADCPs, and OBS sensors, are not included here, as their data are still undergoing validation and post-processing. Preliminary steps have been completed, but full processing will be continued.

3.5.1. Pressure sensors: Data Processing

Several steps were applied to process and filter the raw pressure data collected from the sensors:

1. **Atmospheric Pressure Correction:** The raw pressure signal was corrected for atmospheric pressure variations using data from the KNMI measurement station at Hoek van Holland.
2. **Burst Segmentation:** The continuous pressure signal was divided into 20-minute bursts, which served as the basic units for all subsequent processing steps.
3. **Dry Sensor Detection and Removal:** To exclude periods when sensors may have been exposed above the water surface, all individual relative pressure readings below 3 kPa (approximately 0.3 m water depth) were removed. In addition, entire bursts were excluded if the standard deviation of the pressure signal within the burst was less than 70 Pa, indicating likely dry conditions.
4. **Outlier Removal:** A statistical filter was applied to remove outliers. Pressure values falling outside the range $\mu \pm 3\sigma$ were identified as outliers and excluded. Missing values resulting from this filtering were then linearly interpolated.
5. **Bandpass Filtering:** A bandpass filter was applied to retain wave-relevant pressure fluctuations while removing low-frequency tidal trends and high-frequency noise. The filter passed signals within the frequency range of 0.004 to 1.5 Hz, isolating infragravity and wind-wave components.

This multi-step approach enhances data accuracy and ensures that only relevant hydrodynamic signals are retained for further analysis.

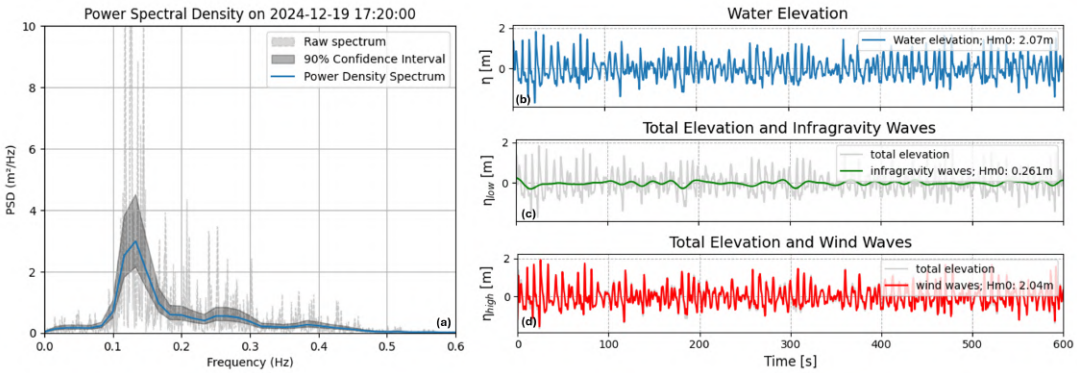

Figure 3.12: Surface elevation time series and corresponding spectral analysis for the second high-water event of Storm 2 (High water 2.b). The left panel shows the power spectral density (PSD) of the full surface elevation signal, highlighting the dominant energy contributions across the frequency range. The right panel presents the reconstructed surface elevations from the full wave spectrum (blue), the infragravity band (0.004–0.05 Hz, green), and the wind-wave band (0.05–1.5 Hz, red).

Following initial filtering, the pressure signal was analyzed across three frequency bands:

- Low frequency (0.004–0.05 Hz): Infragravity waves
- High frequency (0.05–1.5 Hz): Wind waves
- Full spectrum (0.004–1.5 Hz): Infragravity + wind waves

For each of these bands, surface elevation was reconstructed from the subsurface pressure signal using a frequency-domain attenuation correction based on linear wave theory; the derived waves from this spectrum can be seen in Figure 3.12. The attenuation factor was computed as:

$$K(f) = \left(\frac{\cosh(k(f) \cdot h)}{\cosh(k(f) \cdot z)} \right) \cdot M(f)$$

where $k(f)$ is the wavenumber derived from the linear dispersion relation $\omega^2 = gk\tanh(kh)$, h is the local water depth, and $z =$ elev is the height of the pressure sensor above the bed. The multiplicative tapering mask $M(f)$ linearly reduces the correction factor from one at a trusted frequency ($f_{\text{corrmaxBelieve}} = 1.0$ Hz) to zero at a hard cutoff ($f_{\text{corrmax}} = 1.5$ Hz). To ensure numerical stability and avoid over-amplification of noise, the correction factor was capped at a maximum of 5. In the implementation, the square of the attenuation factor $K(f)^2$ was computed for power spectral purposes, but the square root was taken before applying the correction to the Fourier-transformed signal, to correctly scale amplitudes. The corrected spectrum was then inverse-transformed to the time domain using an inverse FFT to obtain the surface elevation time series. This attenuation procedure is adapted from the code of M. van der Lugt (2021) and will be made available in the data repository.

Wave spectra were computed from the reconstructed elevation time series using the Welch method, with a Hann window and a segment length equal to $\frac{1}{30}$ of the 20-minute burst duration. This configuration provided a frequency resolution of approximately 0.017 Hz.
From the resulting spectra, the following wave parameters were derived:

- **Hm0** – Significant Wave Height (m): Calculated as $H_{m0} = 4\sqrt{m_0}$, where m_0 is the zeroth-order spectral moment.
- **Tp** – Peak Wave Period (s): Defined as $T_p = 1/f_p$, where f_p is the frequency at which the spectral energy is maximized.
- **Tm01** – Mean Wave Period (s): Based on the ratio of the zeroth to first spectral moments: $T_{m01} = m_0/m_1$. This parameter is commonly used in wave energy flux and sediment transport calculations.
- **Tm02** – Mean Zero-Crossing Period (s): Computed as $T_{m02} = \sqrt{m_0/m_2}$, representing the average time between successive zero-upcrossings.
- **$T_{-1,0}$** – Mean Absolute Wave Period (s): Calculated as $T_{-1,0} = m_{-1}/m_0$, this parameter emphasizes longer-period wave energy by incorporating the negative first spectral moment.

3.5.2. LiDAR scanners

The LiDAR scanner recorded point data in polar coordinates and internally converted it into Cartesian coordinates. However, these Cartesian outputs were relative to the orientation of the LiDAR itself and therefore required transformation to real-world orientation through geo-referencing. This is done by first determining a transformation matrix, see rotation matrices below, and then applying it to the dataset. After geo-referencing, the data were converted back to polar coordinates and stored in NetCDF format to reduce storage volume.

Rotation around the x-Axis

$$P_x = \begin{bmatrix} 1 & 0 & 0 \\ 0 & \cos\theta & -\sin\theta \\ 0 & \sin\theta & \cos\theta \end{bmatrix}$$

Rotation around the y-Axis

$$P_y = \begin{bmatrix} \cos\theta & 0 & \sin\theta \\ 0 & 1 & 0 \\ -\sin\theta & 0 & \cos\theta \end{bmatrix}$$

Rotation around the z-Axis

$$P_z = \begin{bmatrix} \cos\theta & -\sin\theta & 0 \\ \sin\theta & \cos\theta & 0 \\ 0 & 0 & 1 \end{bmatrix}$$

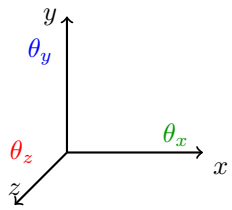

To ensure accurate geo-referencing, ground control points (GCPs) were established during deployment. Aluminum poles with reflective stickers were placed within the scanning range of each LiDAR unit. A SICK LiDAR sensor was used during setup to confirm that the reflectors were clearly visible within the scanner's field of view.

Each scan included seven GCPs, along with the position of the LiDAR sensor itself. These were all surveyed using RTK-GPS to obtain precise coordinates in the Dutch national RD (Rijksdriehoek) system. While only three GCPs are theoretically required for a rigid transformation, additional points provided redundancy and allowed for cross-checking in case of poor visibility or misalignment. Geo-referencing was carried out using the open-source software CloudCompare. The visible GCPs and the scanner location were manually selected and matched with their corresponding RD-coordinates. CloudCompare then calculated a transformation matrix and reported a root-mean-square error (RMSE) for each point cloud, allowing for quality control of the alignment. The calibration and alignment process is illustrated in Figure 3.13. The left panel shows the frame-mounted LiDAR scanner, which was deployed during each storm event. The middle panel depicts the placement of ground control points (GCPs), which were used to align the LiDAR point cloud. The right panel presents a sample output of a single LiDAR scan, where each point is geo-referenced in the Dutch RD coordinate system.

Figure 3.13: Calibration and deployment of the LiDAR system. The left panel shows the frame-mounted LiDAR scanner used during each storm event. The middle panel illustrates the placement of ground control points (GCPs), which were used to align the LiDAR point cloud. The right panel displays the resulting point cloud from a single scan, with all points geo-referenced in the Dutch RD coordinate system.

Once geo-referenced, further processing was performed. The LiDAR scanner recorded 16 scanning transects across 360°, and for most analyses, the transect perpendicular to the dune (transect 3) was selected.

To improve data accuracy, specific regions were systematically removed from the LiDAR point cloud. These included parts of the LiDAR frame itself, as well as noisy reflections caused by rain, airborne particles, birds, or other transient objects occasionally detected by the scanner. All measurements above 5.0 m NAP were excluded to eliminate noise from reflections in the sky, since the maximum dune elevation did not exceed 4.8 m NAP. Additionally, a zone extending 0.2 m in front of and 1.1 m behind the scanner was removed to exclude the LiDAR frame and structural interference from the mounting system.

3.6. Technical validation

To ensure the accuracy and reliability of the dataset, multiple quality control measures, validation methods, and error mitigation strategies were implemented.

3.6.1. Pressure sensors

To validate the S3.P3 pressure sensor data, water level measurements were compared with records from the Rijkswaterstaat (RWS) monitoring station in Scheveningen, located approximately 6.5 km north of the experimental site. Time series analysis revealed a strong visual correlation between the two datasets, with a minor phase lag attributable to tidal propagation differences along the coast. For the full overlapping period, the Root Mean Squared Error (RMSE) between the S3.P3 sensor and the RWS station was 0.146 m, indicating good agreement and confirming the overall reliability of the pressure sensor.

For water levels exceeding 1.5 m +NAP, relevant for the storm conditions which are the primary focus of this study, the agreement between the datasets increases further, with an RMSE of 0.106 m. This supports the accuracy of the S3.P3 pressure sensor in capturing high-water events, which are critical for evaluating storm-induced coastal processes. For lower water levels, some calculated surface elevations fell below the local bed level. These unrealistic outliers were excluded from further analysis, as they fall outside the intended measurement range. Likely, they are not indicative of sensor malfunction, but reflect limitations related to boundary conditions in shallow water.

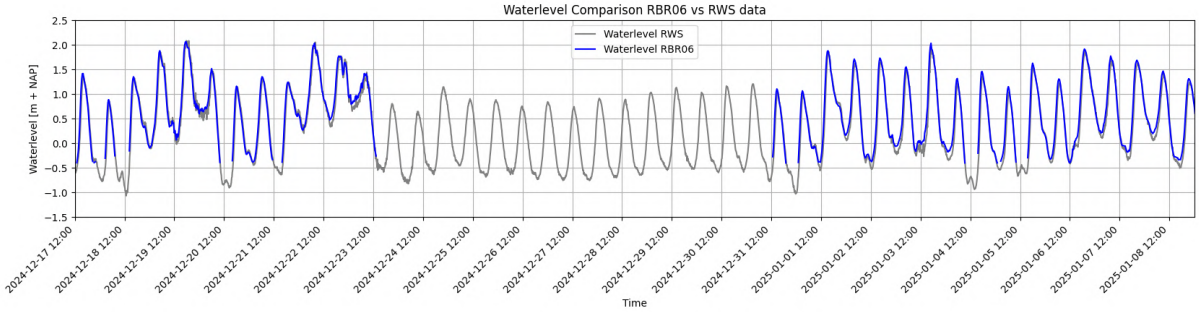

Figure 3.14: Comparison of water level time series from RWS (gray) and measured water level 80 m in front of the dune by S3.P3 (blue). The data demonstrate strong agreement, validating the RBR-derived water levels used in the field experiment.

3.6.2. LiDAR sensor

The LiDAR data were initially processed following the procedure described in Section 3.3.3, which includes the removal of outliers and geo-referencing of the point cloud. To validate the geo-referencing accuracy, the position of the ground control points (GCPs) as measured by RTK-GPS was compared to their location in the LiDAR point clouds after geo-referencing. Since LiDAR geo-referencing was conducted for each LiDAR and deployment , the validation procedure was repeated accordingly. This comparison showed good alignment, with an average root mean square error (RMSE) of 5 cm, and RMSE per scan better than 10 cm in all cases (Table 3.4).

The computed RMSE provides an estimate of systematic error based on the 3D distance between GCP locations and corresponding LiDAR points. The RMSE represents the average deviation of individual points in the point cloud from their true positions. In this dataset, the RMSE indicates that each point in the cloud has an average spatial distortion of the order of centimeters. Given that the LiDAR measurements are used to determine dune topography and bathymetry within 10 m seaward of the dune toe, such small RMSE values are negligible relative to the spatial scale of the observed morphodynamic features.

Table 3.4: The geo-referencing accuracy of for each LiDAR deployment. Values show the RMSE in cm between the GPS-measured GCP locations and the geo-referenced LiDAR point clouds.

Storm	1	2	3	4	5
LiDAR 1	9.2	6.8	7.6	N/A	N/A
LiDAR 2	4.8	5.7	3.5	N/A	4.6
LiDAR 3	7.6	4.2	2.6	N/A	N/A
LiDAR 4	4.8	4.8	4.2	N/A	4.3

To further validate the spatial accuracy of the LiDAR output, GPS-measured points such as the dune crest, dune foot, and exposed hard elements, were integrated into the point cloud, showing good alignment. Subsequent overlaying of different cross-sections recorded throughout the experiment to assess consistency in stable regions (e.g. dune crest heights, hard elements) confirmed that deviations were minimal: observed offsets were below 5 cm, indicating a high degree of consistency in the LiDAR dataset.

3.7. Data paper overview

This data paper presents a comprehensive set of high-resolution field measurements capturing the morphological and hydrodynamic response of hybrid and sandy dunes under storm conditions. The successful deployment and operation of over 30 instruments, including pressure sensors, LiDAR scanners, ADVs, OBS sensors, and ADCPs, during five consecutive storm events yielded a rich dataset of wave forcing, sediment transport, and morphological evolution.

The field campaign at the Sand Motor was executed under challenging winter conditions and achieved its goal of monitoring real-time dune erosion and hydrodynamic interaction across four distinct dune-dike configurations. The LiDAR systems consistently delivered accurate surface elevation data, as validated by GPS reference points with sub-decimeter RMSE. Pressure sensor data, corrected for atmospheric and tidal effects and rigorously processed, provided reliable reconstructions of wave parameters and surface elevation dynamics. These measurements enable detailed investigation of erosion processes and wave-structure interactions at the beach-dune interface. The dataset supports both empirical analysis and model validation of hybrid dune performance and is intended to inform future coastal protection strategies. Overall, the success of the fieldwork demonstrates the feasibility and value of in-situ experiments in advancing our understanding of nature-based and hybrid coastal defenses.

3.8. Recommendations

To improve the efficiency, accuracy, and continuity of future field campaigns involving (hybrid) dune monitoring, the following methodological recommendations are made based on the lessons learned during this project:

- **Simplify and automate LiDAR calibration procedures.** The calibration of the LiDAR scanners (e.g., alignment, position referencing) was time-consuming and manually intensive. Future campaigns should explore automated calibration routines inspired by mobile robotics, where LiDAR self-localization and point cloud registration are routine.
- **Increase frequency and coverage of beach GPS surveys.** Outside the LiDAR's scanning reach, beach morphology changes were only coarsely captured. Frequent GPS wheel surveys, ideally daily during storms, can efficiently map beach slopes and berms. Interpolating these measurements can generate high-resolution beach profiles that improve understanding of foredune evolution and sediment supply to the toe.
- **Improve nighttime visibility for GoPro image sequences.** Time-lapse monitoring of the dune face using GoPro cameras was hindered at night due to limited flashlight battery life. Future setups should consider high-capacity external battery packs or low-power infrared lighting to maintain continuous imaging and better capture wave runup and slump events during nighttime high-water periods. In addition, the spreading angle of the light beam should be wider than the field of view of the cameras, to ensure captured photos have consistent brightness over the full image.

3.9. Acknowledgments

This study was conducted as part of the NWO Perspectief project ‘Future Flood Risk Management Technologies’ and received additional funding from Rijkswaterstaat.

Note to the reader:
This chapter presents the draft of a data paper outlining the data collection methods employed during the field experiment. It functions as the methodology chapter of this thesis. The subsequent chapters will focus on the analysis and interpretation of selected results to evaluate the performance of hybrid dunes and address the core research questions.

Readers are advised to familiarize themselves with the classification of high-water events (e.g., 1.a, 1.b, 2.a, etc.) and the associated data processing procedures. The analysis in the following chapters primarily draws on data obtained from the LiDAR system and the intertidal pressure sensors.

4
Results

This chapter presents the results of the Hybrid-Dune field experiment, focusing on the morphological evolution of different (hybrid) dune sections in response to a sequence of winter storms. The analysis combines LiDAR-based topographic measurements, wave and water level data, and supplementary video observations to quantify erosion dynamics and structural exposure.

Section 4.1 provides a general overview of the morphological development across the monitored dune profiles, along with a summary of the incoming wave conditions. Sections 4.2, 4.3, 4.4 present a detailed breakdown of the erosion response during Storms 1, 2, and 3, respectively. Each storm is divided into separate high-water events, allowing for event-scale comparisons of dune face retreat, sediment loss, and structural transitions. Section 4.5 examines beach morphology at the base of hard structures, comparing the Dike-in-Dune and Dike sections. Section 4.6 summarizes the main findings. These findings are interpreted in detail in Chapter 5.

4.1. General overview

This section provides a general overview of the field measurement campaign. It begins with the morphological evolution of the monitored cross-shore profiles, based on LiDAR measurements for each of the (hybrid) dune sections. This is followed by a description of the offshore and nearshore wave conditions recorded during the observation period.

4.1.1. Morphological Evolution Overview

Fig. 4.1 shows the cross-shore morphological evolution of the Sandy Dune section (S2), based on LiDAR measurements. The 0° transect, located at the center of the section, was selected as a representative cross-shore profile. The morphological development is shown from the initial profile up to the period following Storm 4.

Sandy dune (S1)

LiDAR measurements were taken at low tide, before and after each high tide event, allowing for a direct measurement of the dune profiles without any water or wave interference. These measurements showed that the Sandy Dune section continued to erode throughout the monitoring period, Fig. 4.1. For this reason, data are shown through Storm 4. However, the analysis in the remainder of this chapter focuses only on Storms 1 through 3, as the Dike-in-Dune section (S1) and the Dike section (S3) failed after the third storm, preventing further data collection from those sections.

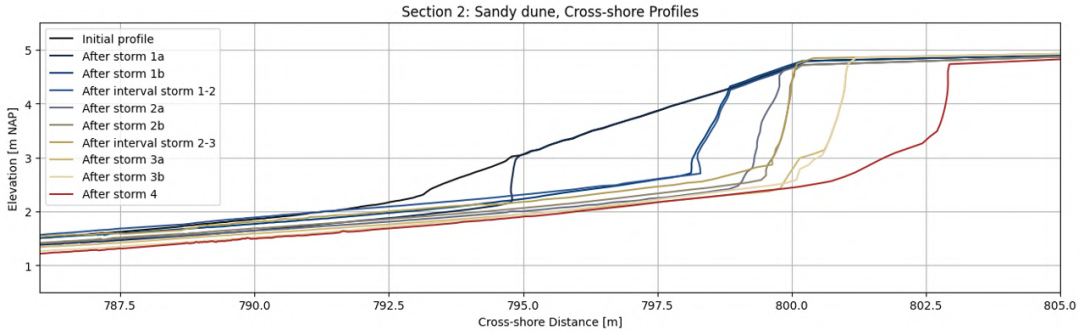

Figure 4.1: Cross-shore profile evolution of the Sandy Dune section (S2) over the course of the first four storms, based on the 0° transect extracted from LiDAR measurements. This transect represents the central cross-section of the dune.

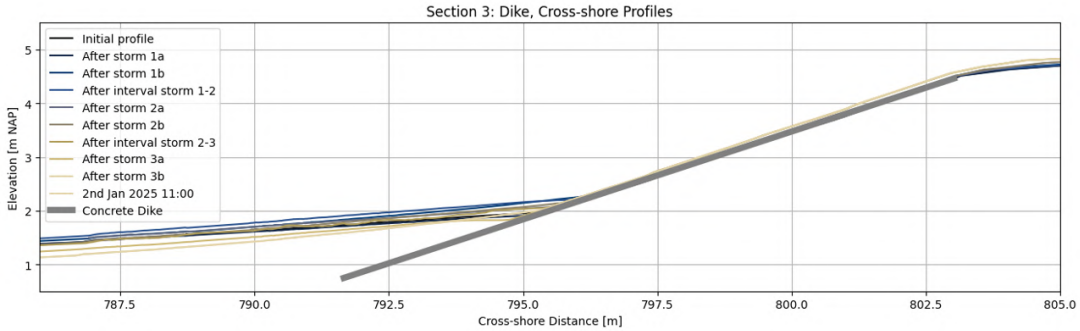

Figure 4.2: Cross-shore profile evolution of the Dike section (S3) during the first three storm events, based on LiDAR-derived measurements.

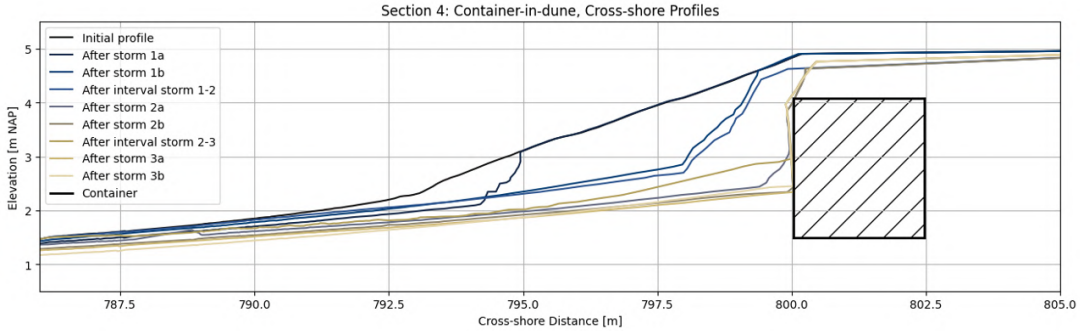

Figure 4.3: Cross-shore profile evolution of the Wall-in-Dune section (S4) during the first three storms, as recorded by LiDAR scans.

Dike-in-dune section (S1)

Fig. 4.4 shows the evolution of the first hybrid dune, the Dike-in-Dune section (S1). The sand layer atop the concrete dike element eroded throughout the storms. The hard element became exposed after the second high tide of the first storm (event 1.b). Erosion continued in subsequent events, resulting in a landward retreat of the dune face. The beach in front of the dike fluctuated between accretion and erosion, with a total elevation variation of approximately 45 cm recorded at x = 786 m. Overall, the section experienced net erosion, reducing the beach level and further exposing the dike. Dune face erosion ceased after the high water event 3.a.

Wall-in-dune section (S4)

The morphological development of the second hybrid dune, the Wall-in-Dune section (S4), is shown in Fig. 4.3. The sand layer in front of the seawall eroded progressively with each high-water event. The hard seawall element was exposed during the second storm. Similar to the other sections, the beach in front of the seawall experienced both accretion and erosion between events. A total elevation variation of approximately 30 cm was recorded at x = 786 m. Although the Wall-in-Dune section did not fail after the third storm, only data from Storms 1 to 3 are included in the comparative analysis to maintain consistency across all sections.

Dike section (S3)

Fig. 4.2 illustrates the morphological evolution of the Dike section (S3). As a hard structure, the slope of the dike itself remains unchanged throughout the events. However, the beach in front of the dike (from approximately x = 796 m seaward) exhibits both erosion and accretion over time. A total elevation variation of roughly 40 cm was observed between the highest and lowest beach levels during the monitoring period. After the third storm, the concrete dike elements failed, making further measurements in this section not possible.

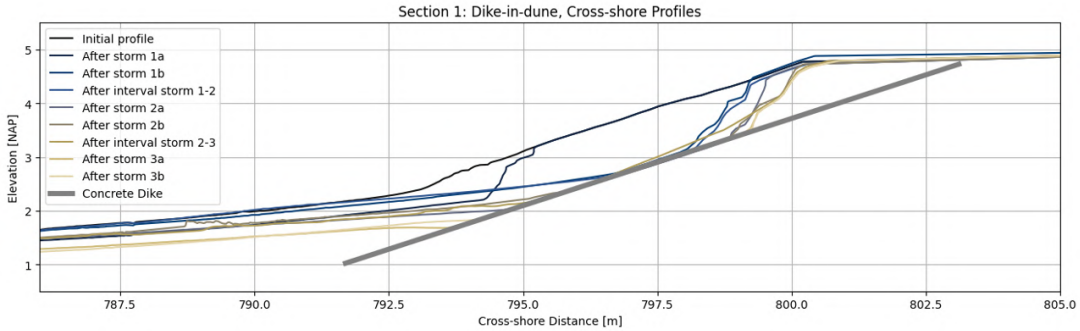

Figure 4.4: Cross-shore profile evolution of the Dike-in-Dune section (S1) over the first three storms. Profiles are based on LiDAR scans taken before and after each high tide.

4.1.2. Incoming wave conditions overview

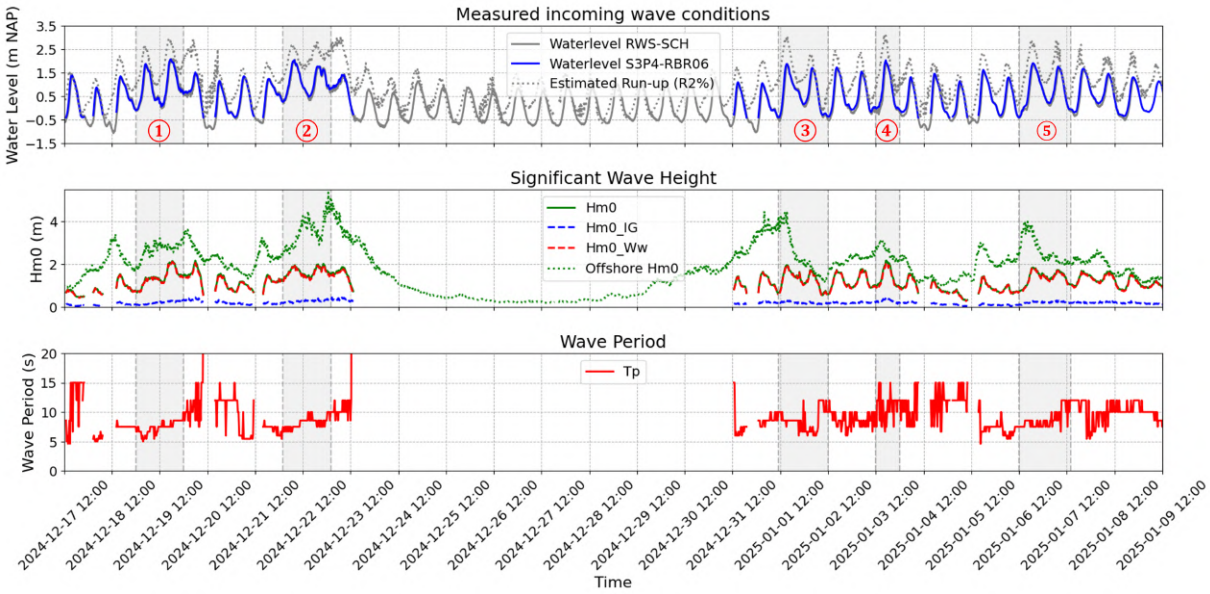

Figure 4.5: Time series of measured wave and water level conditions. The upper panel shows nearshore water levels (Scheveningen, RWS), nearshore water levels (S3.P3), and estimated wave runup ($R_{2\%}$) using Equation 2.1 from Stockdon et al. (2006). The middle panel presents significant wave heights from S3.P3 and offshore measurements from Europlatform 2 (EPL2). The lower panel shows peak wave periods (T_p) measured by S3.P3.

The incoming nearshore wave conditions, measured at S3.P3-RBR06 (introduced in Chapter 3, see Fig. 3.7), are presented in Fig. 4.5. The top panel shows the measured water level, overlaid with estimated wave runup ($R_{2\%}$), calculated using Equation 2.1 from Stockdon et al. (2006). The runup estimates are based on an idealized, uniformly sloping beach with a constant foreshore slope of 0.069. This slope was derived from GPS-based cross-shore transects and LiDAR elevation data collected on 19 December 2024. While this approach simplifies the actual, evolving beach morphology during storm events, it offers a useful first-order approximation of maximum wave runup potential. The input parameters for the runup calculation, significant wave height, peak period, and water level, were taken from measurements at the Europlatform 2 (EPL2) station, located approximately 50 km offshore from Hoek van Holland.

In contrast to Fig. 3.7 in Chapter 3, Fig. 4.5 additionally includes the offshore significant wave height (H_{m0}), shown in the second panel as a green dashed line, measured at EPL2. The estimated runup is also included in the top panel. The figure shows that high offshore wave conditions do not necessarily correspond to high nearshore wave conditions or elevated water levels. For example, during the high water events preceding Storms 1, 2, and 3 (on *2024-12-18 00:00*, *2024-12-21 06:00*, and *2024-12-31 08:00*, respectively), the offshore significant wave heights were relatively high, 3.30 m, 3.15 m, and 4.50 m, but did not result in proportionally elevated nearshore wave heights or water levels.

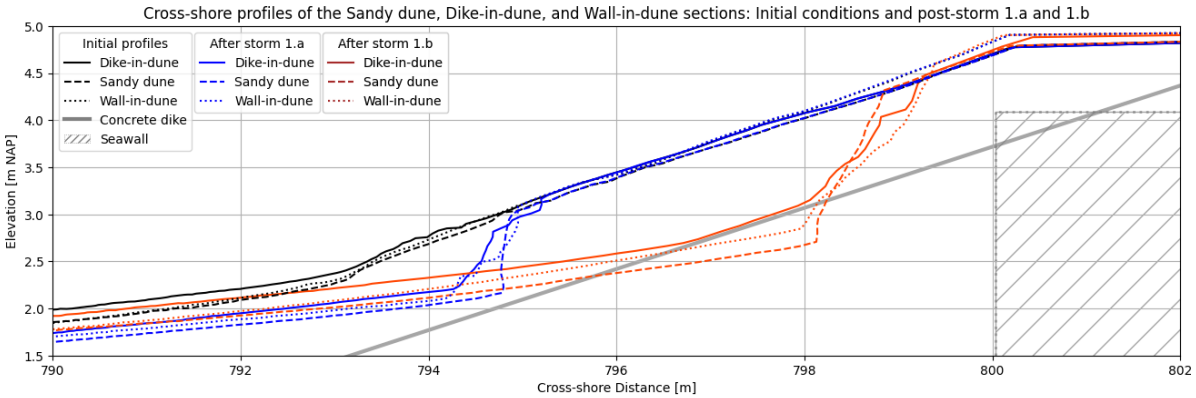

Figure 4.6: Erosion patterns during the first storm event (high waters 1.a and 1.b) for the Dike-in-Dune (S1), Sandy Dune (S2), and Wall-in-Dune (S4) sections.

4.2. Storm 1

During the first storm event of the experiment from the 19th to 20th of December 2024, all (hybrid) dune sections exhibited similar erosion patterns, as shown in Fig. 4.6. The initial high-water peak (1.a) caused erosion primarily at the dune foot across all sections. This trend continued during the second high-water event (1.b), with comparable erosion rates observed. However, this marked a key divergence in behavior: the hard structural core of the Dike-in-Dune section (S1) began to emerge as the overlying, originally 1.0 m thick, sand layer eroded. Consequently, the elevation at the dune foot in this section stabilized, whereas both the Sandy Dune (S2) and Wall-in-Dune (S4) sections continued to erode vertically. Although the elevation at the dune foot in the Dike-in-Dune section began to differ, the overall slope of the dune faces remained consistent across all sections, ranging between 45° and 55°.

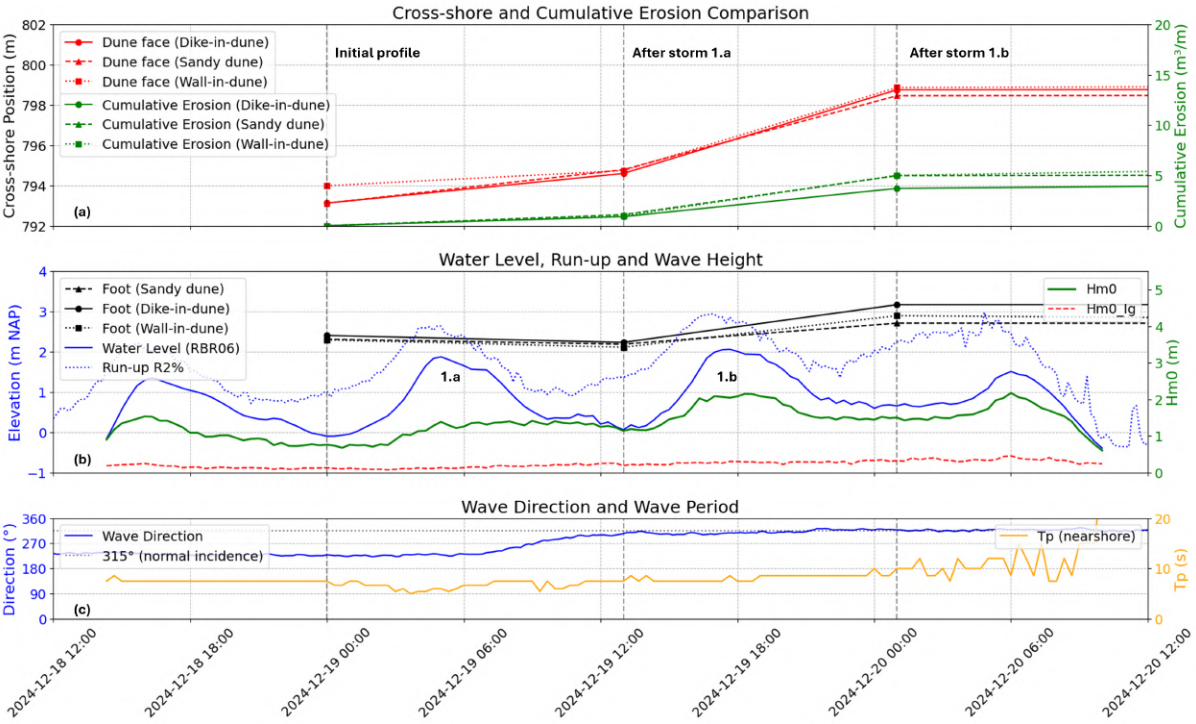

Figure 4.7: Wave conditions and morphological response during Storm 1. **(a)** Cross-shore position of the dune face for the Sandy Dune (dashed), Dike-in-Dune (solid), and Wall-in-Dune (dotted) sections based on LiDAR measurements. Cumulative erosion volumes between cross-shore positions 792–805 m are shown on the secondary (right) axis. **(b)** Water levels and estimated wave runup (R%2, left axis), along with dune foot elevation for each section. Nearshore significant wave height (green) and infragravity wave component (red dashed) are shown on the right axis. **(c)** Peak wave period (T_p) measured at S3.P3-RBR06 and wave direction recorded at the HKWZ offshore wind farm.

Fig. 4.7 illustrates the relationship between incoming wave conditions and morphological changes observed during Storm 1. Panel (a) presents the cross-shore positions of the dune face for the Dike-in-Dune and Wall-in-Dune sections (hybrid dunes), compared to the Sandy Dune. These are represented by solid, dotted, and dashed lines, respectively. A landward shift in the dune face position indicates erosion. Each cross-shore profile was derived from LiDAR measurements, and by comparing successive profiles (between cross-shore positions 792 and 805 m), the amount of erosion or accretion between time intervals was determined. The wave characteristics at the peak of each high-water event are summarized in Table 4.1 (Section 4.6). The table also presents the corresponding erosion volumes, the cross-shore displacement of the dune face, and the change in elevation of the dune foot for each section. The cumulative erosion for each section is shown in Panel (a), plotted on the secondary (right-hand) vertical axis in green.

Panel (b) shows the water level and estimated wave runup ($R_{2\%}$), calculated using Equation 2.1 from Stockdon et al. (2006). These values, along with the elevation of the dune foot for each section, are plotted against the left vertical axis. On the right vertical axis, the panel displays significant wave height: the nearshore values measured 80 m in front of the dune (S3.P3-RBR06) are shown in green, while the contribution from infragravity waves is indicated by the red dashed line. Panel (c) displays the peak wave period (T_p) measured 80 m in front of the dune (S3.P3-RBR06), along with wave direction data obtained from HKWZ, an offshore wind farm located approximately 18 km from the experimental site.

4.2.1. High water 1.a

During the first high-water event (1.a), both the Dike-in-Dune (S1) and Sandy Dune (S2) sections exhibited approximately 1.5m of landward retreat of the dune face. The peak water level reached 1.85m +NAP, while the significant wave height remained moderate at 1.39m. Despite the relatively low infragravity wave height ($H_{m0,IG}$ = 0.14m), the elevated water level allowed wave runup to reach and impact the dune toe, initiating erosion. This event resulted in eroded volumes of 1.10 m^3/m, 0.91 m^3/m, and 0.97 m^3/m for the Sandy Dune (S2), Dike-in-Dune (S1), and Wall-in-Dune (S4) sections, respectively, measured over the cross-shore interval from 792 to 805m. An additional factor influencing erosion during this event was the wave angle of incidence. Offshore, waves approached predominantly from the southwest (approximately 260°), typically generating longshore-directed currents. However, due to refraction as the waves approached the coast, their direction became more shore-normal. As a result, the wave direction (blue line) in Fig. 4.7(c) remained closer to the 315° reference line in the same panel, indicating a more perpendicular approach relative to the shoreline.

4.2.2. High water 1.b

The second high-water event (1.b) resulted in significantly more erosion compared to the first. Total eroded volumes were approximately 3.87 m^3/m for the Sandy Dune (S2), 2.81 m^3/m for the Dike-in-Dune (S1), and 4.04 m^3/m for the Wall-in-Dune (S4). These values represent 3 to 4.5 times the erosion observed during the preceding high-water event (1.a). During this period, the peak water level reached 2.05m +NAP, with a significant wave height of 2.07m. The infragravity wave component ($H_{m0,IG}$) was 0.26m, and the peak wave period was 7.5s, all measured at S3.P3. Notably, the wave direction during high water 1.b shifted to 315°, resulting in near-shore-normal wave incidence. This alignment concentrated wave energy directly on the beach, intensifying cross-shore sediment transport and reducing the influence of longshore processes, unlike the more oblique wave approach observed during high water 1.a.

Following this second high-water event, the beach profile in front of the dune exhibited approximately 10 cm of accretion. During the rising tide, wave runup continued to reach the dune foot, eroding the dune face. However, due to relatively low wave energy during the ebb tide, the mobilized sediment was not transported offshore but instead deposited locally, leading to temporary beach accretion. These observations suggest a potential influence of tidal phase and wave energy variability on short-term sediment transport and morphological response. Up to this point, the Dike-in-Dune (S1) followed a similar erosion pattern to the Sandy Dune (S2). However, after high water 1.b, the protective sand layer over the concrete core was fully removed, exposing the underlying hard structure (see Fig. 4.6). This marks the transition from an unconstrained to a structurally constrained erosion regime, where the presence of a hard element limits further landward retreat of the dune face.

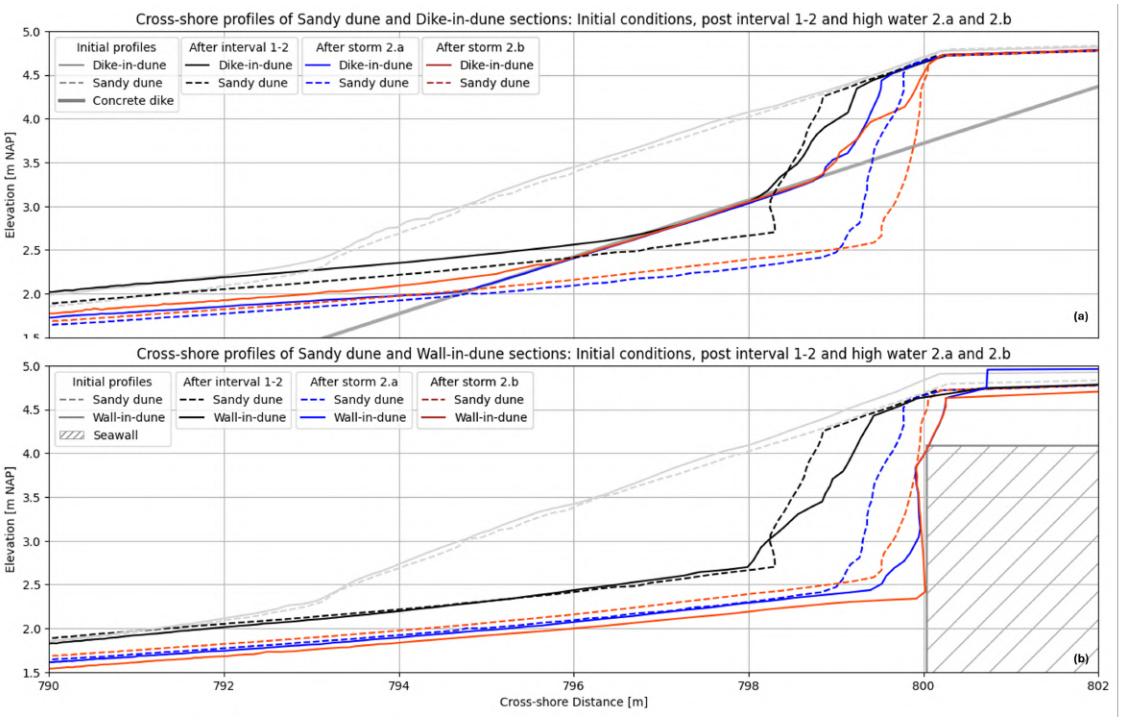

Figure 4.8: Cross-shore profiles of the Sandy Dune (S2) compared with the Dike-in-Dune (S1, top panel) and the Wall-in-Dune (S4, bottom panel). Dashed lines represent the Sandy Dune; solid lines represent the hybrid dunes. Profiles are shown after the Storm 1–2 interval (black), after high water 2.a (blue), and after high water 2.b (brown).

4.2.3. Summary of storm 1 findings

During Storm 1, all three dune sections, the Sandy Dune (S2), Dike-in-Dune (S1), and Wall-in-Dune (S4), exhibited very similar erosion patterns, particularly during the first high-water event (1.a), with comparable dune face retreat and sediment losses. Erosion was primarily concentrated at the dune foot across all sections. However, following the second high-water event (1.b), the hard structure within the Dike-in-Dune (S1) became exposed due to continued erosion of the overlying sand layer. This marked the beginning of a transition from uniform morphological behavior to a structurally influenced regime in S1, while the Sandy and Wall-in-Dune sections continued to erode more freely.

4.3. Storm 2

The second storm occurred from the 22nd to the 23rd of December 2024. During this event, the sand layers in front of the hybrid dunes (Dike-in-Dune – S1 and Wall-in-Dune – S4) were further eroded, resulting in exposure of both of the underlying hard structures by the end of the storm.

The cross-shore profiles of the Sandy Dune (S2) and the hybrid dunes are compared in Fig. 4.8. In both panels, dashed lines represent the Sandy Dune, while solid lines represent the hybrid dune sections. The black, blue, and brown profiles correspond to post-Storm 1–2, high water 2.a, and high water 2.b, respectively. In the top panel, the Sandy Dune shows continued landward retreat during both high-water events. The dune face receded by 0.91m during high water 2.a and by 0.46m during 2.b. In contrast, the Dike-in-Dune retreated by only 0.60m and 0.32m during the same intervals. The difference in erosion volumes was even more pronounced: the Sandy Dune lost 3.54m^3/m and 0.31m^3/m during high waters 2.a and 2.b, respectively, while the Dike-in-Dune eroded only 1.44m^3/m and 0.09m^3/m. This results in a cumulative difference of 2.32 m^3/m in erosion volume between the two sections. The lower panel compares the Sandy Dune with the Wall-in-Dune. During high water 2.a, the Wall-in-Dune (solid lines) eroded relatively rapidly, with a 0.92m retreat of the dune face, while the Sandy Dune retreated by only 0.47m in the same interval. After high water 2.a, the seawall of the Wall-in-Dune became exposed, effectively halting further cross-shore erosion of the dune face during high water 2.b due to the limiting effect of the hard structure.

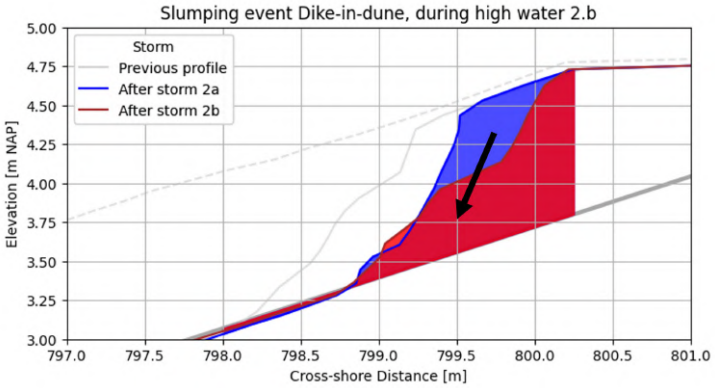

Figure 4.9: LiDAR-derived cross-section of the Dike-in-Dune (S1) showing slumping behavior during high water 2.b. Accumulated sand at the dune base partially covers the exposed dike.

Wave-induced slumping was also observed during high water 2.b. Fig. 4.10 presents sequential video frames captured by a GoPro mounted on the Dike-in-Dune (S1). In panel (a), the hybrid dune is shown just before wave impact. Panel (b) captures the wave runup, and panel (c) shows the result: rapid slumping event of the dune face and downslope sand movement. The collapsed sand accumulates at the dune base, and the slumped volume is highlighted in gray.

Figure 4.10: Slumping event observed by GoPro_01 during high water 2.b on 22 December 2024. Sequential frames show the collapse of the dune face and sand movement over a two-second interval: (a) 08:38:29, (b) 08:38:30, and (c) 08:38:31. This illustrates the dynamics of mass failure under wave loading.

This slumping behavior is further supported by LiDAR data, as shown in Fig. 4.9. The profile for Section 1 (Dike-in-Dune) before and after high water 2.b clearly shows slumped sediment accumulating at the dune base, partially covering the exposed concrete dike. These observations highlight the localized nature of sediment redistribution processes during storm events and demonstrate how structural elements influence erosion dynamics.

4.3.1. High water 2.a

At high water 2.a, which peaked on 22 December at 07:30 (see Fig. 4.11), the water level reached 1.97m +NAP with a significant wave height (H_{m0}) of 1.89m. The infragravity wave energy was notably high during this event, with $H_{m0,IG}$ reaching 0.25m, representing 13.2% of the total significant wave height across the full spectrum. These relatively energetic hydrodynamic conditions resulted in a 91cm landward retreat of the dune face in Section 2 (Sandy Dune), corresponding to an erosion volume of 3.54m^3/m. A comparable dune face retreat was observed in Section 4 (Wall-in-Dune), which retreated by 92cm with a total eroded volume of 4.41m^3/m. In contrast, Section 1 (Dike-in-Dune) experienced only a 60cm retreat and a much lower sediment loss of 1.43 m^3/m.

Video footage captured during high water 2.a at 09:38 supports these observations (see Fig. 4.12). It shows wave runup reaching the dune foot in Section 2, while in Section 1 the wave runup did not reach the dune toe. This visual evidence aligns with the runup estimates shown in Fig. 4.11(b). At the peak of high water 2.a, the estimated wave runup based on the Stockdon equation (Eq 2.1) reaches the elevation of the dune foot in the Sandy Dune but not in the Dike-in-Dune. It should be noted that this runup estimation assumes a uniformly sloping beach and does not account for the presence of a hard structure, such as the dike, which likely alters local wave interactions and reduces runup reach.

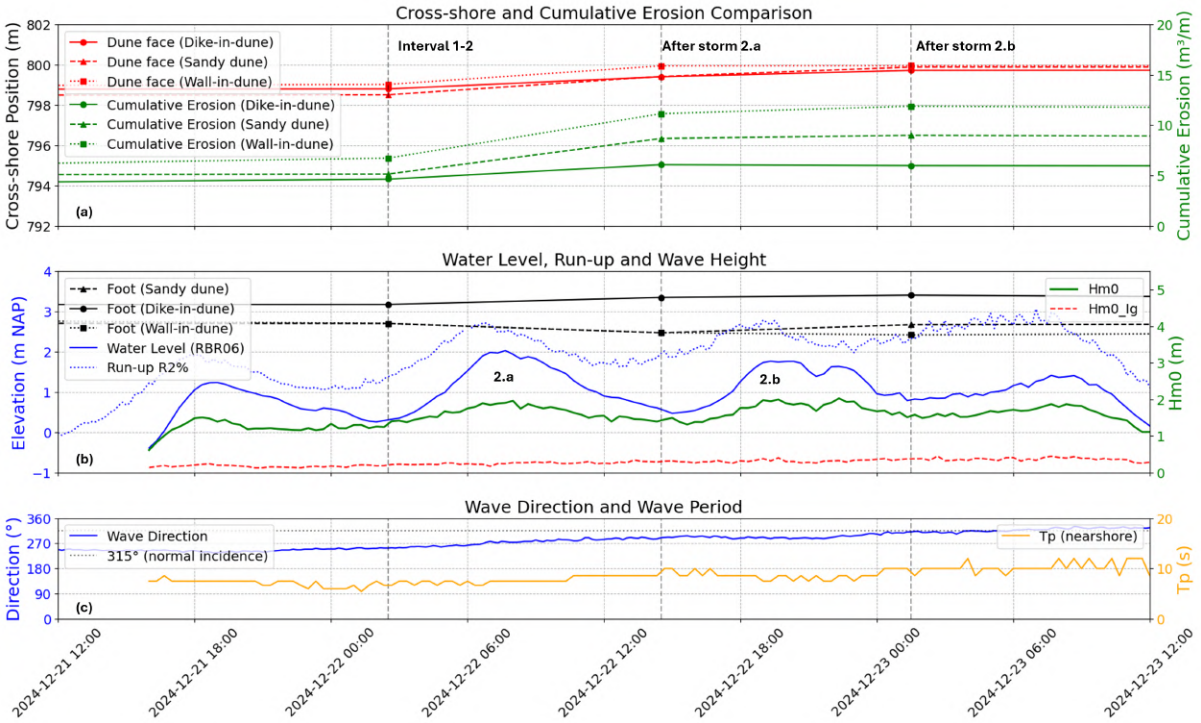

Figure 4.11: Comparison of wave forcing and resulting morphological response in Section 1 (Dike-in-Dune) and Section 2 (Sandy Dune) during Storm 2.

Analysis of beach elevation data offers additional insight into the observed erosion patterns. As shown in Fig. 4.8(a), following the Storm 1–2 interval, the beach elevation in front of the Dike-in-Dune section (S1) was approximately 26cm higher than that in front of the Sandy Dune (S2), measured at x = 794m. After high water 2.a, the beach at S1 dropped by approximately 40cm, reducing it to the same elevation as in S2. In Section 4 (Wall-in-Dune), the beach elevation remained similar to that of the Sandy Dune throughout the interval (Figure4.8(b)), but experienced a drop of about 33cm during high water 2.a, also at x = 794m.

Figure 4.12: Video frames from high water 2.a (22 December, 09:38) illustrating difference in wave runup between Section 1 and Section 2. **Left:** Wave backwash following a runup event. **Right:** The wave runup reaches the dune foot in Section 2 (Sandy Dune), whereas it does not reach the dune foot in Section 1 (Hybrid Dune with concrete core), demonstrating the runup-dampening effect of the hard structure.

4.3.2. High water 2.b

The second high-water event of the storm 2 (2.b) occurred on 22 December at 20:00, as shown in Fig. 4.11. Incoming wave conditions were similar to those observed during high water 2.a, with a significant wave height of 1.89m and an infragravity wave component ($H_{m0,IG}$) of 0.30m, which is 15% of the total wave energy spectrum. However, the peak water level was lower, at 1.76 m +NAP, resulting in reduced wave runup and, consequently, less erosion compared to the earlier event.

In the Sandy Dune section (S2), the dune face retreated by 47cm, while the elevation of the dune foot increased by approximately 20cm. The total eroded volume between x = 792–805m was 0.31 m^3/m, significantly lower than the volume lost during high water 2.a. Additionally, the beach profile in front of the dune accreted by nearly 13cm, measured at x = 798m. Section 1 (Dike-in-Dune) experienced the least erosion among the (hybrid) dune sections. The dune face retreated by only 32cm, with a total eroded volume of 0.08 m^3/m. Meanwhile, the beach in front of the dike element accreted by 20cm, measured at x = 794.5m. In the Wall-in-Dune section (S4), the vertical seawall, already exposed after high water 2.a, effectively halted further landward retreat of the dune face. As shown in Fig. 4.8, the dune face remained at the same cross-shore position during high water 2.b. However, erosion continued at the base of the structure, and the beach profile adjusted accordingly, forming a smoother slope up to the seawall. The total eroded volume during this event was 0.75 m^3/m, with most of the sediment loss occurring in the beach zone between x = 792m and the base of the seawall.

4.3.3. Summary of storm 2 findings

Overall, Storm 2 demonstrated how differences in dune composition and structural reinforcement significantly influenced erosion behavior under similar wave forcing. The Sandy Dune (S2) consistently exhibited the greatest dune face retreat and sediment loss, particularly during high water 2.a. In contrast, the Dike-in-Dune (S1) showed reduced erosion volumes and more limited retreat, aided by both the presence of a hard core and initially higher beach elevation. The Wall-in-Dune (S4) initially eroded rapidly but transitioned to a structurally constrained erosion regime once the seawall was exposed, halting further dune face retreat. Additionally, wave-induced slumping was observed in S1 during high water 2.b, highlighting the complex interaction between wave impact, structural exposure, and sediment redistribution. These results show that the presence of structural elements could influenced the magnitude and pattern of dune erosion during high-energy storm events

4.4. Storm 3

During the third storm event, both hybrid dune sections (Dike-in-Dune and Wall-in-Dune) effectively prevented further retreat of the dune face, in contrast to the continued landward erosion observed in the Sandy Dune (S2), as shown in Fig. 4.1. This difference is illustrated in Fig. 4.13, where the profiles of the hybrid dunes are compared to the Sandy Dune during high water 3.a.

In the top panel (a), the Dike-in-Dune (solid line) is compared with the Sandy Dune (dashed line). The Sandy Dune shows a dune face retreat of 0.99 m, highlighted by a red arrow. In contrast, the Dike-in-Dune exhibits no further retreat of the dune face. Instead, erosion occurred at the base of the dune, indicated by the blue arrow. In the lower panel (b), the Wall-in-Dune (solid line) is compared with the Sandy Dune (dashed line). Again, the dune face erosion of the Sandy dune is indicated in red, while the Wall-in-Dune shows no landward retreat due to the presence of the exposed seawall, as previously discussed in Section 4.3. Instead, the base of the Wall-in-Dune eroded downward by approximately 62 cm, indicated in blue. The beach profile in front of the seawall also eroded, forming a smooth slope up to the structure. Notably, this erosion did not result in the formation of a scour hole in front of the structure.

In both comparisons, the data show that dune face retreat in the hybrid sections (S1 and S4) did not continue once the hard structures were exposed. Under similar hydrodynamic conditions, the Sandy Dune (S2) continued to erode landward, while no further retreat was observed in the Dike-in-Dune and Wall-in-Dune sections. This trend persisted during high water 3.b, where Sections 1 and 4 showed no additional dune face erosion, in contrast to continued retreat in Section 2. These observations indicate different erosion patterns between the natural and hybrid dune systems. While landward erosion continued in the Sandy Dune, the presence of exposed hard elements in the hybrid sections occurred at the same time as the end of dune face retreat.

4.4.1. High water 3.a

High water 3.a produced wave and water level conditions similar to those observed during high water 2.a. The water level peaked at 1.86m +NAP, with a significant wave height of 1.96m. The infragravity wave component ($H_{m0,IG}$) reached 0.31 m, and the peak wave period was 8.6 seconds. The event featured a steep rising tide followed by a prolonged ebb, which is characteristic of storm surges in the North Sea. These conditions caused significant erosion in the Sandy Dune section (S2). Based on LiDAR data, the dune face retreated by 0.99m, resulting in an eroded volume of 3.82m^3/m.

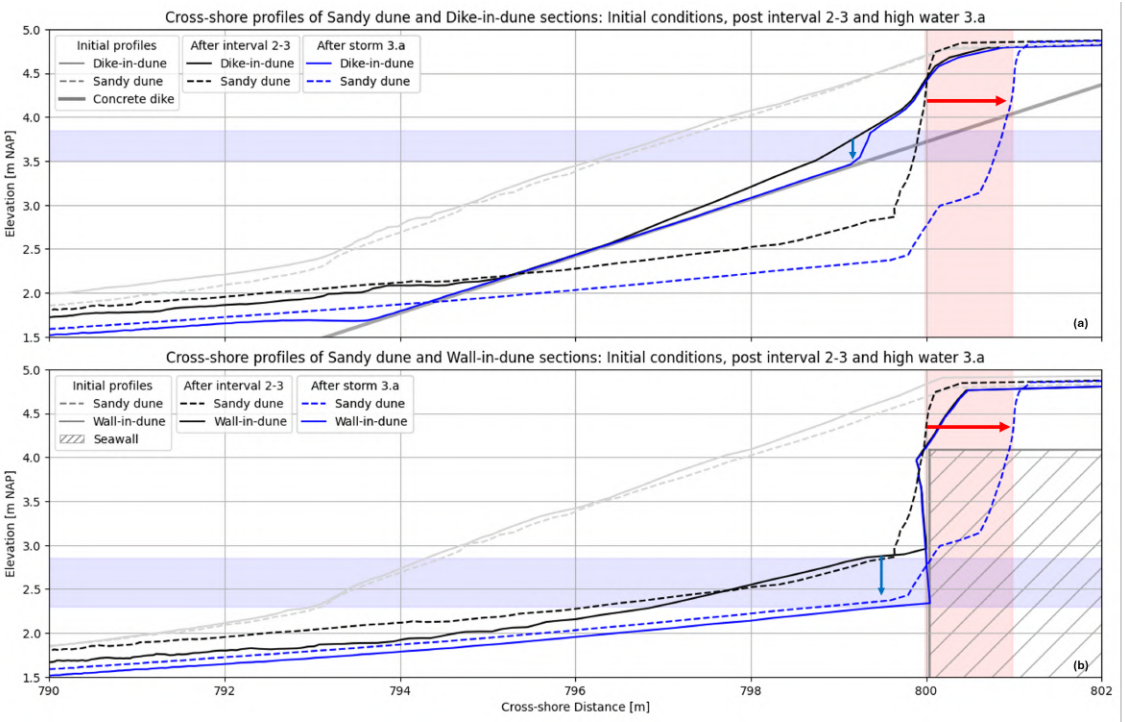

Figure 4.13: Dune face response during high water 3.a. **(a)** Dike-in-Dune (solid) vs. Sandy Dune (dashed): dune face retreat in the Sandy Dune (red) and base erosion in the Dike-in-Dune (blue). **(b)** Wall-in-Dune (solid) vs. Sandy Dune (dashed): dune face retreat in the Sandy Dune and downward erosion at the base of the Wall-in-Dune.

In the Dike-in-Dune section (S1), no dune face retreat was observed. However, minor erosion occurred at the dune base, as previously shown in Fig. 4.13(a). The total eroded volume was 0.97m^3/m, with local beach lowering of up to 75cm (measured at x = 793.5 m) in front of the dike. This could even be seen as a very small scour hole, as it has a small deviation from the sloping beach to the hard structure. The Wall-in-Dune section (S4) also showed no landward retreat of the dune face. However, the beach in front of the seawall eroded by 62cm (measured just seaward of the wall), as seen in Figure4.13(b). This resulted in a total eroded volume of 2.10m^3/m over the cross-shore interval from x = 792 to 805m.

4.4.2. High water 3.b

The second high water during Storm 3 featured lower wave energy compared to 3.a. The peak water level reached 1.71m +NAP, with a significant wave height of 1.64m. The infragravity wave component was 0.18m, and the peak period was 7.5 seconds. The tidal profile again showed a steep rise, followed by a steeper falling tide than observed in 3.a (see Figure4.14).

Due to the lower hydrodynamic forcing during high water 3.b, combined with the cumulative effects of the two preceding storm events, erosion was minimal across all sections. In the Sandy Dune (S2), no net volumetric change was observed. While minor erosion occurred at the dune base near x = 800m, this was offset by sediment accretion further seaward. Over the full cross-shore interval (x = 792–805m), LiDAR data indicate a near-zero net volume change between the post-3.a and post-3.b profiles. Although total erosion was limited, morphological indicators of structural weakening were still present. Fig. 4.15(a) shows a notch at the base of the Sandy Dune, suggesting localized undercutting. In Fig. 4.15(b), sediment accumulation at the dune toe suggests a slumping event. Both images were taken after the storm event and therefore only show the result of these processes; the precise timing of when the notching and slumping occurred is therefore unknown. In the Dike-in-Dune section (S1), no change was observed in the upper dune section above the concrete dike. However, the beach profile in front of the structure showed accretion of approximately 0.15 m^3/m. Similarly, in the Wall-in-Dune section (S4), the beach profile showed accretion of 0.28 m^3/m over the same cross-shore interval. No further dune face retreat or base erosion was observed in either hybrid section.

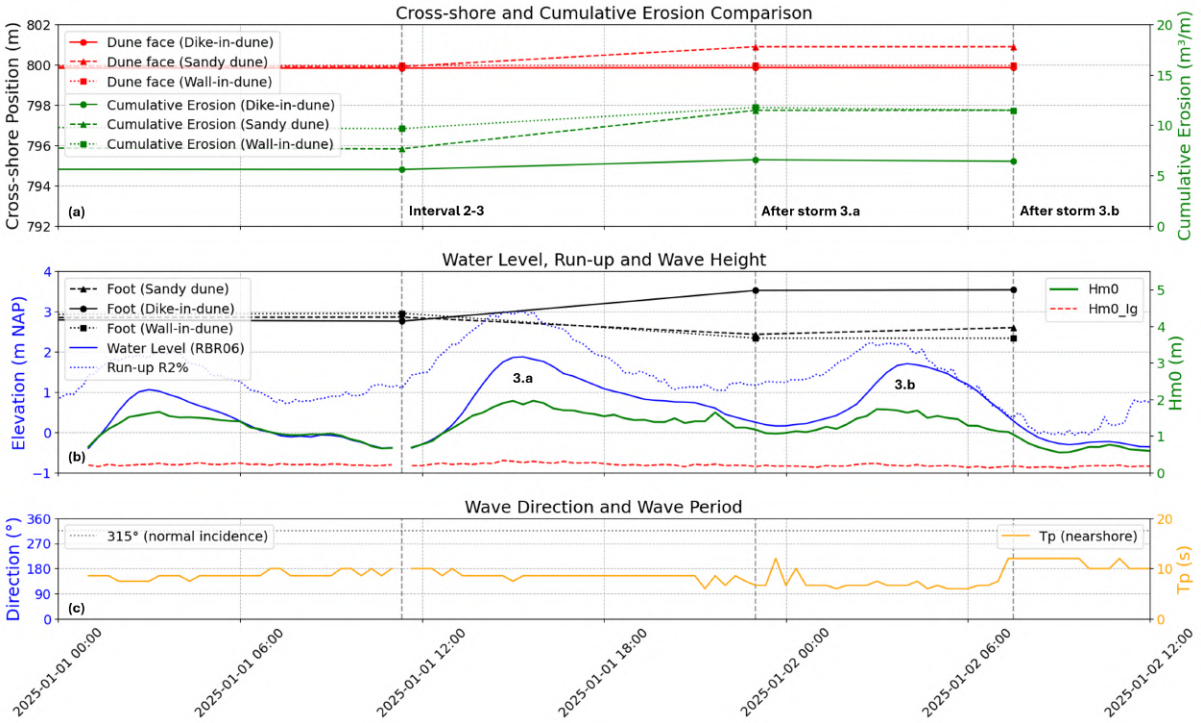

Figure 4.14: Comparison between wave conditions and dune profile positions during Storm 3. Note: wave direction data is not included, as it was unavailable during this period.

4.4.3. Summary of storm 3 findings

Storm 3 further highlighted the contrasting responses between sandy and hybrid dune systems. While the Sandy Dune (S2) continued to erode during high water 3.a, both hybrid sections (S1 and S4) showed no additional dune face retreat once their hard structures were exposed. Erosion in these hybrid dunes was limited to the dune base and beach in front of the structures. By high water 3.b, sediment losses were minimal across all sections, with local accretion observed in front of both hybrid dunes. Morphological signs of notching and slumping were visible in the Sandy Dune, but no further landward retreat occurred in the hybrid sections.

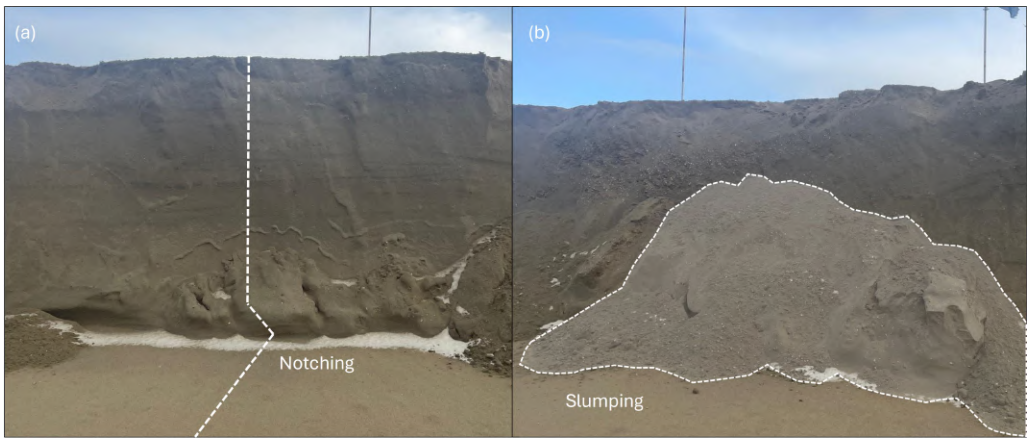

Figure 4.15: (a) Notching at the dune foot caused by repeated wave runup, leading to the development of an undercut. Once the notch becomes sufficiently deep and unstable, the overlying dune material collapses, initiating a slumping event. (b) After the slumping event, a mass of sand is deposited at the base of the dune. Note: white hail is visible on the beach surface, due to a hailstorm that occurred on the morning of 2 January 2025.

4.5. Morphology around sloped dikes

Erosion development at the base of hard structures varied between the hybrid dune sections, revealing key differences in morphodynamic behavior. This section first compares the scour patterns observed in the Dike-in-dune (S1) and the Dike section (S3). Fig. 4.16 illustrates the morphological evolution near the toe of the hard structures for the Dike-in-dune (left panel) and the dike section (right panel) across the three consecutive storm events. The top row shows the cross-shore profiles before and during Storm 1, the middle row shows changes during Storm 2, and the bottom row corresponds to Storm 3.

In the section of the Dike-in-dune, the sandy component of the hybrid dune retreated landward during Storm 1, eventually exposing the underlying hard dike. Notably, following the high water event 1.b, sediment accreted in front of the structure, forming a more stable beach profile. A similar pattern occurred in Section 3, where initial erosion was followed by accretion. This alternating cycle of erosion and accretion continued through subsequent storms. Once the hard structure in Section 1 became exposed, both Sections 1 and 3 exhibited similar behavior. After high water events 2.a and 3.a, only limited erosion was observed at the toe of the structures. However, in both sections (Dike-in-dune and Dike section), the beach profile partially recovered during the lower-energy phases following the second high water events (2.b and 3.b). This dynamic response suggests that although scour develops during peak wave loading, the intervening periods of reduced hydrodynamic energy can promote temporary stabilization through accretion.

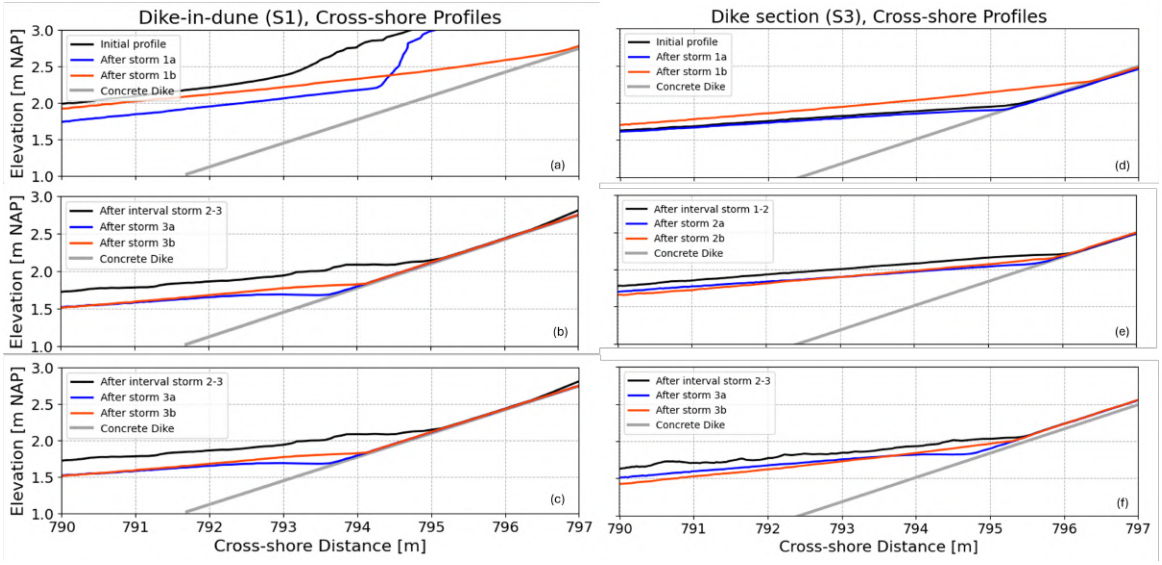

Figure 4.16: Cross-shore profile changes at the base of the Dike-in-Dune (left) and Dike Section (right) over three consecutive storm events. Each row shows LiDAR-derived profiles before and after each storm.

4.6. Main findings

The field measurements during the Hybrid-Dune project revealed distinct erosion behaviors among the tested dune configurations under increasing storm intensity. All sections initially exhibited similar erosion patterns, particularly during Storm 1. However, significant differences emerged as storms progressed and structural elements became exposed in the hybrid dunes.

- The Sandy Dune (S2) consistently experienced the greatest landward dune face retreat and volumetric erosion throughout all storm events.
- In contrast, the Dike-in-Dune (S1) and Wall-in-Dune (S4) sections showed progressively reduced erosion once their hard cores were exposed, effectively halting further dune face retreat by Storm 3. Erosion in these hybrid dunes was largely confined to the dune base and the adjacent beach.
- The Wall-in-Dune exhibited the most abrupt transition to structural control, with the seawall halting retreat immediately after exposure during Storm 2.
- Evidence of wave-induced slumping and notching was observed in both natural and hybrid dunes, highlighting complex local sediment redistribution dynamics.
- Importantly, the presence of hard structures altered erosion regimes, transforming them from unconstrained, retreat-driven processes to localized scour and base adjustment once exposed.
- Morphological comparisons with the Dike-in-dune (S1) and the concrete dike section (S3) revealed similar alternating cycles of erosion and accretion once the hard element of the hybrid dune was exposed.

Overall, these results demonstrate that hybrid dunes provide enhanced resilience to sustained storm conditions by limiting dune retreat after initial sand layer erosion, emphasizing their potential as effective coastal defense strategies.

Table 4.1: Morphological response under various high water conditions

Location		HW 1a	HW 1b	HW 2a	HW 2b	HW 3a	HW 3b
S3.P3- RBR06	Water level [m NAP]	1.85	2.05	1.97	1.76	1.86	1.71
	H_{m0} [m]	1.39	2.07	1.89	1.89	1.96	1.64
	$H_{m0,IG}$ [m]	0.14	0.26	0.25	0.30	0.31	0.18
	T_p [s]	6.00	7.50	7.50	8.60	8.60	7.50
Sandy dune (S2)	Δ Dune face pos. [m]	1.667	3.673	0.912	0.468	0.987	0
	Δ Dune foot elev. [m]	-0.124	0.522	-0.234	0.204	-0.430	0.168
	Erosion [m³/m]	-1.099	-3.874	-3.540	-0.311	-3.821	0
Dike-in dune (S1)	Δ Dune face pos. [m]	1.469	4.154	0.601	0.320	0.019	0
	Δ Dune foot elev. [m]	-0.173	0.936	0.176	0.055	0.765	0.015
	Erosion [m³/m]	-0.906	-2.805	-1.439	0.090	-0.968	0.157
Wall-in dune (S4)	Δ Dune face pos. [m]	0.748	4.130	0.924	0.009	0	0
	Δ Dune foot elev. [m]	-0.183	0.784	-0.229	-0.055	-0.620	0
	Erosion [m³/m]	-0.967	-4.043	-4.413	-0.748	-2.103	0.283

In Table B.1 (Appendix B), a more detailed overview table is given of the changes in dune face, foot, and crest positions, together with measured wave characteristics (offshore and nearshore) and eroded volumes.

5
Discussion

This chapter interprets the experimental results in the context of the research questions and existing literature. The focus lies on understanding how different hybrid dune configurations influence morphological evolution, structural performance, and sediment dynamics under storm conditions.

Section 5.1 addresses the first research question by comparing the cross-shore morphological response of the four dune types. It assesses how the presence and type of hard structure affected erosion progression and stability throughout the experiment. Section 5.2 evaluates how wave and current conditions relate to observed erosion patterns. It discusses key erosion mechanisms, examines correlations with hydrodynamic parameters, and explores how hybrid structures altered wave forcing and sediment transport. Section 5.3 focuses on critical design aspects of hybrid dunes. Drawing on field observations, it outlines structural strengths and weaknesses and reflects on their implications for coastal defense, including the translation to Dutch design storm conditions introduced in Chapter 3. Finally, Chapter 6 builds on this discussion to draw conclusions and assess the broader applicability and limitations of the findings.

5.1. Research question 1: Morphological response over time

In this section, the following research question is addressed: **How do the different hard structures of the hybrid dune influence the cross-shore morphological response over time?** The sections are individually assessed based on their morphological development throughout the experiment. The Sandy dune (S2) and the Dike section (S3) serve as baselines representing configurations without a hybrid dune structure. The response of each hybrid section is then evaluated relative to these references. The research question is answered by analyzing the erosion patterns and changes in dune geometry over time. Observed limitations in the data or setup are discussed, followed by a comparison of results with relevant findings from the literature.

5.1.1. Section 2: Sandy dune

The Sandy Dune (S2) provides a reference for natural morphological response under storm forcing. It experienced waves in the swash-collision regime during the storms of the experiment, characterized by repeated wave runup reaching the dune toe and triggering slope instability (Van Wiechen et al., 2024b). This led to progressive landward retreat of the dune face, driven by notching and gravity-induced slumping.

This erosion followed a cyclic pattern: wave runup reached the dune base (Fig. 4.12), resulting in the notching–slumping mechanism illustrated in Fig. 5.1. As described by Van Wiechen et al. (2024b), repeated runup notches the dune toe, progressively undercutting the face until the overlying sand slumps due to gravity. Evidence of this process in the Sandy Dune is shown in Fig. 4.15. This notching-to-slumping mechanism has been well-documented in both field and flume studies (Erikson et al., 2007; Palmsten and Holman, 2011). The slumped sediment is rapidly entrained into suspension and transported offshore (Larson et al., 2004b; Masselink and Puleo, 2006; Van Thiel de Vries et al., 2007). With no structural elements present to halt this retreat, uninterrupted profile migration was observed (Fig. 4.1). Fluctuations in the phreatic surface within the dune body can further initiate slumping events. Conti et al. (2024) showed that rapid oscillations in moisture content, caused by wave infiltration and drainage, destabilize the dune face and contribute to collapse. Although pressure sensor data was available in this experiment, it was not analyzed in this thesis.

Sediment loss at S2 was further amplified by alongshore sediment transport. During storms with oblique wave incidence from the south-southwest to west-southwest, sediment was transported northward toward neighboring hard-structure sections. Because S2 lacked upstream sandy input from the adjacent Dike section (S3), this resulted in a net sediment deficit and accelerated erosion. The influence of these alongshore effects extended across several tens of meters beyond the transition zone. In summary, the S2 profile reflects the baseline natural response to wave forcing without hard structure interference. It demonstrates that, in the absence of structural reinforcement, storm-driven erosion proceeds continuously

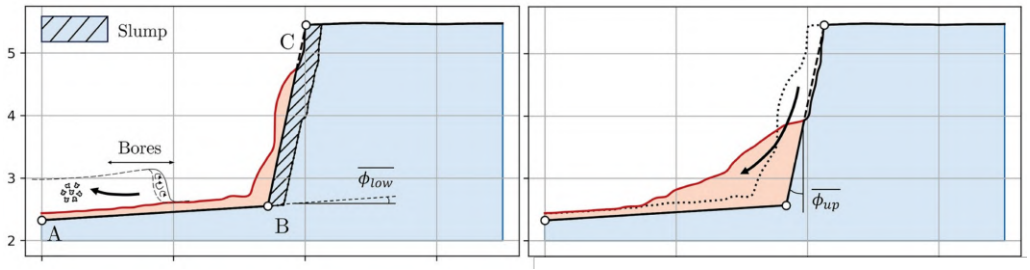

Figure 5.1: Slumping of a sandy dune face following bore impact, illustrating the mass failure mechanism triggered by wave-induced loading. Adapted from Van Wiechen et al. (2024b).

5.1.2. Section 3: Dike

The dike section initially demonstrated structural stability but ultimately failed due to lateral erosion at its boundaries. While the concrete revetment showed no vertical toe scour, the transitions between the hard structure and neighboring sandy dunes were more vulnerable. As erosion advanced from the sides, the foundation beneath the dike was progressively undermined, eventually leading to displacement of the concrete plates and full structural failure after Storm 4.

Despite the absence of a persistent scour hole at the dike toe, the beach in front of the structure exhibited considerable morphological variability throughout the experiment. Alternating phases of accretion and erosion were observed in front of the structure (Fig. 4.16). This dynamic behavior indicates that although vertical scour remained limited, the beach profile was highly responsive to hydrodynamic forcing, suggesting substantial cross-shore sediment mobility. It is possible that scour holes developed during high-energy wave events but were not captured by LiDAR due to elevated water levels or residual water retention within the holes. These scour holes may have been partially infilled with sediment during falling tides and subsequent low-energy conditions, a process described by Van Thiel de Vries et al. (2007) and Boers et al. (2011). This pattern of temporary recovery aligns with findings by Saponieri et al. (2018), who observed similar infill behavior under moderate wave energy conditions when reflective structures are not fronted by steep foreshore slopes.

These findings extend previous work by highlighting the importance of both frontal and lateral stability in hybrid dune design. While studies such as Figlus et al. (2015) and Almarshed et al. (2020) stress the role of wave loading and transition design, this experiment showed that the lack of lateral transition protection led to erosion beneath the flanks of the dike, ultimately compromising structural stability. While no persistent toe scour holes were observed, considered as a primary failure mechanism (Mai et al., 2006), lateral erosion proved dominant under the given boundary conditions. This underscores the need to evaluate hybrid dune integrity in both cross-shore and alongshore directions, particularly at transitions between sandy and armored sections.

5.1.3. Section 1: Dike-in-dune

The Dike-in-Dune (S1) initially exhibited a similar erosion pattern to the natural Sandy Dune (S2), with sediment-dominated retreat. After the first two high waters, the concrete structure became exposed, marking a transition to structure-influenced erosion. Following the second storm, a significant portion of the dike was uncovered, halting further retreat of the dune face, unlike the continued erosion observed in S2 (Fig. 4.1). Once the overlying sand was fully eroded, the beach profile in front of the dike showed similar morphological behaviour to the Dike section (S3) (Fig. 4.16), until structural failure after storm 4.

GoPro footage from the LiDAR frame revealed that erosion at the dune face was primarily due to slumping of the overlying sand, triggered directly by bore impacts (Fig. 4.10). This contrasts with the gravity-driven slumping following toe notching seen in S2. Conti et al. (2024) linked such impact-driven failures to rapid phreatic fluctuations caused by wave infiltration. Although pressure sensors were installed within the dike, their data were not analyzed in this study. Given that hybrid dunes may alter internal flow paths even when buried, future work should include analysis of internal pore pressure data to better understand slumping processes in composite structures. As more of the revetment became exposed during the second storm, wave runup was increasingly attenuated by the structure. Although runup occasionally reached the dune foot (Fig. 4.12), both the frequency and intensity of impacts, and thus erosion, were notably reduced. This reduction is attributed to the elevated position of the dune foot on the dike crest, as well as the energy-dissipating effect of the exposed concrete.

The observed behavior of the Dike-in-Dune is consistent with previous studies. Large-scale flume tests by Van Geer et al. (2009) and Figlus et al. (2015) showed that, once exposed, embedded hard structures can halt landward erosion and stabilize surrounding sediment. In this field experiment, the erosion of the hybrid dune evolved in three distinct phases: (1) undisturbed dune retreat, (2) reduced erosion as the structure became partially exposed, and (3) halted dune face erosion following full exposure, until structural failure occurred. These findings confirm that well-designed hybrid dunes can effectively limit landward erosion and maintain morphological stability under repeated storm loading.

5.1.4. Section 4: Wall-in-dune

The results presented in Chapter 4 demonstrated that the container-in-dune initially showed an erosion pattern similar to that of the sandy dune (Section 2), with significant landward retreat occurring during the initial storms. However, this behavior changed noticeably after Storm 3, when the vertical container core became exposed. Following this exposure, horizontal erosion ceased, and subsequent morphological responses were primarily downward, however, characterized by no toe scour.

The shift from horizontal dune face retreat to vertical erosion aligns with previous research by Figlus et al. (2015), who found that vertical cores, such as T-walls, effectively halt further landward retreat upon exposure. Additionally, Almarshed et al. (2020) highlighted that hybrid dunes typically transition to a more stable morphological regime once their cores become exposed. Compared to the gradual erosion reduction observed in the sloped dike-in-dune (S1), the vertical geometry of the container induced a sharper transition due to the abrupt reflection of wave energy. No scour was observed in front of the container-in-dune, unlike the extensive scour typically seen at traditional dikes (Mai et al., 2006). This is likely due to the sacrificial sand layer, which absorbed wave energy and increased local sediment availability, allowing material to be removed without forming a scour hole. Moderate wave conditions further limited near-bed velocities and pressure gradients, reducing the potential for concentrated toe erosion despite the vertical structure.

In summary, the wall-in-dune section transitioned from natural dune behavior to a stable, structure-controlled profile once the container core became exposed. The absence of toe scour suggests that sacrificial sand layers can effectively mitigate vertical erosion, even under reflective wave conditions. These results underscore the importance of structural geometry, sand buffering, and transition design in the erosion resistance of hybrid dunes.

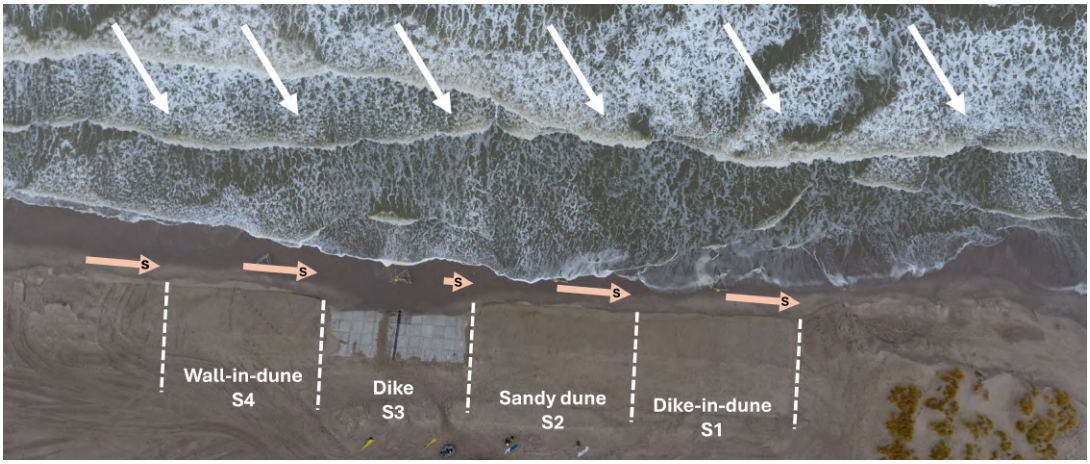

Figure 5.2: Schematic illustration of sediment fluxes under oblique wave conditions. White arrows indicate wave direction; brown arrows show the relative magnitude and direction of longshore sediment transport. The reduced sediment flux in section S3 (Dike-in-Dune) results in a deficit in S2 (Sandy Dune), promoting localized erosion.

5.1.5. Overview

This section addresses the first research question: *How do the different hard structures of the hybrid dune influence the cross-shore morphological response over time?* The results show that hybrid dunes initially behave similarly to natural dunes, with landward erosion driven by notching, slumping, and sediment removal. Once the hard cores become exposed, a shift occurs from sand-dominated to structure-controlled morphology. Erosion of the dune face slows or halts, and subsequent changes are concentrated around the exposed structure. This stabilization persists until structural failure occurs, as seen in the Dike-in-Dune and Dike sections (S1 and S3) after Storm 4.

Hard constructions also influence the morphological response at neighbouring dune stretches. Field observations suggest that longshore flow patterns were relatively uniform along the site. However, increased erosion consistently occurred near transition zones between sandy and armored sections. These areas showed greater dune retreat, typically extending 2–3 meters alongshore from the transition, after which cross-shore erosion appeared more uniform. This indicates that structural transitions can locally increase wave forcing and sediment mobility, likely due to wave reflection or focusing. These effects should be considered in the design and placement of hybrid dunes. The longshore transport process is illustrated in Fig. 5.2. The schematic shows oblique waves approach (white arrows) and the resulting sediment transport (brown arrows). In the Dike-in-Dune section (S3), the outgoing flux is reduced due to structural interruption, creating a sediment deficit in the adjacent Sandy Dune (S2), where erosion is intensified. The figure highlights how hard structures not only affect local erosion but also reduce sediment supply to neighbouring sections.

Several limitations apply to the whole experimental setup. While high-resolution LiDAR enabled detailed morphological tracking, its accuracy is limited near wet surfaces and hard edges, introducing centimeter-scale uncertainty in volume estimates. This is further affected when comparing transects from different deployments, as each scan is calibrated independently. Small misalignments can result in artificial elevation differences. Longshore sediment transport was not directly measured, so interpretations rely on visual observations and inferred patterns. Although flow appeared uniform, small variations in transport near transitions may influence erosion and remain a source of uncertainty. Further analysis of ADV data is recommended to quantify these effects.

In summary, the field results show that hard structures within hybrid dunes shift erosion from progressive retreat to a more stable, structure-controlled profile once exposed. However, they also introduce localized effects at transitions and can reduce sediment supply to adjacent dunes. This highlights the need to consider both local stability and alongshore sediment continuity when designing hybrid dunes for coastal protection.

5.2. Research question 2: Wave and current conditions

This section addresses the second research question: "*What is the correlation between wave and current conditions and the morphological response of hybrid dunes?*" Building on the morphological evolution presented in Section 5.1, this discussion connects observed erosion patterns to wave forcing and structural influence. The section first summarizes key erosion mechanisms, then examines correlations between hydrodynamic parameters and erosion, and finally assesses how hard structures modify these interactions.

5.2.1. Overview of Erosion Processes

All sections experienced dune face retreat triggered by wave runup during the first storms. In this initial phase, hybrid dunes (S1 and S4) behaved similarly to the natural Sandy Dune (S2), with erosion driven by wave-induced notching, slumping, and infiltration. As the hard cores became exposed, erosion transitioned from sand-dominated to structure-controlled, eventually halting landward retreat.

- **Notching at the dune toe**: Caused by repeated wave runup eroding the lower part of the dune face. This process is consistent with findings by Conti et al. (2024) and Van Wiechen et al. (2024b). An example of notching observed during the experiment is shown in Fig. 4.15(a).
- **Slumping of the dune face**: Occurs after notching, when gravitational forces acting on the upper dune exceed the internal shear strength, leading to mass failure. This process, described by Conti et al. (2024) and Van Wiechen et al. (2024b), is illustrated in Fig. 4.15(b), where the post-slump sediment is visible at the dune toe.
- **Bore impact and infiltration**: When a wave bore reaches the dune face, the resulting infiltration and rapid changes in pore pressure and water table height can trigger sudden failure, even in the absence of prior notching. Such a slumping event is captured in Fig. 4.10, consistent with mechanisms described by Conti et al. (2024).

These processes were consistently triggered when wave runup reached the dune face, confirming runup as the dominant driver of erosion (Masselink and Puleo, 2006; Van Thiel de Vries et al., 2007; Van Wiechen et al., 2024b). Once exposed, the hybrid structures altered the flow and reduced runup, thereby limiting further erosion.

5.2.2. Correlation of dune erosion and wave characteristics

To understand which wave conditions most strongly influence dune erosion, erosion volumes were compared against key hydrodynamic parameters for each high-water event. Figure 5.5 provides an overview of wave conditions and morphological response. Panel (a) shows the cross-shore dune face position for the Dike-in-Dune (S1), Sandy Dune (S2), and Wall-in-Dune (S4), alongside cumulative erosion volumes (green, right axis). Run-up was estimated using the empirical formula by Stockdon et al. (2006) (Eq. 2.1) and plotted against dune foot elevations in Panel (b), along with water levels, significant wave height (H_{m0}), and infragravity component ($H_{m0,IG}$). Wave data recorded 80 m seaward of the dune toe (S3.P3-RBR06) showed strong nearshore wave dissipation when compared to offshore wave heights and minimal infragravity energy, with $H_{m0,IG}/H_{m0} < 16\%$, confirming a short-wave-dominated system. Panel (c) presents wave direction and peak period. In all high-water events except Event 3.b, estimated run-up exceeded the dune toe in S2 and S4, aligning with increased erosion and dune retreat. However, the Stockdon formula assumes normally incident waves and uniform sandy slopes. It may overestimate run-up under oblique wave conditions, longshore currents, or near reflective structures. For armored profiles such as the Dike-in-Dune, the formulation by Van Gent (2001) (Eq. 2.6), developed for shallow foreshores with hard revetments, may provide more accurate estimates once the core becomes exposed.

The Pearson analysis used key hydrodynamic parameters of both offshore and nearshore, and erosion volumes per high water event for sections of Dike-in-dune (S1), Sandy dune (S2), and the Wall-in-dune (S4). Wave, water level data, and erosion volumes are summarized in Table 4.1 (Chapter 4). The analysis aimed to identify which parameters were most strongly associated with erosion. Fig. 5.3 illustrates the correlation between measured water levels at 80 m seaward of the dune toe (S2RBR4) [m +NAP] at the peak of the high waters and eroded volumes [m^3/m] over that interval, with color indicating significant wave height (H_{m0}) for each section, indicated in panel (a) Dike-in-dune, (b) Sandy dune, and (c) Wall-in-dune. All three sections, Dike-in-Dune (S1), Sandy Dune (S2), and Wall-in-Dune (S4), exhibit a positive correlation ($r > 0.80, p < 0.05$) between nearshore water level (measured in m +NAP) and

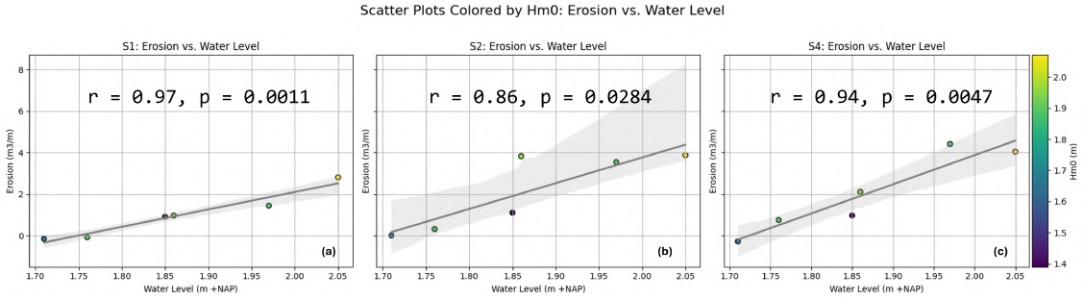

Figure 5.3: Scatter plots showing the relationship between water level, measured 80 m seaward of the dune toe (S3.P3RBR4), and the corresponding dune erosion volume for the (a) Dike-in-Dune (S1), (b) Sandy Dune (S2), and (c) Wall-in-Dune (S4) sections. Point color indicates significant wave height (H_{m0}). A grey linear regression line with a 95% confidence interval illustrates the general trend. These plots highlight the correlation between total water level and erosion, with potential modulation by wave energy.

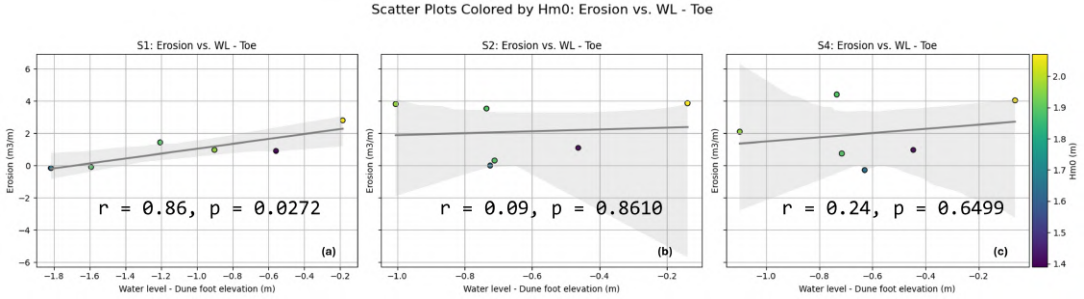

Figure 5.4: Scatter plots showing dune erosion as a function of water level exceedance above the local dune toe elevation ($\mathrm{WL} - z_{\mathrm{toe}}$) for (a) Dike-in-dune (S1), (b) Sandy dune (S2), and (c) Wall-in-dune (S4). Point color represents significant wave height (H_{m0}), illustrating the combined effects of water elevation and wave energy. Linear regression lines with 95% confidence intervals indicate potential relationships between exceedance and erosion intensity.

the corresponding erosion volume [m^3/m] during each high water event (Fig. 5.3). This result supports the findings of Van Wiechen et al. (2024b), who noted that increasing water levels elevate bore height and energy, thereby amplifying the erosive impact at the dune toe. In this figure, the point color denotes significant wave height (H_{m0}). H_{m0} alone had weak correlation (Table B.1 in Appendix B), yet its role in swash dynamics justifies its continued consideration.

Fig. 5.4 further explores the relationship between erosion and the elevation difference between the dune foot's position before the high water and the water level at the peak of the high water. In these figures, a trend line is shown along with a 95% confidence interval (gray). A statistically significant positive correlation is observed for the Dike-in-Dune section (S1) ($r = 0.86, p = 0.0272$). However, this relationship is absent in the Sandy Dune (S2) and Wall-in-Dune (S4) sections. This divergence contradicts earlier findings by Larson et al. (2004a), who linked dune erosion to the square of the runup exceedance over the dune toe. Likewise, Van Wiechen et al. (2024b) found a strong correlation ($r = 0.91, p = 4.505E-07$) between erosion rate and $(\eta_{L,A,2\%} - z_B)^2$, where $\eta_{L,A,2\%}$ represents the lidar-derived water level exceeded 2% of the time, and z_B the dune base elevation.

It is important to acknowledge several limitations of the correlation analysis. First, the dataset contains a limited number of high-water events, and the temporal resolution is coarse: peak water levels were compared to cumulative erosion measured over 12-hour intervals. This mismatch complicates direct cause-and-effect interpretation. Higher-frequency LiDAR data, as used by Van Wiechen et al. (2024b), could support such approaches and improve result reliability. Second, the Pearson correlation assumes statistical independence and linearity among variables, which may not hold for dynamic and interdependent processes such as dune erosion. More advanced regression techniques, accounting for temporal autocorrelation and non-linear interactions, are recommended for future analysis.

5.2.3. Interference of hard structures

Beyond direct wave forcing, hard structures substantially influenced the observed erosion patterns by modifying local hydrodynamics and sediment redistribution. Once exposed, the hybrid structures began to dissipate or deflect wave energy, reducing the runup and limiting further dune retreat (Figlus et al., 2015).

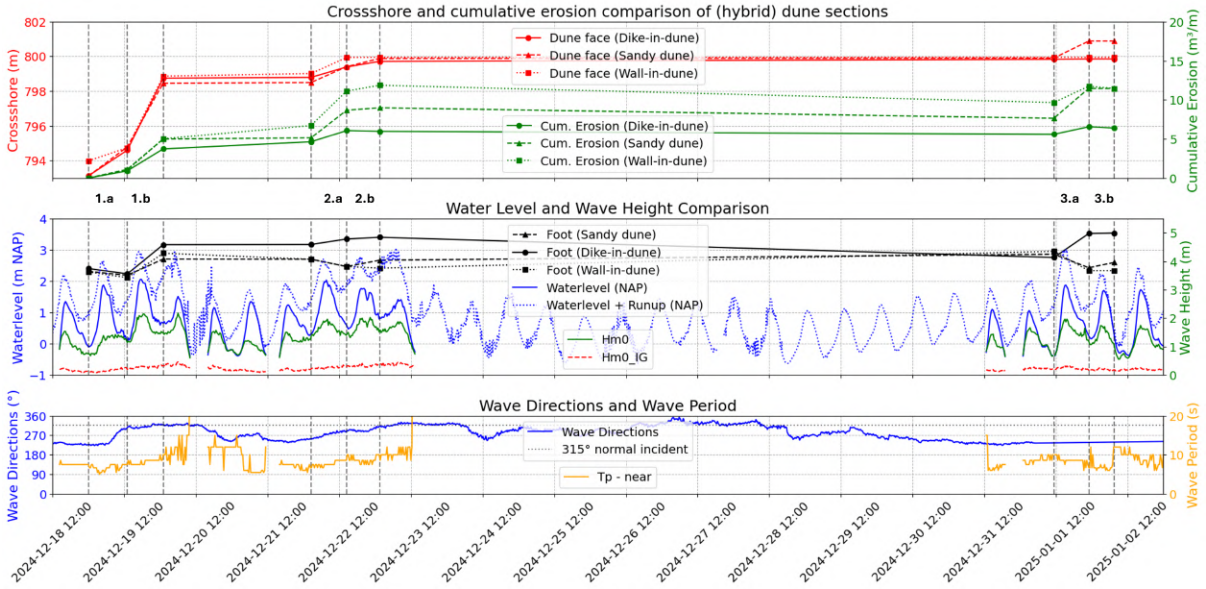

Figure 5.5: Wave conditions and morphological responses during Storms 1–3. **(a)** Cross-shore position of the dune face for the Sandy Dune (dashed), Dike-in-Dune (solid), and Wall-in-Dune (dotted) sections based on LiDAR measurements. Cumulative erosion volumes between cross-shore positions 792–805 m are shown on the secondary (right) axis. **(b)** Water levels and estimated wave runup (R%2, left axis), along with dune foot elevation for each section. Nearshore significant wave height (green) and infragravity wave component (red dashed) are shown on the right axis. **(c)** Peak wave period (T_p) measured at S3.P3-RBR06 and wave direction recorded at the HKWZ offshore wind farm. All panels cover the duration of Storms 1, 2, and 3.

These structural changes altered alongshore sediment pathways. Although longshore transport was not directly measured, oblique wave angles from the west–southwest during High Waters 1.a and 2.a likely generated longshore currents from Wall-in-Dune (S4) toward Dike-in-Dune (S1). Initially, both hybrid sections retained sufficient sediment buffers, but the armored Dike section (S3), lacking this sacrificial sand layer, restricted the sediment availability to the adjacent Sandy Dune (S2). This likely contributed to increased erosion there. By Storm 3, with the adjacent hard elements exposed of the Wall-in-dune (S4), Dike (S3), and Dike-in-dune (S1), this process intensified and further disrupted the updrift supply of the sandy dune section (S2). This interpretation aligns with Van Thiel de Vries et al. (2011), who observed enhanced erosion in dune sections with disrupted sediment supply. The sharp erosion trend at S2 during High Water 3.a in Fig. 5.5(a) supports this pattern. However, the absence of directional wave or current measurements prevents a clear distinction between cross-shore and longshore effects. Neglecting these alongshore dynamics, particularly near structural transitions, where there is increased turbulence and flow alternating, increasing the erosion, risks underestimating their role in localized erosion and post-storm sediment recovery. For hybrid systems, where cross-shore and longshore interactions are closely linked, a fully resolved 3D sediment budget is essential to accurately assess system behavior.

Finally, structural geometry played a key role in modulating wave energy. As shown by Saponieri et al. (2018), vertical seawalls can intensify runup and toe scour. This effect was seen in Wall-in-Dune (S4), where vertical beach erosion developed in front of the structure. In contrast, the sloped Dike-in-Dune (S1) more effectively dissipated energy and reduced dune erosion, consistent with findings of Figlus et al. (2015).

5.2.4. Overview

This section shows that the total water level is a key driver of erosion across both hybrid and natural dune sections. While positive correlations with erosion were found, especially in the Dike-in-Dune section, the limited number of events and coarse data resolution reduce their statistical significance. Hybrid structures altered erosion dynamics over time by dissipating wave energy and retaining sediment once exposed. Longshore transport, though not directly measured, influenced sediment redistribution under oblique wave conditions, contributing to spatial variability. Despite data limitations, the consistent relationship between water level and erosion highlights its importance in assessing dune response. Future studies should resolve both cross- and longshore processes at higher resolution to better understand hybrid dune behavior.

5.3. Research question 3: The design points of hybrid dunes

This section addresses Research Question 3: *"What are the most critical design points of a hybrid dune?"* Drawing on field observations from the Hybrid-Dune experiment, combined with supporting literature, this section identifies key structural strengths and weaknesses of two hybrid dune types. The insights provide design recommendations for applying hybrid dunes as flood defences along the Dutch coast under design storm conditions.

5.3.1. Hybrid dune Section 1: Dike-in-dune

Section 1, containing a concrete dike core buried in sand, initially behaved similarly to the sandy dune during early storm events. However, once the hard structure was exposed after storm 1.b, the erosion dynamics changed significantly. The core began to dissipate wave energy, effectively reducing wave runup, notching, and subsequent slumping erosion. Sediment from the eroded upper dune was transported either offshore during high-energy phases or redistributed alongshore, while moderate conditions allowed sediment deposition in front of the dune, forming a shallower profile and promoting wave energy dissipation (Larson et al., 2004b; Stockdon et al., 2006).

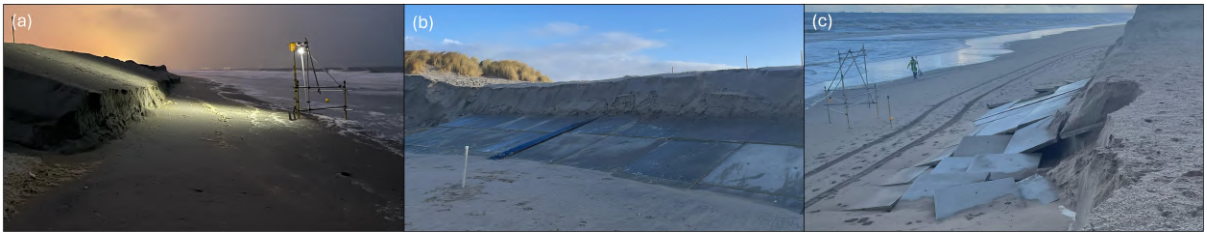

Figure 5.6: Morphological evolution of the hybrid dune (Dike-in-Dune) throughout the experiment, showing changes in dune profile and exposure of the hard core over successive storm events. (a) 19-12-2025, 08:07; (b) 23-12-2024, 11:37; (c) 02-01-2025 15:00

Strengths

Once exposed, the revetment effectively halted further dune face retreat by reducing wave runup and increasing the vertical threshold required for waves to reach the dune toe. This was particularly effective under moderate wave conditions, where swash no longer reached the dune foot, thereby preventing notching and slumping. By increasing the surface roughness (γ_f), the wave runup reduction could be further enhanced (Van der Meer, 2017). This structural response aligns with flume studies by Figlus et al. (2015), demonstrating that core-enhanced dunes can significantly reduce erosion once the core is active. Following the storm peaks, calmer conditions allowed limited beach recovery through onshore sediment transport, reflecting the temporary stabilizing effect of exposed hard elements (Van Thiel de Vries et al., 2007).

Weaknesses

A key vulnerability was identified at the transition zones between the revetment and adjacent sandy sections. These boundaries experienced intensified erosion, forming increased dune erosion over a width of 2–3 meters (Fig. 5.6(c)). Lateral erosion progressively undermined the flanks of the concrete dike, weakening its foundation. As a result, individual concrete plates were displaced, and the structure lost stability. With each successive storm, this flanking effect intensified, ultimately leading to full structural failure after Storm 4 (Fig. 5.7).

Design implications

- **Transition Zone Reinforcement:** The transition between the sand body and the revetment, particularly along the lateral edges, must be reinforced to prevent flanking and local scour. This can be achieved by incorporating geotextile filters and armoring the sides with rock or concrete revetment elements. In addition, the vertical extent of the revetment should exceed the local design water level plus expected wave runup, ensuring that the structure remains effective under storm loading and no overtopping.

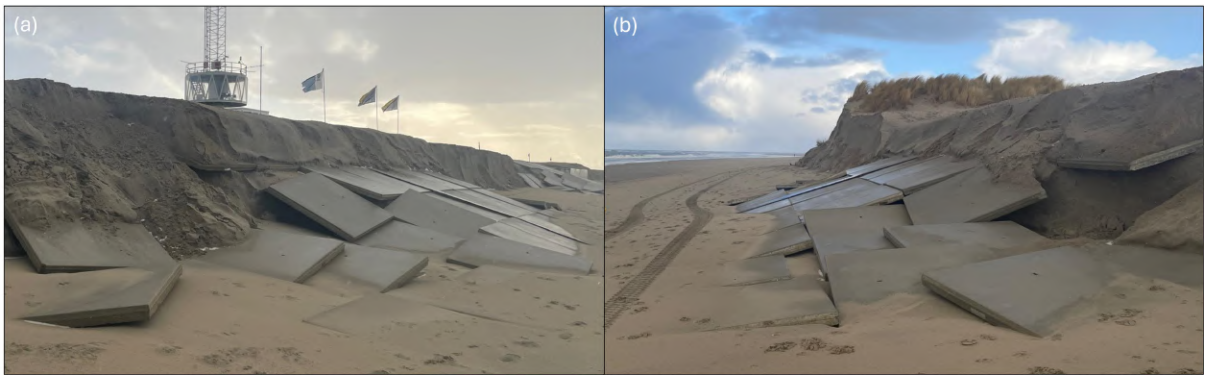

Figure 5.7: Progressive structural failure of the dike segments during the experiment, highlighting the effects of lateral erosion, toe scour, and shifting of concrete elements.*02-01-2025, 14:43*

- **Sand Cover Calibration:** The thickness of the sand cover above the revetment should be carefully designed for each specific location, taking into account local hydrodynamic conditions and desired protection levels. The balance between the volume of sacrificial sand and the strength of the underlying hard structure is crucial. An optimized design ensures that the sand layer provides sufficient buffering during moderate storm events, while the revetment is capable of withstanding more extreme conditions once exposed, together forming a robust, multi-layered flood defense system.
- **Long-Term Sediment Strategy:** A proactive nourishment or sediment management strategy is essential. Although natural recovery occurs during low-energy wave conditions, particularly in summer, these processes are insufficient to fully restore the foredune profile over longer timescales. Periodic nourishment may be required to maintain adequate sand volume and ensure long-term performance.
- **Toe Protection:** Scour protection measures should be installed at the base of the hard structure. While toe scour did not reach critical levels during this experiment, literature suggests that under more extreme conditions, scour can compromise the foundation and lead to structural failure (Boers et al., 2011; Mai et al., 2006).

5.3.2. Hybrid Dune: Wall-in-dune (S4)

Initially, the Wall-in-Dune (S4) section eroded similarly to the Sandy Dune (S2) and Dike-in-Dune (S1). After Storm 2.a, the vertical seawall became exposed, halting further landward erosion. As the wave energy is now reflected downward, this marked the transition from dune retreat to vertical erosion.

Figure 5.8: Overview of erosion progression in Section 4 (Wall-in-Dune). (a) 19-12-2024, 12:51 — Initial state before storm activity. (b) 23-12-2024, 14:28 — Erosion of the sandy layer and partial exposure of the container after Storm 2. (c) 02-01-2025, 14:39 — Continued downward erosion and stabilization of the dune face post-Storm 3.

Strengths

The Wall-in-dune effectively halted dune face retreat after Storm 2.a, with the dune crest remaining stable during subsequent events. Despite its vertical geometry, the core resisted toe undermining, likely due to the moderate wave loading after exposure, increased amount of sediment due to the sacrificial sand layer, and the absence of plunging breakers near the structure. This minimized the formation of deep scour holes, often observed near reflective vertical defenses (Figlus et al., 2015; Saponieri et al., 2018).

Weaknesses

Vertical seawalls are vulnerable to toe scour under high-energy conditions, posing a risk to structural stability (Mai et al., 2006; Saponieri et al., 2018). Although not observed here, it remains a critical concern. Transition zones did experienced localized scour and flanking due to flow divergence and should be reinforced (Fig. 5.9(b)). Unlike the sloped Dike-in-Dune, the Wall-in-Dune does not trap sediment once the fronting sand is eroded. While the thicker sand cover initially provides a larger sacrificial volume, its full erosion leaves the core fully exposed. Recovery of this sand layer is slow without nourishment, reducing resilience and increasing long-term maintenance requirements.

Figure 5.9: Final erosion state of Wall-in-dune (S4). (a) 02-01-2025, 15:08 — Limited toe scour is visible at the base of the container, suggesting wave reflection but no significant undermining. (b) 06-02-2025, 11:29 — The adjacent natural scarp, shaped by wave and wind erosion, retreated further landward following Storms 4 and 5. Backside erosion of the seawall began to emerge.

Design implications

- **Transition zones:** Reinforce the interfaces between the vertical core and adjacent sandy sections to prevent flanking and localized scour.
- **Core setback and sand cover:** Optimize the landward placement and sand thickness to ensure delayed core exposure, allowing the sand buffer to absorb wave energy during initial storm phases.
- **Narrow-profile suitability:** Vertical cores are effective in space-limited locations but require careful toe and transition maintenance.
- **Toe protection:** Include geotextiles or buried rock toes to mitigate toe scour from plunging waves and wave reflection once the core is exposed.

5.3.3. Translation to Dutch design storm

To address the third sub-research question, hybrid dunes must be evaluated under the full range of design storm conditions, including the Dutch 1:10,000-year event. The field experiment was limited to moderate conditions, significant wave heights of 2–3.5 m and water levels measured below +2.5 m NAP, mainly within the collision regime and not representative of extreme storm impacts. In contrast, the Dutch design storm involves H_{m0} values of 11 m, T_p of 12 s, and surge levels up to +5.0 m +NAP along the North Sea coast (Van Der Meer et al., 2016). To assess hybrid dune performance under such conditions, the observed field responses should be extrapolated using validated numerical models. This process, summarized in Fig. 5.10, begins with 1D model validation (e.g., XBeach) and progresses to 2D simulations to capture lateral effects and optimize designs for extreme events.

From field results to model implementation

The first step is to use the field data to validate and calibrate a one-dimensional (1D) XBeach model under the observed storm conditions. This model should accurately reproduce key processes such as dune erosion, core exposure, and beach profile evolution. Due to shorter runtimes, starting with 1D allows efficient testing and refinement. Once the 1D model performs reliably, it can be extended to two-dimensional (2D) simulations to capture lateral variability, including alongshore sediment transport and transition zone effects between hard and soft sections. This step is essential for evaluating the full complexity of hybrid dune behavior under realistic storm conditions.

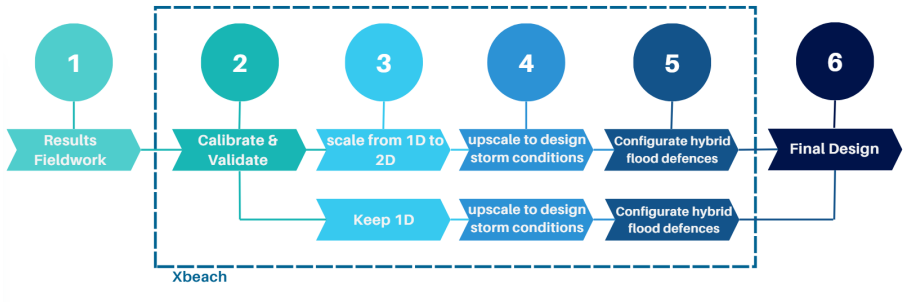

Figure 5.10: Flowchart outlining the process for translating fieldwork findings into practical implementation strategies for hybrid dune design along the Dutch coast. The steps include field data analysis, model validation, design optimization, and site-specific application.

Towards full-scale design storm testing

Once validated, the hybrid dune model can be extended to simulate extreme storm scenarios based on Dutch design standards. Although wave heights during the experiment were modest (2–3.5 m H_s), the prototypes' nearshore placement enabled water levels at the dune foot comparable to those during full-scale storms. In practice, hybrid dunes are located further landward, requiring higher storm surges to reach the structure. Thus, the observed +2.1 m NAP water levels can represent a structure placed at +4.5 m NAP, assuming similar beach slopes. While wave heights must still be scaled, Section 5.2 showed that water level is the primary driver of erosion, supporting this conceptual translation. Model simulations should include varying wave climates, storm intensities, and beach-dune geometries. Long-duration events (>24 hours) are essential to capture cumulative erosion effects critical to long-term performance (Roelvink et al., 2009).

Broader implications for Dutch coastal management

A validated 2D XBeach model enables site-specific optimization of hybrid dune designs along the Dutch coast. Hybrid dunes offer a flexible alternative where traditional dike upgrades are impractical, combining flood protection with natural aesthetics, multifunctional land use, and adaptability to sea-level rise and climate change (Almarshed et al., 2020; Figlus et al., 2015). Compared to hard coastal structures, they reduce environmental impact and allow for maintenance through sand nourishment rather than structural reconstruction. Hybrid systems can also extend the service life of aging dikes and support innovative designs in urban zones, where core structures may double as vertical sea defenses. To ensure viability, designs must be tailored to local conditions, considering beach width, wave loading, and nourishment needs. Key structural requirements for design storm resilience:

- **Crest height:** The hard revetment should extend above expected design runup levels, typically +7.5 to +8.5 m NAP, to prevent overtopping during extreme storm events (Van Der Meer et al., 2016).
- **Sand cover:** A sand buffer needs to be designed to absorb frequent storm energy, with the expectation that it may be fully eroded during a design storm.
- **Transition zones:** Reinforce flanks and boundary zones with geotextiles or armoring to prevent flanking and localized scour, which were critical failure points in the experiment.
- **Toe protection:** Incorporate buried rock layers or geotextile filters at the base of the structure to resist toe scour and foundation undermining during high wave loading.

5.3.4. Overview

This section identifies the critical design points of hybrid dunes based on field observations from the Hybrid-Dune experiment. The Dike-in-Dune showed erosion resistance once its hard core was exposed, but suffered structural failure due to flanking at transition zones. The Wall-in-Dune effectively halted landward erosion after exposure, due to the vertical seawall, it changed from horizontal dune retreat to vertical beach erosion. Key design implications include reinforcing transition zones, optimizing sand cover thickness. Although tested under moderate storm conditions, the findings can be scaled to Dutch design storm scenarios using validated numerical models. Hybrid dunes offer a promising, adaptable solution for coastal defense if tailored to site-specific conditions and maintained through sediment management.

6 Conclusions

This thesis investigated the morphological response of hybrid dunes under storm conditions through a large-scale field experiment conducted at the Sand Engine. The objective was to improve understanding of sediment transport dynamics and structural performance in hybrid dune configurations, systems that integrate sandy elements with engineered hard revetments. The findings contribute to the design of more resilient, adaptive coastal defenses in light of recreation and climate adaptability.

Morphological evolution of hybrid dunes

Hybrid dunes altered the cross-shore erosion response by shifting the system from a sand-dominated to a structure-controlled regime. This transition followed a consistent three-phase pattern:

- **Phase 1 – Sand-dominated response**: All dune types initially showed similar behavior, with toe notching, slumping, and offshore sediment transport. Dune face retreat reached up to 4 m, and erosion volumes ranged from 0.9–4.0 m^3/m during the initial storm event.
- **Phase 2 – Transitional phase**: As storm loading progressed and hard structures became partially exposed (e.g., after Storm 2.a), erosion in the hybrid dunes slowed. The Dike-in-Dune (S1) had 30% less dune retreat and 60-70% less eroded volume compared to the Sandy dune (S2). 1.4 m^3/m
- **Phase 3 – Structure-dominated regime**: Once fully exposed, the structural revetements prevented further landward retreat. During Storm 3, Dike-in-dune (S1) and Wall-in-dune (S4) showed no horizontal erosion, while S2 eroded an additional 1.0 m.

Core geometry significantly affected performance. The concrete revetment in the Dike-in-dune section allowed gradual energy dissipation and supported smoother morphological transitions. The seawall in the Wall-in-dune section halted retreat more abruptly but was associated with localized vertical beach erosion. In contrast, the Sandy dune, lacking structural support, retreated by over 7 m and lost more than 11 m^3/m cumulatively. However, structural stabilization was not permanent. During Storm 4, both the Dike-in-Dune and Dike sections failed due to flanking erosion and undermining. These results show that while embedded structures can locally halt dune face retreat, their long-term effectiveness depends on the stability of adjacent sediment and transition zones.

Hydrodynamic forcing and erosion response

Erosion volumes across all profiles correlated strongly with the duration of total water level exceedance over the dune toe. The correlation was statistically significant ($r > 0.80$, $p < 0.05$), confirming water level as a key predictor of storm-induced erosion. However, the limited number of events, 12-hour measurement intervals, and assumptions of linearity limit the predictive strength of this relationship. More advanced, high-resolution analysis is recommended for future work. Further conclusions or assumptions based on the statistical correlation can therefore not be drawn.

Beyond this first-order driver, hybrid dunes altered erosion patterns by modifying local hydrodynamics. Once exposed, hard structures reduced wave runup and changed energy distribution, influencing sediment mobility and localization of erosion. Vertical designs intensified wave reflection, contributing to vertical erosion in front of the structure, while sloped designs supported energy dissipation. Additionally, longshore sediment transport was likely disrupted by structural exposure. Under oblique wave conditions from the southwest, sediment supply toward the Sandy Dune (S2) appeared limited by the armored Dike (S3), which lacked a sand buffer. As a result, the Sandy dune experienced increased erosion due to this sediment deficit. By Storm 3, with Dike-in-dune (S1), Dike (S3), and Wall-in-dune (S4) fully exposed, this updrift sediment delivery was further constrained, increasing the sediment starvation at the Sandy dune section.

These findings underline that cross-shore erosion cannot be fully understood without accounting for longshore processes, especially near structural transitions where turbulence and flow steering intensify. For hybrid dunes, which inherently disrupt natural continuity, cross- and longshore interactions must be jointly assessed.

Design implications for hybrid dunes

The performance of hybrid dunes depended on a combination of interrelated design factors. The thickness of the sand cover over the structural core strongly influenced erosion resistance. Thicker covers extended the natural sand-buffer phase and delayed the onset of structure-dominated behavior. Once exposed, core geometry played a decisive role. The sloped dike of (S1) supported more gradual energy dissipation and stable profile development, while the vertical seawall (S4) caused a more abrupt change in wave behavior and localized vertical beach erosion. Although both halted landward retreat, the resulting nearshore morphodynamics were very different. Most critically, transition zones between the structure and surrounding sand emerged as key failure points. Side erosion was a dominant mechanism in the Dike-in-Dune section, where unprotected adjacent sand was undermined, leading to structural failure. These findings highlight the need for fully integrated hybrid dune designs that address not only core shape and volume but also lateral continuity, flanking protection, and toe reinforcement.

Final remarks

This research shows that hybrid dunes alter the erosion response of coastal profiles under storm conditions. Their embedded structures shift the dominant erosion mechanism from retreat-driven to structure-constrained, offering localized resistance but also introducing new vulnerabilities. The observed three-phase erosion behavior provides a useful framework for predicting hybrid dune performance. However, long-term effectiveness depends on well-designed transitions, sufficient sand cover, and an integrated understanding of sediment transport at both cross-shore and alongshore scales. When carefully designed, hybrid dunes can serve as adaptable, nature-based coastal defenses, balancing structural stability with morphological flexibility in a changing climate.

7
Recommendations

This chapter presents targeted recommendations derived from the field experiment, data analysis, and limitations encountered in this thesis. The recommendations aim to guide future research efforts, enhance experimental setups, and inform the practical design and implementation of hybrid dune systems.

Recommendations based on current field campaign data

The following recommendations are prioritized to enhance the value and applicability of the Hybrid-Dune field campaign dataset. They focus on improving temporal resolution, data integration, and analysis capabilities to support future morphological process studies and numerical modeling.

- **Increase temporal resolution of LiDAR-based dune profiles.** Morphological change was derived from LiDAR data processed at 12-hour intervals, which is too coarse to capture short-term responses during high-energy storm phases. It is recommended to extract cross-shore profiles at intervals of 10 minutes, particularly during rising tides and wave peaks. This would improve alignment with the measured hydrodynamic forcing and enable detection of rapid erosion phases such as slumping or notching.
- **Derive wave runup statistics from LiDAR time-series.** The LiDAR system operated at 4 Hz and recorded continuous elevation time-series at the dune face. Post-processing this data to extract wave runup maxima, bore heights, and exceedance statistics would directly link hydrodynamic loading to morphological response. This is particularly relevant for evaluating runup attenuation by hybrid structures and identifying storm thresholds.
- **Quantify longshore sediment transport using ADV and OBS measurements.** Differential erosion between dune sections indicates active longshore transport processes. It is recommended to analyze directional flow data from Acoustic Doppler Velocimeters (ADV) in combination with turbidity data from Optical Backscatter Sensors (OBS) to quantify sediment fluxes, especially near structural transitions. This will support 3D sediment budget estimation and clarify sediment redistribution patterns.
- **Analyze internal loading using embedded pressure sensors.** The dataset includes pore pressure sensors embedded in the structural cores. These should be used to assess internal hydrodynamic forcing and its role in initiating slumping or base instability. Future campaigns should consider adding soil moisture sensors in adjacent sand layers to better capture saturation-driven weakening and internal failure mechanisms.
- **Calibrate and validate numerical models using the full integrated dataset.** Bathymetric surveys from Rijkswaterstaat (RWS) should be combined with LiDAR and GPS-based profiles to define offshore boundary conditions and extend the morphological domain. Together with wave, pore pressure, and turbidity data, this dataset offers a robust foundation for calibrating 1D and 2D XBeach models. Simulations should replicate key processes, such as slumping, runup attenuation, and core exposure timing, and be used to explore hybrid dune behavior under specific storm conditions to improve predictive reliability for design and risk assessment.
- **Apply 3D LiDAR analysis to quantify spatial slumping behavior.** Although 16 LiDAR transects were collected, only a single profile was analyzed. Future work should use the full 3D dataset to identify and track slumping volumes across the dune face, capturing lateral variability and sediment redistribution. As shown by Van Wiechen et al. (2024b), linking slump timing and volume to dune base erosion and water level exceedance improves process understanding and supports more accurate, feedback-driven erosion modeling.

Recommendations for future research on hybrid dunes

To advance the understanding of hybrid dune performance, future research should focus on isolating structural effects, minimizing experimental interference, and systematically testing design variables under controlled and natural wave forcing. The following recommendations are prioritized accordingly:

- **Mitigate transitional effects and improve structural performance** Transitions between hybrid and non-hybrid dune sections caused localized turbulence, scour, and sediment steering, contributing to failure in the Dike and Dike-in-Dune sections. Future experiments could extend each profile (e.g, 30–100 meters) to allow wave shoaling and refraction before reaching transitions, ensuring representative cross-sectional behavior. These effects could also be examined in large-scale 3D flume tests (e.g., at Deltares) to quantify flow separation and scour, supporting more robust real-world transition designs.
- **Systematically test structural parameters and define sand cover design criteria.** Key design variables, such as core slope, elevation, sand cover thickness, and vegetation, should be varied in a single, continuous hybrid dune section to isolate their influence. Particular emphasis should be placed on identifying threshold sand cover thicknesses needed to delay core exposure. These results can inform quantitative design rules tailored to local wave climates and desired structural performance.
- **Test hybrid dunes under a range of controlled wave loading conditions.** The performance of hybrid dunes should be tested under systematically varied hydrodynamic conditions. This can be achieved by placing identical hybrid structures at different distances from the shoreline to induce varying wave energy exposure, or by recreating similar setups in a large-scale flume facility. Flume experiments also allow precise control over wave period and spectral shape, enabling investigation of frequency-dependent erosion processes and resonance effects not easily observed in the field.
- **Combine core types for adaptive structural behavior.** Different structural core materials, e.g., T-walls, geotextile containers, clay, or armor stone, offer unique erosion resistance and energy dissipation characteristics. Hybrid dunes that combine materials across different profile zones (e.g., reflective core with dissipative toe) could optimize performance under varied conditions. Testing such composite configurations in flume setups could reveal whether internal structural layering improves resilience, reduces scour, or delays failure mechanisms.

Bibliography

Almarshed, B., Figlus, J., Miller, J., and Verhagen, H. J. (2020). Innovative coastal risk reduction through hybrid design: combining sand cover and structural defenses. *Journal of Coastal Research*, 36(1):174–188.

Bertin, X., de Bakker, A., Van Dongeren, A., Coco, G., André, G., Ardhuin, F., Bonneton, P., Bouchette, F., Castelle, B., Crawford, W. C., et al. (2018). Infragravity waves: From driving mechanisms to impacts. *Earth-Science Reviews*, 177:774–799.

Boers, M., Van Geer, P., and Van Gent, M. (2011). Dike and dune revetment impact on dune erosion. In *The Proceedings of the Coastal Sediments 2011: In 3 Volumes*, pages 810–823. World Scientific.

Bosboom, J. and Stive, M. (2023). *Coastal Dynamics*. TU Delft Open, Delft, The Netherlands, version 1.2 edition. Licensed under Creative Commons Attribution-NonCommercial-ShareAlike 4.0 International (CC BY-NC-SA 4.0).

Castelle, B., Marieu, V., Bujan, S., Splinter, K. D., Robinet, A., Sénéchal, N., and Ferreira, S. (2015). Impact of the winter 2013–2014 series of severe western europe storms on a double-barred sandy coast: Beach and dune erosion and megacusp embayments. *Geomorphology*, 238:135–148.

Conti, S., Splinter, K., Booth, E., Djadjiguna, D., and Turner, I. (2024). Observations on the role of internal sand moisture dynamics in wave-driven dune face erosion. *Geomorphology*, 462:109331.

De Bakker, A. T. M., Tissier, M. F. S., and Ruessink, B. G. (2014). Shoreline dissipation of infragravity waves. *Continental Shelf Research*, 72:73–82.

Dette, H., Larson, M., Murphy, J., Newe, J., Peters, K., Reniers, A., and Steetzel, H. (2002). Application of prototype flume tests for beach nourishment assessment. *Coastal Engineering*, 47(2):137–177.

Elgar, S. and Guza, R. T. (1985). Observations of bispectra of shoaling surface gravity waves. *Journal of Fluid Mechanics*, 161:425–448.

Erikson, L. H., Larson, M., and Hanson, H. (2007). Laboratory investigation of beach scarp and dune recession due to notching and subsequent failure. *Marine Geology*, 245(1-4):1–19.

Figlus, J., West, N. A., Almarshed, B., and Jonkman, S. N. (2015). Conceptual design and physical model study of core-enhanced dunes as hybrid coastal defence structures. In *Coastal Structures and Solutions to Coastal Disasters Joint Conference 2015*, pages 65–73. American Society of Civil Engineers Reston, VA.

Gourlay, M. R. (2011). Wave set-up. In Hopley, D., editor, *Encyclopedia of Modern Coral Reefs*, pages 1144–1148. Springer.

Harris, M. and Ellis, J. (2020). A holistic approach to evaluating dune cores. *Journal of Coastal Conservation*, 24(1):1–15.

Herbich, J. B., Murphy, H. D., and Van Weele, B. (1980). Scour of flat sand beaches due to wave action in front of sea walls. In *Proceedings of Coastal Engineering Conference*, Lehigh University, Bethlehem, Pennsylvania. ASCE.

Kraus, N. C. and McDougal, W. G. (1996). The effects of seawalls on the beach: Part i, an updated literature review. *Journal of coastal research*, pages 691–701.

Larson, M., Erikson, L., and Hanson, H. (2004a). An analytical model to predict dune erosion due to wave impact. *Coastal Engineering*, 51(8):675–696. Coastal Morphodynamic Modeling.

Larson, M., Kubota, S., and Erikson, L. (2004b). Swash-zone sediment transport and foreshore evolution: field experiments and mathematical modeling. *Marine geology*, 212(1-4):61–79.

Mai, C. V., Pilarczyk, K. W., and Van Gelder, P. H. A. J. M. (2006). Foreshore erosion and scour induced failures of sea dikes. In *Third international conference on scour and erosion*, pages 424–433. CURNET.

Masselink, G. and Puleo, J. A. (2006). Swash-zone morphodynamics. *Continental Shelf Research*, 26(5):661–680.

Maximiliano-Córdova, C., Silva, R., Mendoza, E., Chávez, V., Martínez, M. L., and Feagin, R. A. (2023). Morphological performance of vegetated and non-vegetated coastal dunes with rocky and geotextile tube cores under storm conditions. *Journal of Marine Science and Engineering*, 11(11):2061.

Nordstrom, K. F. (2019). Coastal dunes with resistant cores. *Journal of Coastal Conservation*, 23(1):227–237.

Palmsten, M. L. and Holman, R. A. (2011). Infiltration and instability in dune erosion. *Journal of Geophysical Research: Oceans*, 116(C10).

Poppema, D., Vries, S. D., and Antonini, A. (2025). Hybrid dune voor rws, waterschappen. Presentation. Presented on January 10, 2025. TU Delft. Includes field experiment on hybrid dune construction and erosion measurement.

Reniers, A., Thornton, E., Stanton, T., and Roelvink, J. (2004). Vertical flow structure during sandy duck: observations and modeling. *Coastal Engineering*, 51(3):237–260.

Roelvink, D., Reniers, A., Van Dongeren, A., De Vries, J. V. T., McCall, R., and Lescinski, J. (2009). Modelling storm impacts on beaches, dunes and barrier islands. *Coastal engineering*, 56(11-12):1133–1152.

Ruessink, B., Houwman, K., and Hoekstra, P. (1998). The systematic contribution of transporting mechanisms to the cross-shore sediment transport in water depths of 3 to 9 m. *Marine Geology*, 152(4):295–324.

Ruessink, B. G., Michallet, H., Abreu, T., Sancho, F., van der A, D. A., van der Werf, J. J., and Silva, P. A. (2009). Modeling sediment transport beneath skewed asymmetric waves above a plane bed. *Journal of Geophysical Research: Oceans*, 109.

Ruessink, B. G., Michallet, H., Abreu, T., Sancho, F., Van Der A, D. A., Van der Werf, J. J., and Silva, P. A. (2011). Observations of velocities, sand concentrations, and fluxes under velocity-asymmetric oscillatory flows. *Journal of geophysical research: Oceans*, 116(C3).

Ruggiero, P. and McDougal, W. G. (2001). An analytic model for the prediction of wave setup, longshore currents and sediment transport on beaches with seawalls. *Coastal Engineering*, 43(3-4):161–182.

Sallenger, J. r. and Asbury, H. (2000). Storm impact scale for barrier islands. *Journal of coastal research*, pages 890–895.

Saponieri, A., Di Risio, M., Pasquali, D., Valentini, N., Aristodemo, F., Tripepi, G., Celli, D., Streicher, M., and Damiani, L. (2018). Beach profile evolution in front of storm seawalls: A physical and numerical study. *Coastal Engineering Proceedings*, (36):70–70.

Schiereck, G. J. and Verhagen, H. J. (2012). *Introduction to Bed, Bank and Shore Protection: Engineering the Interface of Soil and Water*. VSSD, Delft, The Netherlands, 2nd edition edition.

Small, C. and Nicholls, R. J. (2003). A global analysis of human settlement in coastal zones. *Journal of coastal research*, pages 584–599.

Steendam, G. J., Van Hoven, A., Van der Meer, J., and Hoffmans, G. (2014). Wave overtopping simulator tests on transitions and obstacles at grass covered slopes of dikes. volume 1, page 79. Citeseer.

Stive, M. and Wind, H. (1986). Cross-shore mean flow in the surf zone. *Coastal Engineering*, 10(4):325–340.

Stockdon, H. F., Holman, R. A., Howd, P. A., and Sallenger Jr, A. H. (2006). Empirical parameterization of setup, swash, and runup. *Coastal engineering*, 53(7):573–588.

Sutherland, J., Obhrai, C., Whitehouse, R., and Pearce, A. (2006). Laboratory tests of scour at a seawall. In *Proceedings 3rd International Conference on Scour and Erosion, CURNET, Gouda, The Netherlands*. Technical University of Denmark.

TAW (1998). *Guidelines for Geotechnical Design of Dikes*. Technical Advisory Committee on Water Defences.

Thao, N. T. P. and Tuan, T. Q. (2019). Influences of geometrical and structural configurations on beach and sea-dike toe scour during storms. In *International Conference on Asian and Pacific Coasts*, pages 401–406. Springer.

Turner, I. (1993). The total water content of sandy beaches. *Journal of Coastal Research*, pages 11–26.

Van der Meer, J. W. (2017). Wave run-up and overtopping. In *Dikes and revetments*, pages 145–160. Routledge.

Van Der Meer, J. W., Allsop, N., Bruce, T., De Rouck, J., Kortenhaus, A., Pullen, T., Schüttrumpf, H., Troch, P., Zanuttigh, B., et al. (2016). Eurotop-manual on wave overtopping of sea defences and related structures. an overtopping manual largely based on european research, but for worldwide application.

Van Geer, P., Boers, M., and van Gent, M. (2009). Measurements on the interaction between dunes and dikes during extreme storm events. In *Proceedings Of Coastal Dynamics 2009: Impacts of Human Activities on Dynamic Coastal Processes (With CD-ROM)*, pages 1–14. World Scientific.

Van Gent, M. R. (2001). Wave runup on dikes with shallow foreshores. *Journal of waterway, port, coastal, and ocean engineering*, 127(5):254–262.

Van Gent, M. R. A., De Vries, J. S. M. v. T., Coeveld, E. M., De Vroeg, J. H., and Van de Graaff, J. (2008). Large-scale dune erosion tests to study the influence of wave periods. *Coastal Engineering*, 55(12):1041–1051.

Van Thiel de Vries, J., Van Gent, M., Walstra, D., and Reniers, A. (2008). Analysis of dune erosion processes in large-scale flume experiments. *Coastal Engineering*, 55(12):1028–1040.

Van Thiel de Vries, J. S. M., Clarke, L. B., Aarninkhof, S. G. J., Coeveld, E. M., Holman, R. A., Palmsten, M. L., Reniers, A. J. H. M., Stive, M. J. F., and Uijttewaal, W. S. J. (2007). Interaction of dune face and swash zone. In *Coastal Sediments' 07*, pages 1975–1987.

Van Thiel de Vries, J. S. M., Van Dongeren, A. R., McCall, R., and Reniers, A. J. H. M. (2011). The effect of the longshore dimension on dune erosion.

Van Wiechen, P. P. J., de Vries, S., and Reniers, A. J. H. M. (2024a). Field observations of wave-averaged suspended sediment concentrations in the inner surf zone with varying storm conditions. *Marine Geology*, 473:107302.

Van Wiechen, P. P. J., De Vries, S., Reniers, A. J. H. M., and Aarninkhof, S. G. J. (2023). Dune erosion during storm surges: A review of the observations, physics and modelling of the collision regime. *Coastal engineering*, 186:104383.

Van Wiechen, P. P. J., Mieras, R., Tissier, M., and de Vries, S. (2024b). Coastal dune erosion and slumping processes in the swash□dune collision regime based on field measurements. *Journal of Geophysical Research: Earth Surface*, 129(10):e2024JF007711.

A

GPS survey & Beach profiles

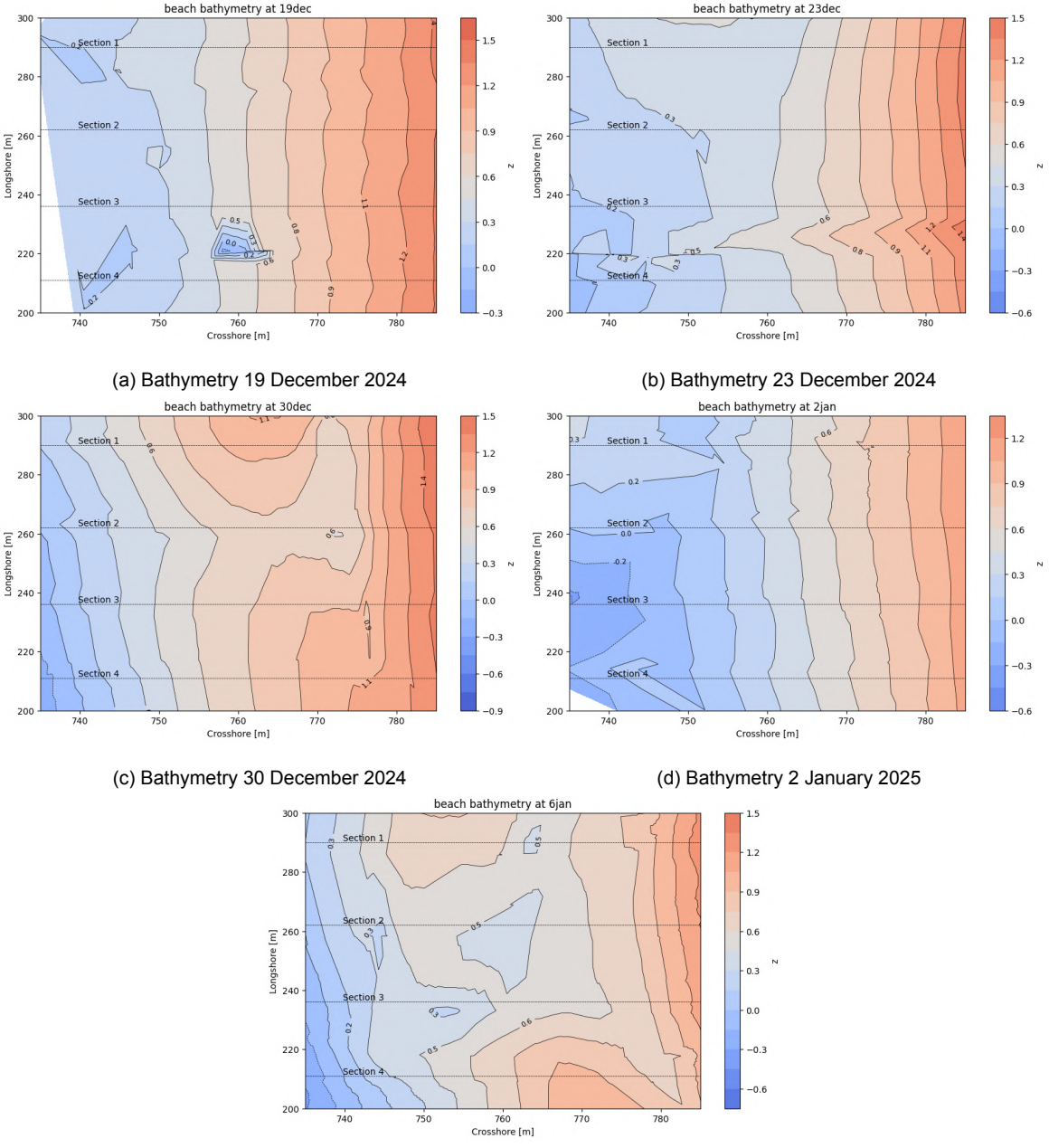

(a) Bathymetry 19 December 2024

(b) Bathymetry 23 December 2024

(c) Bathymetry 30 December 2024

(d) Bathymetry 2 January 2025

(e) Bathymetry 6 January 2025

Figure A.1: Overview of five plots representing beach bathymetry derived from interpolated RTK-GPS data.

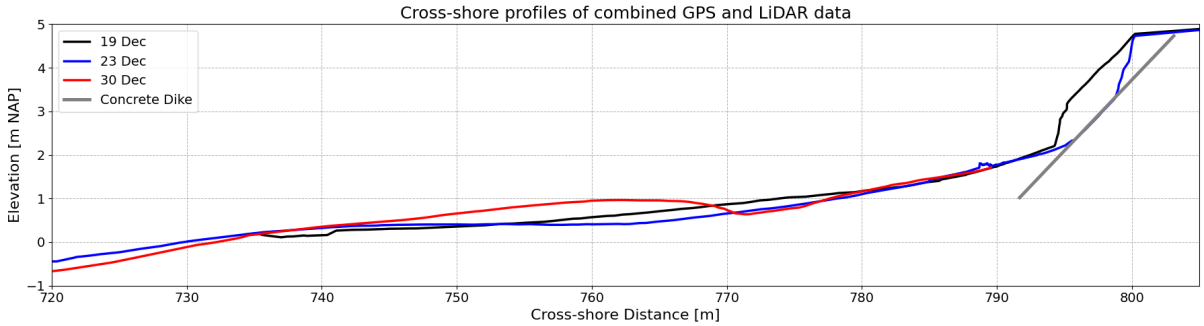

Figure A.2: Cross-shore beach profiles from GPS and LiDAR data for December 19 (black), December 23 (blue), and December 30 (red). The December 30 profile is based solely on GPS measurements, as no LiDAR data were available for that day. The concrete dike is shown in grey. Combining GPS and LiDAR data extends profile coverage across the beach-dune transition. Due to rapid morphological changes in the study area, co-located measurements on the same day are essential for reliable comparisons.

Bathymetry Data Collection and Processing

The bathymetric data presented in this section were obtained by interpolating Real-Time Kinematic GPS (RTK-GPS) measurements collected on specific survey dates. For this purpose, the RTK-GPS device was mounted on a wheeled cart and configured to record data at a frequency of 0.5 Hz, resulting in one measurement every two seconds. This setup allowed for efficient and continuous coverage of the intertidal zone within the experimental area.

The gathered data points were interpolated using the nearest-neighbour method to generate spatially continuous bathymetric maps. This interpolation approach provided a practical balance between preserving local detail and filling gaps in areas of lower measurement density.

The resulting bathymetry plots offer a more comprehensive view of the beach morphology in the experimental zone, extending beyond the spatial limits of the LiDAR systems. These maps support a more accurate interpretation of cross-shore and longshore beach features relevant to the hybrid dune system's behavior.

Beach Profile

A detailed beach profile was established by combining GPS and LiDAR measurements, allowing for an extended cross-shore reach beyond the typical LiDAR coverage (see Figure A.2). In this figure, the beach cross-section derived from GPS measurements is matched with LiDAR data collected on the same date and time. The black line represents data from December 19, the blue line from December 23, and the red line shows only the GPS measurements from December 30, as no corresponding LiDAR data was available for that date. It is important to note that, due to the high morphological variability of the study area, significant changes in beach and dune profiles can occur on a daily basis. Therefore, GPS and LiDAR data should be collected on the same date to ensure accurate and meaningful comparisons.

B

High water characteristics & Eroded Volumes

Table B.1, on the next page, provides a comprehensive overview of the incoming wave conditions, dune retreat, eroded sediment volumes, and relevant morphological parameters derived from LiDAR profile data. These measurements offer detailed quantitative insight into the evolution of both natural and hybrid dune sections during the first three storm events of the Hybrid Dune project. Wave characteristics, including significant wave height and peak period, were recorded at the measuring sensor S3.P3-RBR06. This data forms the basis for interpreting the hydrodynamic forcing acting on the dune profiles during each storm. The morphological changes presented in the table reflect differences in dune crest position, toe retreat, and volume loss, providing a direct link between storm intensity and structural response. This appendix supports the main findings by offering precise data on how each dune type performed under varying storm conditions and highlights the sediment dynamics crucial for understanding erosion resistance and recovery potential

Correlation table

Table B.1 presents Pearson correlation coefficients (r) between hydrodynamic parameters and erosion volumes per high water event for Sections S1 (Dike-in-Dune), S2 (Sandy Dune), and S4 (Wall-in-Dune). Parameters include water level, H_{m0}, $H_{m0,IG}$, T_p, and estimated runup ($R_{2\%}$).

Across all sections, water level showed the strongest and most consistent correlation with erosion volume. Correlations with H_{m0} and T_p were weaker. Runup ($R_{2\%}$) showed moderate correlation, but its simplified assumptions may limit reliability in hybrid systems.

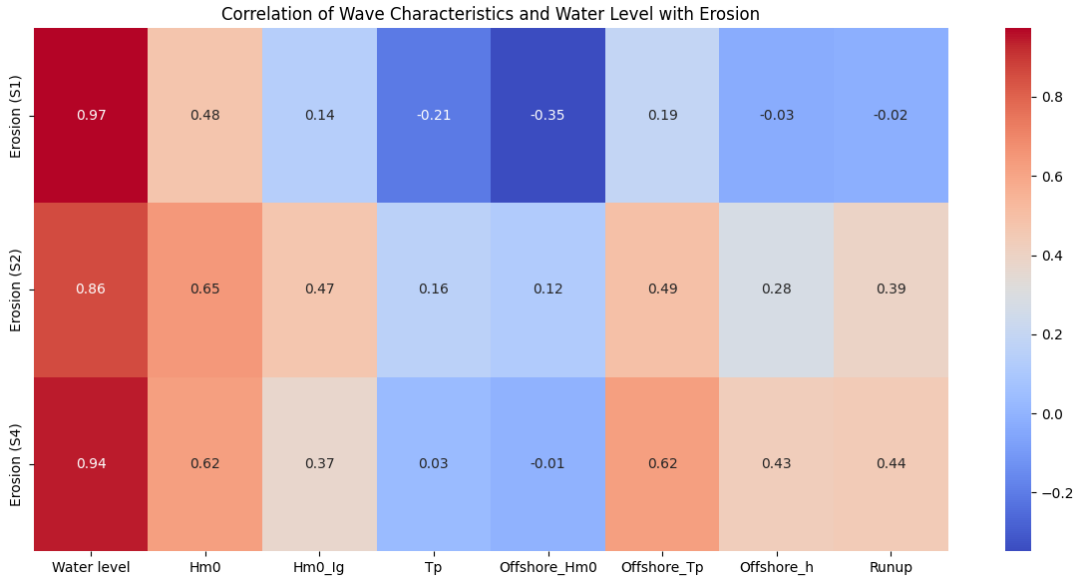

Figure B.1

Table B.1: Overview of wave conditions and morphological evolution during the hybrid dune field campaign. Columns represent successive high-water events, with **X** marking moments of LiDAR-based dune profile measurements. For each section (Sandy Dune, Dike-in-Dune, and Wall-in-Dune), wave conditions (water level, H_{m0}, $H_{m0,IG}$, and T_p) are listed, alongside changes in dune face position, dune foot elevation, and erosion or accretion volumes. Cumulative erosion is expressed in $[\mathrm{m^3/m}]$ relative to the initial profile.

	Initial	**HW 1.a**	**X**	**HW 1.b**	**X**	**HW 2.a**	**X**	**HW 3.a**	**X**
Wave Conditions									
Water level [m NAP]		1.85		2.05		1.97		1.86	
Hm0 [m]		1.39		2.07		1.89		1.96	
Hm0_Ig [m]		0.14		0.26		0.25		0.31	
Tp [s]		6		7.5		7.5		8.6	
Sandy dune									
Cross-shore dune face [m]	793.117	1.667	794.784	3.673	798.457	0.912	799.413	0.987	800.892
Elevation dune foot [m NAP]	2.313	-0.124	2.189	0.522	2.711	-0.234	2.471	-0.43	2.434
Erosion/accretion [m³/m]		-1.0992		-3.8744		-3.5404		-3.8214	
Cum. erosion/accretion [m³/m]	0		-1.0992		-4.9736		-8.6709		-11.4665
Dike-in dune									
Cross-shore dune face [m]	793.127	1.469	794.596	4.154	798.75	0.601	799.396	0.019	799.853
Elevation dune foot [m NAP]	2.407	-0.173	2.234	0.936	3.17	0.176	3.351	0.7649	3.526
Erosion/accretion [m³/m]		-0.9061		-2.8053		-1.4392		-0.9676	
Cum. erosion/accretion [m³/m]	0		-0.9061		-3.7114		-6.0633		-6.5575
Wall-in dune									
Cross-shore dune face [m]	793.987	0.748	794.735	4.13	798.865	0.9241	799.94	0	799.949
Elevation dune foot [m NAP]	2.296	-0.183	2.113	0.784	2.897	-0.229	2.475	-0.62	2.339
Erosion/accretion [m³/m]		-0.9669		-4.0432		-4.4129		-2.1031	
Cum. erosion/accretion [m³/m]	0		-0.9669		-5.0101		-11.1294		-11.7511